

**ROLE OF POLYMER FUNCTIONALITY  
AND ARCHITECTURE ON MORPHOLOGY  
OF GOLD NANOPARTICLES**

A THESIS SUBMITTED TO  
UNIVERSITY OF PUNE

FOR THE DEGREE OF  
DOCTOR OF PHILOSOPHY  
(CHEMISTRY)

BY

**SATISH C. BIRADAR**  
(M.Sc. CHEMISTRY)

UNDER THE GUIDANCE OF  
**DR. MOHAN G. KULKARNI**

POLYMER SCIENCE AND ENGINEERING DIVISION  
NATIONAL CHEMICAL LABORATORY  
PUNE 411008 (INDIA)

OCTOBER 2012

## **DECLARATION**

I hereby declare that the work presented in the thesis entitled “**Role of polymer functionality and architecture on morphology of gold nanoparticles**” submitted for Ph.D. degree to the University of Pune, has been carried out by me at the National Chemical Laboratory, Pune, under the guidance of **Dr. M. G. Kulkarni**. The work is original and has not been submitted in part or full by me for any degree or diploma to this or any other university.

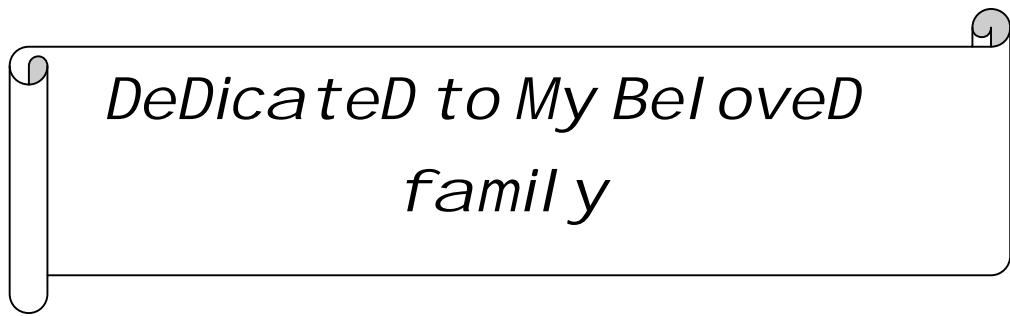
**Date:**

**National chemical laboratory**

**Pune - 411008**

**Satish C. Biradar**

**(Research Student)**



*DeDicated to My Bel oved  
family*

## *Acknowledgements*

*I would like to take this opportunity to pay first my sincere thanks to Dr. M. G. Kulkarni, whose motivation, guidance, advice and encouragement have lead me to bring my dream to reality. I am very much privileged to work under his esteemed guidance.*

*It is my pleasure to acknowledge Dr. S. Sivaram, former Director, NCL, and Dr. Sourav Pal, present Director, NCL, Pune for permitting me to present this work in the form of thesis.*

*I would like to acknowledge the financial support received from UGC-CSIR in the form of Fellowship.*

*I am grateful to Dr. V. K. Pillai and Mr. Dhanraj for their collaborative work. My sincere thanks to Dr. M. V. Badiger, Mr. M. J. Thakar, Dr. G. V. N. Rathna, Dr. P.G. Shukla, Dr. P.P. Wadgaonkar, Ms. D. A. Dhobale, Dr. Suresh Bhatt Dr A.S. Jadhav Dr. Mahesh Kulkarni, Dr. Amol Kulkarni and Dr. Satish Ogale for their suggestions and encouragement.*

*I sincerely thank my labmates Dr. Santosh, Dr. Sachin Dr. Hemant Dr. Ujwal Dr. Prerana Dr. Sunita, Dr. Shubhangi, Dr. Jiten, Dr. Aarti, Dr. Rupali Dr. Anupa, Dr Gore, Dr. Bharate, Dr. Swapnil, Dr. Nitin, Suresha, Manjusha, Nivika, Sameera, Anumun, Arun, Raju, Asmita, Pawan, Mayur, Vrushali, Arpita, Monzy, Harshal, Tushar, Shubhang, Irfan, Komal, Maya and Vishal who extended help throughout the tenure of my work at NCL. I would like to thank Mr. Dhavale, Mr Saroj Mr. Bharti and Mr. Mahajan for all the help rendered by them.*

*My sincere thanks to all NCL mates especially Dr. Rahul, Dr. Dr. Korbad Dr. Sachin Dr. Kishor, Dr. Ankush, Dr. Bharat, Dr. Sharan, Lalit, Krishna Pradeep, Chinmai, Satej, Dr. Laxman, Dr. Suleman, Dr. Abasaheb, Dr. Manmath, Santosh, Nagesh, Prakash, Balaji, Sharad, Dr Bhaskar, Shashikant, Khupse, Dr. Ravi, and Sutar for their cheerful environment.*

*The words are not enough to express all my love and thankfulness towards my parents, brothers and sister. I would like to express my deep gratitude to my mother in law. I could not have completed my research work without her support and blessings. Lastly, I would like to thank my wife Meera and my son Dnyanesh for their sacrifices and cheerful environment.*

**Satish C. Biradar**

## Table of Contents

|   |        |
|---|--------|
| List of Figures                                 | vi     |
| List of Tables                                  | xii    |
| Abbreviations and Symbols                       | xii    |
| <br>  |        |
| <b>Chapter 1</b>                                |        |
| <b>Literature review</b>                        | 1 - 49 |
| 1.1 Nanomaterials: origin and importance        | 1      |
| 1.2 Nanotechnology                              | 1      |
| 1.3 History of nanomaterials                    | 2      |
| 1.4 Classification of nanomaterials             | 3      |
| 1.4.1 Organic nanoparticles                     | 3      |
| 1.4.2 Inorganic nanomaterials                   | 4      |
| 1.4.2.1 Magnetic nanoparticles                  | 4      |
| 1.4.2.2 Semiconductor nanoparticles             | 4      |
| 1.4.2.3 Noble metal nanoparticles               | 4      |
| 1.4.2.3.1 Gold nanoparticles                    | 5      |
| 1.5 Properties of nanomaterials                 | 5      |
| 1.5.1 Catalytic properties                      | 6      |
| 1.5.2 Mechanical properties                     | 6      |
| 1.5.3 Magnetic properties                       | 6      |
| 1.5.4 Biocompatibility                          | 7      |
| 1.5.5 Melting point                             | 7      |
| 1.6 Applications of AuNPs                       | 8      |
| 1.6.1. Drug delivery                            | 8      |
| 1.6.2 Imaging                                   | 8      |
| 1.6.3. Photothermal Therapy                     | 9      |
| 1.6.4. Catalysis                                | 9      |
| 1.7 Methods for synthesis of gold nanoparticles | 11     |
| 1.7.1 Physical methods (“top down approach”)    | 11     |
| 1.7.1.1 Sonochemical methods                    | 12     |
| 1.7.1.2 Radiolysis method                       | 12     |

|   |    |
|---|----|
| 1.7.1.3. UV Irradiation method                              | 13 |
| 1.7.1.4. Laser ablation                                     | 13 |
| 1.7.2. Biological Methods (Bottom up approaches)            | 13 |
| 1.7.3. Chemical methods                                     | 14 |
| 1.8 Characterization techniques                             | 16 |
| 1.8.1 UV-Visible spectroscopy                               | 16 |
| 1.8.2 Fourier transforms infrared spectroscopy (FT-IR)      | 18 |
| 1.8.3 Transmission electron microscopy (TEM)                | 19 |
| 1.8.4 Atomic force microscopy (AFM)                         | 19 |
| 1.8.5 Thermo gravimetric analysis (TGA)                     | 19 |
| 1.8.6 X-ray photoelectron spectroscopy (XPS)                | 19 |
| 1.9 Ligand-protected AuNPs                                  | 20 |
| 1.10 Role of polymer in stabilization of gold nanoparticles | 25 |
| 1.11 Stability of AuNPs                                     | 29 |
| 1.12 Nanocapsules synthesis                                 | 32 |
| 1.13 Synthesis of gold nanochains                           | 36 |
| 1.14 Our approach   | 43 |

## **Chapter 2**

|                            |         |
|----------------------------|---------|
| <b>Objective and scope</b> | 50 - 51 |
| 2.1 Introduction           | 50      |
| 2.2 Objectives             | 50      |

## **Chapter 3**

|   |        |
|---|--------|
| <b>Shell crosslinked AuNPs for enhanced thermal stability</b> | 52 -68 |
| 3.1 Introduction  | 52     |
| 3.2 Experimental section                                      | 53     |
| 3.2.1 Materials   | 53     |
| 3.2.2. Measurements   | 54     |
| 3.2.3. Synthesis of DSDMA                                     | 54     |
| 3.2.4. Synthesis of AuNPs                                     | 55     |
| 3.3. Results and discussion                                   | 56     |
| 3.3.1 Synthesis and characterization of AuNPs.                | 56     |
| 3.3.1.1 UV, IR and TEM analysis                               | 56     |

|   |    |
|---|----|
| 3.3.1.2. Thermal - crosslinking of DSDMA stabilized AuNPs | 59 |
| 3.3.1.3. Photo - crosslinking of DSDMA stabilized AuNPs   | 60 |
| 3.3.2. Stability of AuNPs                                 | 61 |
| 3.3.2.1 Solvent stability                                 | 61 |
| 3.3.2.2. Stability against DTT                            | 62 |
| 3.3.2.3. Thermal stability                                | 63 |
| 3.3.2.4 Nanocapsules synthesis                            | 66 |
| 3.4. Conclusions  | 67 |

## **Chapter 4**

|   |          |
|---|----------|
| <b>Polydentate disulfides for enhanced stability of AuNPs and facile nanocavity formation</b> | 69 - 100 |
| 4.1. Introduction   | 69       |
| 4.2. Experimental section   | 71       |
| 4.2.1. Materials  | 71       |
| 4.2.2. Measurements   | 71       |
| 4.2.3. Synthesis  | 72       |
| 4.2.3.1. Inclusion complex of DSDMA (Precipitation method)                                    | 72       |
| 4.2.3.2. Polymerization of DSDMA - $\beta$ CD inclusion complex                               | 73       |
| 4.2.3.3. Preparation of gold nanoparticles  | 73       |
| 4.2.3.4 Thermal stability   | 74       |
| 4.2.3.5 Nanocapsules synthesis  | 74       |
| 4.3. Results and discussion   | 74       |
| 4.3.1. Poly(DSDMA) characterization   | 76       |
| 4.3.2 Synthesis and characterization of poly(DSDMA) stabilized AuNPs                          | 79       |
| 4.3.2.1 UV, IR and TEM analysis   | 79       |
| 4.3.3 Stability of AuNPs  | 82       |
| 4.3.3.1 Solvent stability   | 82       |
| 4.3.3. Stability against DTT  | 83       |
| 4.3.3.3 Thermal stability   | 85       |
| 4.3.4 Nanocapsules  | 92       |
| 4.3.4.4. Synthesis of nanocavities from 3.2 nm AuNPs  | 92       |
| 4.3.5.2 Synthesis of nanocavities from 6 nm AuNPs   | 97       |

|       |             |    |
|-------|-------------|----|
| 4.4.0 | Conclusions | 97 |
|-------|-------------|----|

## **Chapter 5**

|   |  |     |
|---|--|-----|
| <b>Characterization of gold nanoparticles</b> | 101 - 112  |     |
| 5.1   | Introduction   | 101 |
| 5.2.  | Experimental section                                   | 101 |
| 5.2.1   | Materials  | 101 |
| 5.2.2   | Instrumentation  | 101 |
| 5.3   | Results and discussion                                 | 102 |
| 5.3.1   | XRD Analysis   | 102 |
| 5.3.2   | X-ray photoelectron spectroscopy (XPS)                 | 102 |
| 5.3.3   | Differential pulse voltametry (DPV)                    | 104 |
| 5.3.4   | Scanning tunnelling microscope (STM)                   | 106 |
| 5.3.5   | Electron paramagnetic resonance (EPR) characterization | 107 |
| 5.4   | Conclusions  | 109 |

## **Chapter 6**

|   |  |     |
|---|--|-----|
| <b>One pot room temperature synthesis of robust gold nanochains</b> | 113–144  |     |
| 6.1.  | Introduction   | 113 |
| 6.2.  | Experimental section   | 116 |
| 6.2.1.  | Materials  | 116 |
| 6.2.2.  | Measurements   | 116 |
| 6.2.3   | Polymer synthesis  | 117 |
| 6.2.4   | AuNP synthesis   | 117 |
| 6.3.  | Results and discussion   | 118 |
| 6.3.1.  | PAmAm characterization   | 119 |
| 6.3.1.1.  | Confirmation of polymerization by FT-IR                          | 119 |
| 6.3.1.2.  | Confirmation of polymerization by <sup>1</sup> H NMR             | 119 |
| 6.3.2   | Effect of PAmAm concentration on morphology of AuNPs             | 120 |
| 6.3.2.1   | In situ investigation of nanochain formation                     | 123 |
| 6.3.2.2   | Effect of polymer concentration on AuNP morphology<br>at pH 3.3  | 126 |
| 6.3.2.3   | Effect of polymer concentration on AuNPs morphology<br>at pH 8.3 | 129 |



|   |     |
|---|-----|
| 6.3.2.4 Effect of pH on morphology of AuNPs prepared<br>at constant polymer concentration | 130 |
| 6.3.2.5 Effect of solvent on chain length   | 132 |
| 6.3.3 Stability   | 134 |
| 6.3.3.1 Effect of pH on stability.  | 134 |
| 6.3.3.2 Stability against temperature   | 137 |
| 6.3.3.3 Stability against thiol exchange  | 138 |
| 6.3.3.4 Stability against salt  | 139 |
| 6.4 Conclusions   | 141 |

## **Chapter 7**

|   |           |
|---|-----------|
| <b>Conclusions and recommendations for further work</b> | 145 - 148 |
| 7.1 Introduction  | 145       |
| 7.2 Significant findings                                | 145       |
| 7.3 Recommendation for further work                     | 147       |

## List of Figures

### Chapter 1

#### Literature review

|      |  |    |
|------|--|----|
| 1.1  | Use of nanomaterials in (a) Lycurgus Cup, (b) Damascus Sword.                                      | 4  |
| 1.2  | UV-Vis spectra for the synthesis of p-aminophenol.   | 10 |
| 1.3  | Schematic for homocoupling phenyl boronic acid   | 10 |
| 1.4  | Flowchart for biosynthesis of nanoparticles  | 14 |
| 1.5  | Schematic presentations for AuNPs formation  | 15 |
| 1.6  | Polarization of a spherical metal particle by the electrical field<br>vector of the incoming light | 18 |
| 1.7  | Ligand stabilized gold nanoparticles   | 20 |
| 1.8  | Schematic for dendron-stabilized AuNPs   | 22 |
| 1.9  | Structures of alkane thiols  | 23 |
| 1.10 | Structure of monothiol and trithiol ligand   | 24 |
| 1.11 | Structure of thioctic acid and dihydrolipoic acid  | 24 |
| 1.12 | Schematic for reduction of $I_2$ by $NaBH_4$   | 25 |
| 1.13 | Structures of dendrimers   | 25 |
| 1.14 | Polymer stabilized AuNPs   | 26 |
| 1.15 | Schematic for preparation polymer-stabilized transition<br>metal nanoparticles                     | 27 |
| 1.16 | Multidentate ligands for stabilization of AuNPs  | 29 |
| 1.17 | G2 alkyl dendrimer   | 30 |
| 1.18 | G2 aromatic dendrimer  | 31 |
| 1.19 | Norbornene functionalized AuNPs  | 31 |
| 1.20 | Polyamine crosslinked AuNPs  | 32 |
| 1.21 | Schematic representation of the synthesis of<br>vesicle-templated nanocapsules                     | 33 |
| 1.22 | Schematic for nanocapsules via the 'self-templating' approach.                                     | 34 |
| 1.23 | Synthesis for nanocapsules using AuNPs as sacrificial templates                                    | 35 |
| 1.24 | Schematic of nanocapsules synthesis  | 35 |
| 1.25 | Octanethiol and 12-( <i>N</i> -Pyrrolyl)dodecanethiol stabilized AuNPs                             | 37 |
| 1.26 | Schematic of light triggered Covalent assembling of AuNPs  | 38 |

|      |  |    |
|------|--|----|
| 1.27 | Schematic for nanochains formation   | 39 |
| 1.28 | UV-visible spectra of nanochains before and after silica coating                               | 39 |
| 1.29 | TEM images of photo-polymerized DA-PEG and silica coated AuNPs nanochains.                     | 40 |
| 1.30 | Schematic for preparation of chainlike assemblies of Au NPs                                    | 40 |
| 1.31 | TEM images before and after silica-coating of chainlike assemblies of Au NPs                   | 41 |
| 1.32 | Schematic for the preparation of the HPAMAM-N(CH <sub>3</sub> ) <sub>2</sub> /AuNPs composite. | 42 |

### Chapter 3

#### Shell crosslinked AuNPs for enhanced thermal stability

|      |  |    |
|------|--|----|
| 3.1  | <sup>1</sup> H NMR spectrum of DSDMA   | 55 |
| 3.2  | Schematic for DSDMA stabilization AuNPs  | 57 |
| 3.3  | UV-Visible spectra of AuNPs at disulfide to Au ratio a) 1 b) 10 c) 25 mM DSDMA concentration                           | 58 |
| 3.4  | TEM images of DSDMA AuNPs at a) 1 b) 10 c) 25 mM concentration   | 58 |
| 3.5  | IR Spectrum of DSDMA stabilized AuNPs  | 59 |
| 3.6  | TEM images of DSDMA AuNPs at disulfide: Au a) 1:5 b) 1: 10   | 59 |
| 3.7  | UV-Visible spectra of DSDMA AuNPs after a) before b) after heating at 140 °C for 1 h                                   | 60 |
| 3.8  | TEM image of DSDMA stabilized AuNPs after heating at 140 °C for 1h   | 61 |
| 3.9  | UV-Visible spectra of DSDMA AuNPs after a) 1 day b) 15 days.   | 62 |
| 3.10 | TEM image of DSDMA stabilised AuNPs 1:1 molar ratio after a) 1 day b) 15 days.   | 62 |
| 3.11 | UV-Visible spectra of DSDMA AuNPs stability against DTT  | 63 |
| 3.12 | UV-Vis spectra of DSDMA AuNPs at a) 50 b) 90 c) 100 °C   | 65 |
| 3.13 | UV-Vis spectra of crosslinked DSDMA stabilized AuNPs at a) room temperature b) 140 °C after 1 h c) 140 °C after 1.25 h | 65 |
| 3.14 | AuNPs with 1:1 ratio of disulfide: Au a) 40 °C b) 100 °C   | 66 |
| 3.15 | AuNPs with 1:1 ratio of disulfide : Au a) 40 °C b) 140 °C after 1h   | 66 |

## Chapter 4

### Polydentate disulfides for enhanced stability of AuNPs and facile nanocavity formation

|      |  |    |
|------|--|----|
| 4.1  | DSDMA inclusion complex synthesis  | 77 |
| 4.2  | <sup>1</sup> H NMR spectrum of DSDMA – β CD inclusion complex  | 77 |
| 4.3  | Poly(DSDMA) synthesis 1) DSDMA; β-CD inclusion complex<br>2) Poly(DSDMA) with β-CD 3) Poly(DSDMA) with free vinyl group.                   | 78 |
| 4.4  | <sup>1</sup> H NMR of poly(DSDMA)  | 78 |
| 4.5  | UV-Vis spectra of poly(DSDMA) AuNPs at disulfide: Au ratio<br>a) 1:1, b) 10:1, c) 25:1   | 79 |
| 4.6  | TEM images of AuNPs stabilized on poly(DSDMA) at<br>disulfide: Au ratio a) 1:1 b) 10:1 c) 25: 1 show particle<br>size 3.2, 2.8 and 2.2 nm. | 80 |
| 4.7  | UV-Visible spectra of AuNPs at disulfide: gold ratio a) 1:5 b) 1: 10   | 81 |
| 4.8  | TEM images AuNPs at disulfide: gold ratio a) 1: 5 b) 1: 10   | 81 |
| 4.9  | IR spectrum of poly(DSDMA) stabilized AuNPs  | 82 |
| 4.10 | UV-Visible spectra of poly (DSDMA) AuNPs in solution after<br>a) 1 day b) 1 year   | 83 |
| 4.11 | TEM of poly(DSDMA) AuNPs in solution after 1 year.   | 83 |
| 4.12 | UV-Visible spectra of DSDMA AuNPs stability against DTT.   | 84 |
| 4.13 | Poly(DSDMA) AuNPs stability against DTT a) before and<br>b) after addition 5 h c) 72 h d) 80 h.  | 84 |
| 4.14 | UV-Vis spectra of poly(DSDMA) AuNPs at a) 40 °C<br>b) at 140 °C after 4 h c) after 4.5 h.  | 87 |
| 4.15 | AuNPs with 10:1 ratio of poly(DSDMA) and auric chloride<br>a) room temperature b) 140 °C after 4 h.  | 88 |
| 4.16 | IR spectrum of noncrosslinked and crosslinked poly(DSDMA)<br>AuNPs.  | 89 |
| 4.17 | UV-Vis spectra of poly (DSDMA) AuNPs at a) 40 °C b) at 140 °C<br>after 1.5 h c) after 1.75 h   | 90 |
| 4.18 | AuNPs with 1:5 ratio of poly(DSDMA) and auric chloride<br>a) room temperature b) 140 °C at 1.75 h.   | 91 |
| 4.19 | DLS of poly(DSDMA) AuNPs before and after crosslinking.  | 91 |

|      |   |    |
|------|---|----|
| 4.20 | TGA of AuNPs stabilized by a) DSDMA b) Poly(DSDMA) at 1: 10<br>c) 10: 1                 | 92 |
| 4.21 | UV-Visible spectra of etched poly(DSDMA) AuNPs a) before<br>b) after washing            | 95 |
| 4.22 | IR spectrum of etched poly(DSDMA)   | 95 |
| 4.23 | TEM images of nanocavities from crosslinked poly(DSDMA).                                | 95 |
| 4.24 | AFM of a) Poly(DSDMA) nanocapsules b) height profiles of<br>selected particles.         | 96 |
| 4.25 | DLS of gold etched from before crosslinking and after<br>crosslinking of poly(DSDMA)    | 96 |
| 4.26 | TEM images of a) Poly(DSDMA) stabilized 6 nm AuNPs<br>b) Nanocapsules formed on etching | 97 |

## **Chapter 5**

### **Characterization of gold nanoparticles**

|     |   |     |
|-----|---|-----|
| 5.1 | XRD of AuNPs  | 103 |
| 5.2 | Binding energies of poly(DSDMA) stabilized AuNPs  | 103 |
| 5.3 | Superimposed DPV responses of AuNPs   | 106 |
| 5.4 | DPV responses of AuNPs size 3 nm before and<br>after heating.   | 106 |
| 5.5 | STM image of a) AuNPs with height profile b) AuNPs<br>c) I-V profile on HOPG surface d) I-V curve on AuNPs.   | 107 |
| 5.6 | Electron Paramagnetic Resonance spectra (EPR) of AuNPs<br>stabilized on Poly (DSDMA) of size a) 2.2 nm b) 2.8 nm<br>c) 3.2 nm d) 6 nm e) 8 nm f) DSDMA stabilized 2.8 nm AuNPs. | 109 |

## **Chapter 6**

### **One pot room temperature synthesis of robust gold nanochains**

|     |   |     |
|-----|---|-----|
| 6.1 | Schematic for synthesis of gold nanoparticles and nanochains                              | 118 |
| 6.2 | FT-IR spectrum of PAmAm   | 119 |
| 6.3 | <sup>1</sup> H NMR of PAmAm with terminal amine   | 119 |
| 6.4 | UV spectra of AuNPs prepared at PAmAm concentration<br>a) 30 mM b) 20 Mm c) 10 mM d) 5 mM | 121 |
| 6.5 | TEM images of AuNPs formed at PAmAm concentration   |     |

|      |  |     |
|------|--|-----|
|      | a) 30 mM b) 20 mM c) 10 mM d) 5 mM.  | 122 |
| 6.6  | UV –Vis spectra of AuNPs at PAmAm concentration a) 3 mM<br>b) 1.5 mM.  | 122 |
| 6.7  | TEM images of AuNPs prepared at concentration a) 3 mM<br>b) 5 mM   | 123 |
| 6.8  | UV – Vis spectra of Au nanochain formed at 3 mM PAmAm  | 124 |
| 6.9  | TEM images of AuNPs formed at 3 mM PAmAm concentration at<br>a) 5 min b) 20 min c) 60 min d) 200 min         | 124 |
| 6.10 | HR-TEM image of Au nanochains  | 125 |
| 6.11 | Schematic for pH dependent morphology of gold nanoparticles  | 127 |
| 6.12 | UV- Vis spectra of AuNPs formed at pH 3.3 and concentration<br>a) 3 mM b) 5 mM c) 10 mM                      | 128 |
| 6.13 | TEM images of AuNPs at a) 5 mM b) 10 mM and pH 3.3   | 128 |
| 6.14 | UV-Vis spectra of AuNPs prepared at pH 8.3 using polymer<br>concentration a) 5 mM b) 10 mM c) 20 mM          | 129 |
| 6.15 | TEM images of AuNPs formed at PAmAm concentration a) 5 mM<br>b) 10 mM d) 20 mM at pH 8.3.                    | 130 |
| 6.16 | UV - Visible spectra at pH a) 3.3 b) 4.3 c) 5.3 d) 6.3 e) 7.3 f) 8.3   | 131 |
| 6.17 | TEM analyses of AuNPs formed at pH a) 4.3 b) 5.3 c) 7.3 d) 8.3   | 132 |
| 6.18 | UV-Vis spectra of AuNPs prepared in the presence of cosolvent<br>a) Acetonitrile b) Methanol (50% vol /vol). | 133 |
| 6.19 | TEM of AuNPs prepared in the presence of a) Acetonitrile<br>b) methanol (50% vol / vol)                      | 134 |
| 6.20 | UV-Vis spectra of nanochains a) before and b) after addition<br>of NaOH at pH 8.3                            | 135 |
| 6.21 | TEM of AuNPs formed at 3 mM a) at pH 3.3 b) on switching<br>to 8.3.  | 136 |
| 6.22 | UV-Vis spectra of isolated AuNPs a) at pH 8.3 b) on switching<br>to 3.3                                      | 136 |
| 6.23 | TEM of AuNPs at 3 mM concentration a) at pH 8.3<br>b) on switching to pH 3.3                                 | 137 |
| 6.24 | UV-Vis spectra of AuNPs at 70 °C, after a) 1 h b) 12 h<br>c) 24 h e) at 100 °C                               | 138 |
| 6.25 | UV-Vis spectra of Au nanochains exchanged with thiol   |     |

|      |  |     |
|------|--|-----|
|      | a) before addition b) 24 h after addition of 10 mM thiol.                | 139 |
| 6.26 | TEM of AuNPs against thiol exchange before and after.                    | 139 |
| 6.27 | UV-Vis spectra of a) AuNPs b) 1h c) 24 h after addition of<br>1 mM NaCl  | 140 |
| 6.28 | Uv-Vis spectra of a) AuNPs b) 1h c) 24 h after addition of<br>10 mM NaCl | 140 |

## List of table

### Chapter 6

#### One pot room temperature synthesis of robust gold nanochains

|                                     |     |
|-------------------------------------|-----|
| 1 Effect of pH on SPR and LSPR peak | 131 |
|-------------------------------------|-----|

#### Abbreviations and Symbols

|                   |  |
|-------------------|--|
| AIBN              | Azobisisobutyronitrile                       |
| AFM               | Atomic force microscopy                      |
| AuNPs             | Gold nanoparticles                           |
| $\beta$ -CD       | $\beta$ -Cyclodextrin                        |
| CHCl <sub>3</sub> | Chloroform                                   |
| DCM               | Dichloromethane                              |
| DMF               | N,N Dimethyl formamide                       |
| DSDMA             | Bis (2-methacryloyl hydroxyl ethyl)disulfide |
| DRS               | Diffuse reflectance spectroscopy             |
| DLS               | Dynamic light scattering                     |
| DPV               | Differential pulse voltametry                |
| EPR               | Electron paramagnetic resonance              |
| FTIR              | Fourier transform infrared spectroscopy      |
| GPC               | Gel permeation chromatography                |
| Mw                | Weight average molecular weight              |
| Mn                | Number average molecular weight              |
| NMR               | Nuclear magnetic resonance spectroscopy      |
| Poly              | Polymer                                      |
| SPR               | Surface plasmon resonance                    |
| STM               | Scanning tunnelling microscope               |
| SERS              | Surface enhancement Raman spectroscopy       |
| TGA               | Thermo gravimetric analysis                  |
| TEM               | Transmission electron microscopy             |
| UV-Vis            | Ultraviolet visible spectroscopy             |
| XRD               | X-ray diffraction                            |
| XPS               | X-ray photoelectron spectroscopy             |



---

---

**Chapter 1**  
**Literature review**

---

---

### **1.1 Nanomaterials: origin and importance**

The word nano, comes from the Greek “nanos” meaning “Dwarf”. Nano refers to the  $10^{-9}$ , or one billionth fraction. When it refers to a meter (m), or a nanometer (nm), it is on the scale of atomic diameters. Thus nanomaterial science involves the study of atoms, molecules, and their assembly whose size is on the nanometer scale ( $< 100$  nm) (Whitesides 2005, Polizzi et al 2007, Lieber 2003).

Materials at nanolevel exhibit different properties and their study leads to new materials. There are others reasons why nanomaterials is becoming such an interesting field. One is availability of new instruments which are able to visualise at this scale. Secondly physical and chemical properties of nanomaterials are different than their bulk counterpart (Ozin and Arsenault 2005). The scanning tunnelling microscope was invented at IBM-Zurich in Switzerland (Herring 1952). This was the first instrument that was able to see atoms. A few years later, the atomic force microscope (AFM) was invented Mullins (1963), expanding the capabilities and types of materials that could be investigated. Since then many similar techniques have evolved from these instruments to evaluate various properties of materials at the nanometer scale. Emergence of these tools has enabled structural studies of nanomaterials and given an impetus to the research in nanomaterials. Currently, there are a large number of complementary instruments such as TEM, XPS, XRD, and DLS that help researcher to analyse nanomaterials at different scale.

### **1.2 Nanotechnology**

Nanotechnology encompasses design, synthesis and application of nanomaterials. Research and development in this field is growing rapidly throughout the world. For example, band gaps of semiconductors can be tuned by varying material size at the nanometer scale. These new physical properties can lead to newer applications not

otherwise possible. The other important aspect is the miniaturization of current and new instruments, sensors and machines that will greatly impact the world we live in. Examples of miniaturization are: computers with great power that calculate algorithms to mimic human brains, nanorobots that can repair internal damage and remove chemical toxins in human bodies, biosensors that warn us at the early stage of the onset of disease and preferably at the molecular level and target specific drugs that automatically attack the diseased cells on site, and nanoscale electronics that constantly monitor our local environment. Nanotechnology has broad range of potential applications, and requires contributions from multidisciplinary teams comprising chemists, physicists, engineers, material scientists, molecular biologists, pharmacologists to work together on synthesis and processing of nanomaterials, understanding the physical properties at nanometer scale, design and fabrication of devices using nanomaterials as building blocks, and design and construction of novel tools for characterization of nanomaterials. Synthesis and processing of nanomaterials are essential aspects of nanotechnology. Studies on new physical properties and applications of nanomaterials are possible only when nanomaterials are made available with desired size, shape, morphology as well as chemical composition. The research has significantly intensified in the last few decades, resulting in increasing number of publications in journals across different disciplines as research on nanotechnology is evolving and expanding very rapidly (Zhao et al 1999).

### **1.3 History of nanomaterials**

Nanotechnology as is presently defined is relatively new. The study of biological systems and the engineering of many materials such as colloidal dispersions, metallic quantum dots, and catalysts in the nanometer form has been in progress for centuries. For example, the Chinese are reported to have used AuNPs as an inorganic dye to

introduce red color into their porcelains more than thousand years ago (Ayers et al 1992, Zhao and Ning 2000). The Lycurgus cup, a glass cup of 4th century AD, appears red in transmitted light and green in reflected light (Figure 1.1a). This effect, which can be seen in the cup preserved in the British museum in London, is because of Au and Ag nanocrystals present in the walls of the cup so also the ‘Damascus Sword’ containing the nanoscale carbon particles (Figure 1.1b). Michael Faraday (1857) demonstrated the synthesis of AuNPs in 1857 in his paper titled ‘Experimental relations of gold (and other metals) to light’ published in Philosophical Transactions. It is in the last few decades that this field has scaled new heights for many reasons including invention of revolutionary imaging methods and techniques that made the characterization of the materials at nanoscale easier. Medical applications of colloidal gold present another example. Colloidal gold was and is still used for the treatment of arthritis. A number of diseases were diagnosed by the interaction of colloidal gold with spinal fluids obtained from the patient. What has revolutionized the field is our ability to image, engineer and manipulate systems at the nanometer scale, and the combination of our ability to see and manipulate matter on the nanoscale as well as our understanding of interactions at atomic scale.

#### **1.4 Classification of nanomaterials**

Prathna et al (1999) described details of classification of nanoparticles. Nanoparticles can be broadly grouped into two parts: namely organic and inorganic nanoparticles.

##### **1.4.1 Organic nanoparticles**

Organic nanomaterials are composed of mostly carbon and are in the form of hollow spheres, ellipsoids, or tubes. Spherical and ellipsoidal carbon nanomaterials are referred to as fullerenes, while cylindrical ones are called nanotubes.



**Figure 1.1** Use of nanomaterials in (a) Lycurgus Cup, (b) Damascus Sword.  
(Verhoeven et al 1998 and Freestone et al 2007)

#### 1.4.2.1 Magnetic nanoparticles

The nanoparticles of Iron, Nickel and Cobalt belong to this category and have potential applications in biomedicine, magnetic resonance imaging, catalysis, nanofluids and optical filters.

#### 1.4.2.2 Semiconductor nanoparticles

The nanoparticles of zinc oxide and titanium oxide are classified into this category. Zinc oxide nanoparticles are soluble in water and have antimicrobial properties, are non toxic and compatible with skin, which make them suitable additives for textiles and surfaces. Zinc Oxide nanoparticles are also an effective additive for packaging plastics to prevent UV damage. Titanium dioxide too is an extensively investigated metal oxide. It is an important material for industrial applications in pigments, semiconductors, filler, coating and cosmetics.

#### 1.4.2.3 Noble metal nanoparticles

Gold and silver nanoparticles of various size and shape have been investigated and found various applications in catalysis, as SERS substrates and in drug delivery.

#### **1.4.2.3.1 Gold nanoparticles**

AuNPs are the most investigated nanoparticles amongst the metal nanoparticles, over 70 000 publications have appeared on AuNPs to date (Zhao et al 2012). Also gold is the most electronegative element and can be generated from its salts by a various reducing species. Not only classical reducing agent such as hydrides, hydrazine, hydroxylamine, alcohols etc. can be used, but also organic species with some reducing character are suited to produce gold nanoparticles from salts. “Green chemistry” has evolved in recent years. Gold nanoparticles can be generated using natural organic materials as reducing agents. Different types of fungi have been found to reduce gold salts into elemental gold. Relative ease of gold nanoparticle preparation, stability of nanoparticles in various solvents, resistance to oxidation, and simultaneously the active interaction with various organic ligands, including oligomeric and polymeric ligands, especially those bearing Thiol, Nitrogen, and other heteroatoms has spurred research in gold nanoparticles (Bakeeva et al 2008).

The AuNPs exhibit unique physical properties such as mechanical, thermal and magnetic as well as catalytic properties and biocompatibility find various applications in drug delivery, Catalysis and as a SERS substrate.

#### **1.5 Properties of nanomaterials**

A number of physical properties become more pronounced as the particle size decreases. Certain properties may not be evident as the size is lowered from macro to micro level but may be significant at the nano scale. The increase in surface area to volume ratio leads to increasing dominance of the behaviour of atoms on the surface of the particle over that of those in the interior of the particle (Prathna et al 1999). This leads to remarkable modification of many fundamental properties such as electrical and thermal conductivity, band gap, density of states, electron affinity,

mechanical, magnetic and optical properties. These properties are a strong function of size, shape and distribution of the nanoparticles.

### **1.5.1 Catalytic properties**

The field of nanocatalysis has witnessed exponential growth during the last few decades. As nanoparticles have a large surface to volume ratio compared to bulk materials, they are attractive as catalysts, since catalysis is a surface phenomenon. It has been shown that the activities of gold nanoparticles of different shapes are indeed different for the same electron-transfer reaction in colloidal solution. This shape dependent catalysis adds to the advantage of using nanoparticles as catalysts. In addition to being small they have corners and edges, which make the surface atoms of the nanoparticles unstable during the chemical reaction they catalyze. The reactant molecules also show different affinity in adsorption towards different faces of the catalyst. Hence gold nanoparticles of different shapes covered by different faces could be used to increase the selectivity of a catalyst. Oxidation and reduction reactions were carried out using gold nanoparticles as catalyst.

### **1.5.2 Mechanical properties**

Mechanical properties of a material depend strongly on the density of dislocations, particle size and the surface interface to volume ratio. The strength and hardness of the material could be severely affected with decrease in particle size. As compared to the bulk material, a nanoparticle has more defects because of the high surface to volume ratio. The ability of nanomaterial to undergo extensive tensile deformation without destroying the structure is well reported and is called superplasticity.

### **1.5.3 Magnetic properties**

The magnetic properties of nanoparticles differ from those of bulk in two ways. The large surface to volume ratio results in a different local environment for the surface

atoms in their magnetic coupling / interaction with neighbouring atoms, leading to the mixed volume and surface magnetic characteristics. Unlike bulk ferromagnetic materials, which usually form multiple magnetic domains, several small ferromagnetic particles could consist of only a single magnetic domain. In such cases superparamagnetism is exhibited wherein the magnetizations of the particles are randomly distributed and they are aligned only under an applied magnetic field, and the alignment disappears once the external field is withdrawn. This could have important implications for example, in ultra-compact information storage where the size of the domain determines the limit of storage density.

#### **1.5.4 Biocompatibility**

One of the important aspects in the study of nanoscience and nanotechnology is to assess the cytotoxicity levels of nanoparticles in living systems. Nanoparticles have been used for various biological applications. They hold future in biodiagnostics, therapeutics, drug delivery, bioimaging, immunostaining and biosensing. Thus, it becomes an important issue to study the short and long term effect of size, shape, and surface functional groups on the biocompatibility, uptake, subcellular distribution, metabolism, and degradation of these nanostructures. Some of the efforts made in this direction are the studies using gold nanoparticles. Sastry et al (2003) have studied the uptake of AuNPs by mammalian cells by pinocytosis and its compartmentalization in lysosomal bodies. With high scattering cross-section of AuNPs in the near infrared region. They are also being considered for use as intravenous contrast enhancers in medical imaging.

#### **1.5.5 Melting point**

The melting point of the nanocrystals has a direct relation with the size of the nanoparticles i.e. smaller is the size of a nanoparticle lower will be the melting point.



The surface atoms in the solid phase are coordinatively unsaturated and thus high amount of surface energy is associated with them and the surface energy is always lower in the liquid phase as compared to the solid phase. The process of melting starts from the surface and thus, the nanoparticle system is much more stable in the liquid phase due to reduced surface energy. A dramatic decrease in the melting point is observed in the nanoparticles that are smaller than 3-4 nm in size.

## **1.6 Applications of AuNPs**

Gold colloids have fascinated scientists for over a century and are now heavily utilized in chemistry, biology, engineering, and medicine. AuNPs have recently emerged as an attractive candidate for various applications as discussed below.

### **1.6.1. Drug delivery**

Programmed release of the drugs to physiological targets has been a major challenge in molecular and macromolecular therapeutics (Torchilin 2006). Highly tunable and multivalent surface architecture of gold nanoconjugates offers the potential to incorporate multiple therapeutic agents as well as to target and protect molecules on the surface of a single nanoparticle, and thus are expected to improve the delivery and efficacy of therapeutic payloads Giljohann et al (2010). The payloads could be small drug molecules or large biomolecules like proteins, DNA, or RNA. Efficient release of these therapeutic agents is a prerequisite for effective therapy. The release could be triggered by internal or external stimuli [glutathione (Hong et al 2006), pH (Polizzi et al 2007, Han et al 2006)].

### **1.6.2 Imaging**

AuNPs modified with antibodies specific to cancer associated proteins have been used to image cancerous cells. Light microscopy experiments show that conjugates exhibit six times greater affinity to cancerous cells than the noncancerous controls, thus

making this technique potentially useful for the detection of cancer cells (Sayed et al 2005).

### **1.6.3. Photothermal therapy**

Gold nanorods and nanoshells conjugated with antibodies are being developed as photothermal therapy agents that use antibody-coated surfaces to destroy cancerous cells. For example, nanoshells conjugated to antibodies against human epidermal growth factor receptor 2 (HER2) were incubated with cancerous cells over-expressing HER2 receptors. These cells were then irradiated with near- IR light at a frequency that is resonant with the surface plasmon resonance of the nanoshells. Light absorption leads to heating, which causes cell death.

### **1.6.4. Catalysis**

Nanoparticulate Au catalysts are active under mild conditions, even at ambient temperature or less, and this makes them unique. These catalysts are effective in reducing running costs of chemical plants and could increase the selectivity of the reactions involved where applicable, e.g. in pollution control applications, such as air cleaning, low light-off autocatalysts, and purification of hydrogen streams used for fuel cells.

Size dependent effects of metal clusters have been studied for long time and are importance in catalysis. Fenger et al (2012) synthesized AuNPs of size 3.5, 10, 13, 28, 56 nm diameters using CTAB as stabilizer and tested for catalytic activity of the p-nitro phenol to p-aminophenol reaction (Figure 1.2). The result showed that neither very small (3.5 nm) nor large nanoparticles (28 nm - 56 nm) exhibit high catalytic activity. Rather the particles in the intermediate size range (13 nm) exhibit higher activity.

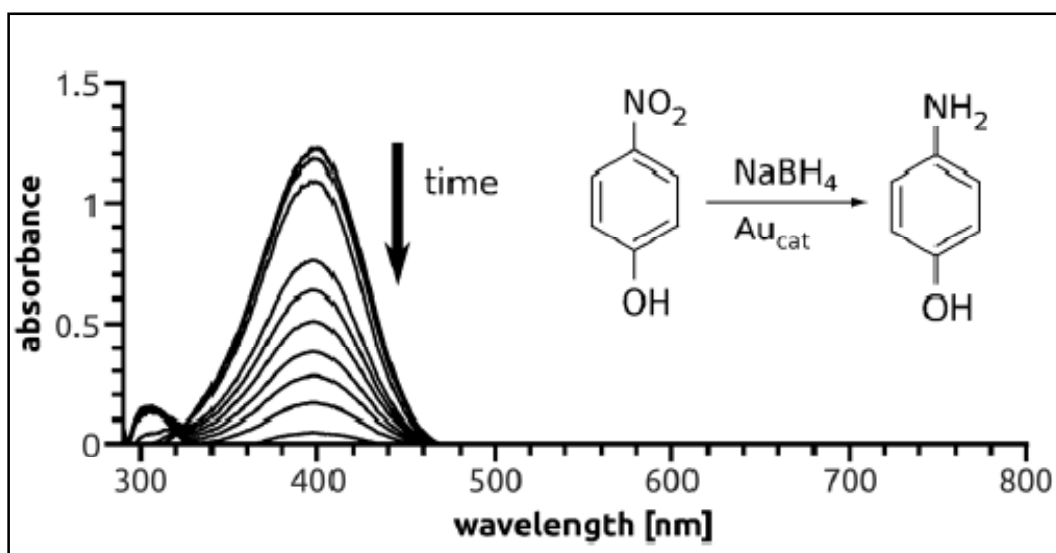


**Figure 1.2** UV-Vis spectra of the catalytic process for p-nitro phenol to p-aminophenol. (Fenger et al 2012)

Tsunoyama et al (2004) reported synthesis of PVP stabilized 2 nm AuNPs and showed their use for the homocoupling of phenylboronic acid in water under aerobic conditions and proposed a mechanism for their activity (Figure 1.3).

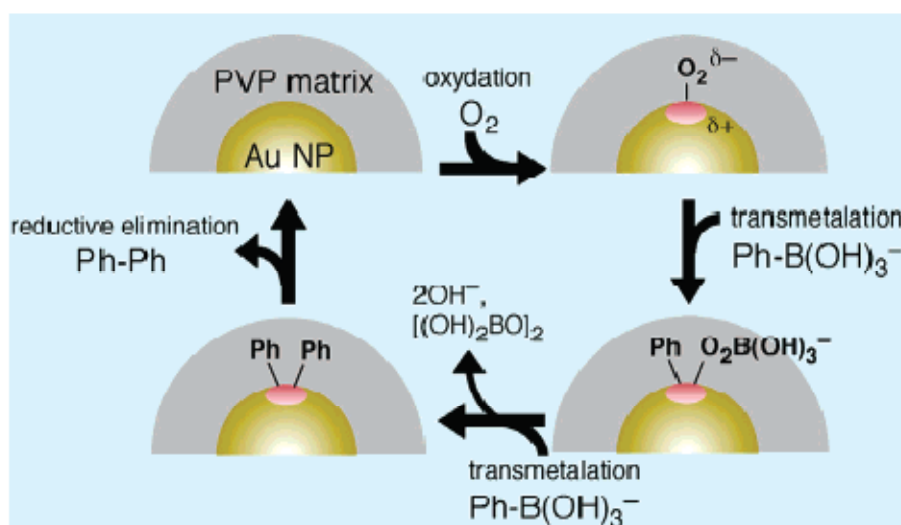


**Figure 1.3** Schematic for homocoupling phenyl boronic acid (Tsunoyama et al 2004).

The AuNPs are also used in oxidation of many compounds ambient air at low temperatures, particularly CO and nitrogen-containing malodorous compounds, such as trimethylamine. This offers scope for applications in air quality improvement and control of odors etc.

## 1.7 Methods for synthesis of gold nanoparticles

After the initial report by Faraday in 1857 of the reduction of auric chloride solution by phosphorus in carbon disulfide, the preparation of AuNPs with controlled sizes and shapes received increased attention during the second half of the 20<sup>th</sup> century. The breakthroughs came through Turkevich et al in 1951 with the citrate method which was improved by Frens in 1973. In 1981 Schmid et al reported a Au<sub>55</sub>-phosphine cluster and the notion of quantum dot, followed by Mulvaney and Giersing who in 1993 reported first synthesis and stabilization of AuNPs by thiolates. Schiffrin group in 1994 reported most convenient Brust-Schiffrin biphasic method of thiolate-stabilized AuNPs (Daniel and Astruc 2004). Improvisations of these methods during the last decade, especially the seed growth synthesis, have now led to promising applications.

AuNPs can be prepared by both “top down” and “bottom up” approaches. For “top down” procedures, a bulk state Au is systematically broken down to generate AuNPs of desired dimensions. The “top down” method has limitation in the control of the size and shape of particles as well as functionalization (Nguyen et al 2011). In contrast, in the “bottom up” strategy, the formation of AuNPs originates from individual molecules, because it involves a chemical or biological reduction (Parab et al 2011).

A number of procedures are available in the literature for synthesis of gold nanoparticles. Most of them have been known for decades. For this reason only some of relevant and most useful synthesis method shall be discussed here briefly.

### 1.7.1 Physical methods (top down approach)

The simplest way of obtaining nanoparticles is the generation of gold atoms in the gas phase followed by their controlled condensation to nanoparticles. This is the well-

known metal- vapour synthesis. In special cases the colloidal metals can be studied in the gas phase. However, in order to obtain them as matter, the vapours have to be condensed into a dispersing medium. Only some more common technique shall be discussed.

#### **1.7.1.1 Sonochemical methods**

Jin et al (2007) reported synthesis of gold nanoparticles using Sonochemical method. An aqueous solution of auric chloride (0.25 mM, 5 ml) was added to the [1-(2, 3-dimercaptoacetoxypropyl)- 3-methylimidazolium, 3-mercapto-1- propanesulfonic acid (TFIL) solution. The solution was stirred for 5 min and then 30% hydrogen peroxide (1.5 ml) was added to the solution mixture, finally it was subjected to ultrasonic irradiation at 25 °C. The color of solution changed gradually from yellow to red with increasing irradiation time, indicating the formation of AuNPs. In order to get various size of particles, thiol to gold ratio was varied in the range 2:1, 1:1, 1:2, 1:4 and 1:8, respectively. UV-Visible spectra showed peak in the range of 525.6 nm to 539.2 nm and corresponding TEM showed particle size in the range of 9.5 to 5.5 nm.

#### **1.7.1.2 Radiolysis method**

Radiolysis of aqueous solutions involves the radiolytic reduction of auric chloride to zero-valent nanoparticles. Choofong et al (2010) synthesized gold nanoparticles in aqueous solution in the presence of Chitosan as stabilizer. In aqueous solution,  $\gamma$  - rays induce radiolysis of water to form solvated electrons (hydroxyl radicals (OH•), hydrogen atoms (H•), hydrogen peroxide (H<sub>2</sub>O<sub>2</sub>), hydrogen gas (H<sub>2</sub>). The OH• and H• species react with Chitosan molecules by H-abstraction on carbon atoms (C<sub>1</sub>-C<sub>6</sub>) within glucosamine unit. Radicals can form at C<sub>1</sub> and C<sub>4</sub> atoms that involve the

scission of 1-4 glycosidic linkages. The solvated electron species reduce gold ion ( $\text{Au}^{+3}$ ) to gold atom ( $\text{Au}^0$ ).

#### **1.7.1.3. UV Irradiation method**

Sau et al (2001) reported gold nanoparticles synthesis using UV radiation with an ordinary germicidal lamp (Philips, Holland G15T8Uvc, 15 W). Chloroauric acid and TX-100 solutions were photo-irradiated for 25 min. The photo activation produced pink colored Au(0) particles of size 5 and 20 nm by varying the ratio of gold ion concentration to stabilizer. 20–110 nm particles were formed by the reduction of fresh Au(III) ions on the surface of presynthesized nanoparticles.

#### **1.7.1.4. Laser ablation**

Mafune et al (2011) synthesized Gold nanoparticles by laser ablation of metal gold plate in aqueous solution of sodium dodecyl sulfate (SDS). The gold metal plate was irradiated with laser beam. Upon irradiation of the laser beam, the solution gradually turned to wine red indicating formation of nanoparticles. The concentration of SDS was varied in the range 0.001 M to 0.1 M in order to get particles of different size. UV-Vis spectrum showed absorption at 517 nm and increase in concentration lead to peak broadening. Corresponding TEM showed particles size in the range 1-15 nm.

#### **1.7.2. Biological methods (bottom up approaches)**

Biosynthesis of nanoparticles is a kind of bottom up approach where the main reaction occurring is reduction / oxidation (Kruger et al 2008). The microbial enzymes or the plant photochemical with anti oxidant or reducing properties are usually responsible for reduction of metal compounds into their respective nanoparticles. Biological methods mainly employ fungus, bacteria and leaf extract to reduce metal ions to form nanoparticles (Figure 1.4).

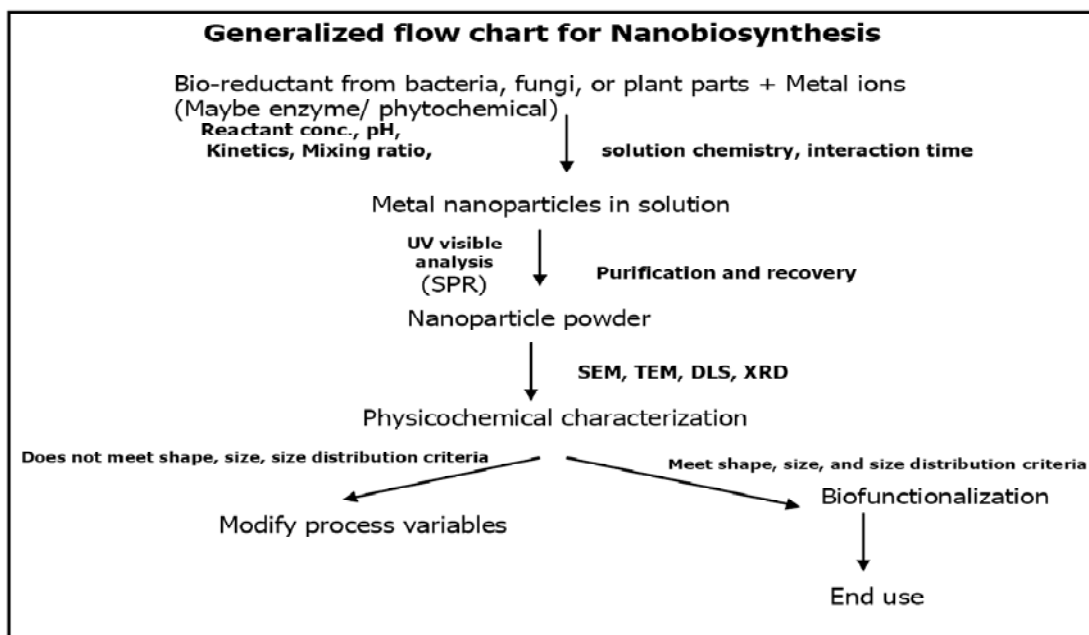


**Figure 1.4** Flowchart for biosynthesis of nanoparticles (Prathna et al 1999)

The AuNPs synthesis using natural-source extracts involves mixing the extracts with aqueous auric chloride until the color changes to red or purple. Although biological methods produce AuNPs at room temperature, control of particle size and distribution is difficult.

### 1.7.3. Chemical methods

Synthesis of AuNPs using chemical methods has been more popular and gained wide acceptance because of its easy protocols and the fine shape and size control provided by this method (Alkilany et al 2010). It involves the reduction of chloroaurate ions with reducing agents such as borohydride, aminoboranes, hydrazine, formaldehyde, hydroxylamine, saturated and unsaturated alcohols, citric and oxalic acids, polyols, sugars, hydrogen peroxide, sulfites, carbon monoxide, hydrogen and acetylene in the presence of a capping agent. In the course of the last century, numerous easier to handle reducers were identified. A few of the more relevant procedures are mentioned below. Sodium citrate is most commonly used for reduction of gold salt. Citrate acts as a capping agent and also a mild reducing agent at elevated temperature. Polte et al

(2010) reported the synthesis of AuNPs using citrate as reducer and stabilizer. The formation of nanoparticles involves first rapid formation of nuclei followed by aggregation of the nuclei into larger particles which further slow diffusion growth of nanoparticles sustained by ongoing reduction of gold precursor as well as further coalescence. Subsequently, particles grow rapidly to their final size, the final particle size governed by complete consumption of the precursor species (Figure 1.5).

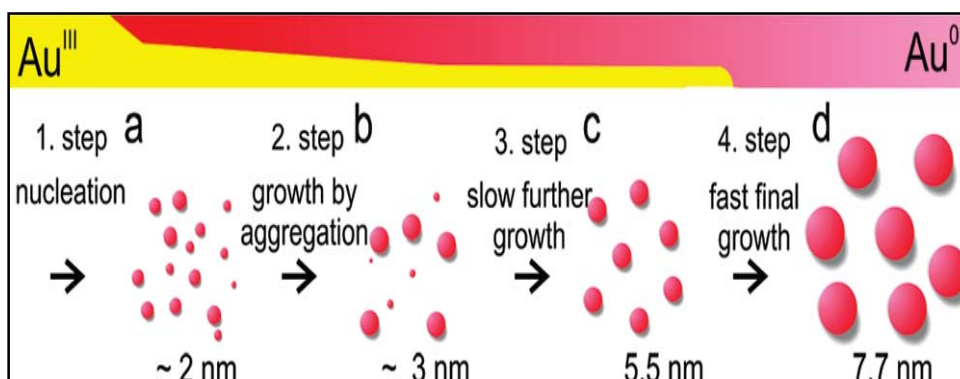


**Figure 1.5** schematic presentations for AuNPs formation (Polte et al 2010)

Although citrate can be used as reducing and stabilizing agent, it takes long time to stabilize nanoparticles and due to very weak binding the resultant particles are not so stable.

Borohydride method has also been used for long time to synthesize AuNPs at room temperature. Brust et al (1994) introduced a two-phase method. This was followed by a one phase method, which allowed working without a phase-transfer agent and thus avoided the phase-transfer step and need for further purification from tetraoctylammonium bromide impurities. The single phase hydrazine and borohydride method has been most frequently used since the strong reducing characteristics of these reducing agent lead to nanoparticles in shorter time.

Hussain et al (2009) reported AuNPs synthesis using hydrazine as reducing agent. 75 mL of 5% starch aqueous solution was diluted in 15 mL of ethylene glycol at room temperature with stirring. After 30 min 2 ml of 1% auric chloride aqueous solutions



was added and stirred. Addition of aqueous hydrazine to the above solution led gold nanoparticles as evident from red color.

Borohydride is one of the most useful reducing agent for synthesis of AuNPs (Aryal et al 2006, Frenkel et al 2005, Male et al 2008, Shimmin et al 2004, Bhat and Maitra 2008). The synthesis of gold nanoparticle using borohydride as reducing agent is discussed below in brief. Shimmin et al (2004) reported synthesis of Gold nanoparticles using borohydride as reducing agent, where in  $\text{HAuCl}_4 \cdot 3\text{H}_2\text{O}$  was dissolved in 2-propanol and acetic acid solution, and Me-PEG-SH was then added followed by vigorous stirring of the solution for 15-30 min. On rapid addition of borohydride, the above solution turned dark immediately, indicating the formation of gold nanoparticles, and was further stirred for at least 1 h in order to stabilize nanoparticles.

## **1.8 Characterization techniques**

### **1.8.1 UV-Visible spectroscopy**

UV-Visible range is a small window of total electromagnetic spectrum, which ranges from 190 nm to 800 nm. Appearance of colour arises from the property of the colored material to absorb selectively and reflect its complementary colour which falls within the visible region of the electromagnetic spectrum.

Light absorption by small metal particles is best described by Mie's theory. The absorption spectrum of particles in a given solvent can be calculated from the optical constants of the bulk metal, although the absorption of the particles is often vastly different from that of the bulk metal itself. The simplest case is when the particles are spherical and their size is small compared to the wavelength of light and the particles are well separated in solution. At particle sizes in the range 3 to 20 nm, the dependence of the absorption spectra on particle size is not strong. This is because the

particles are below the size at which higher order terms in the Mie formula for the absorption constant become significant. Thus, one has to regard only the dipole term, which depends only on the total metal concentration in the solution and not on particle size. The absorption coefficient in  $\text{mol}^{-1} \cdot \text{L} \cdot \text{cm}^{-1}$  is calculated from the relation

$$\alpha = \frac{18\pi}{\ln 10} \frac{10^5}{\lambda} \frac{Mn_0^3}{\rho} \frac{\varepsilon_2}{(\varepsilon_1 + 2n_0^2) + \varepsilon_2^2}$$

Where,  $\lambda$  is the wavelength of light in nanometers,  $M$  and  $\rho$  are the molecular weight and density of the metal,  $n_0$  is the refractive index of the solvent and  $\varepsilon_1$  and  $\varepsilon_2$  are the real and imaginary parts of the dielectric constant of the metal. When the size of the particles becomes smaller than the mean free path of the electrons, the absorption bands are broadened; this is accounted for by using size corrected values of  $\varepsilon_2$

$$\varepsilon_2 = \varepsilon_{2(bulk)} + \left( \frac{\omega_p^2}{\omega^3} \right) (V_F / R)$$

where  $\omega$  is the light frequency,  $\omega_p$  the plasmon frequency,  $v_F$  the electron velocity at the Fermi level and  $R/V_F$ , mean time of the free movement of the electrons. Resonance with the incident light is reached at the wavelength, where the negative value of  $\varepsilon_1$  of the metal is equal to twice the dielectric constant of the medium. For example, gold particles possess plasmon resonances in the visible range (~514 nm). When a small spherical metallic nanoparticle is irradiated by light, the oscillating electric field causes the conduction electrons to oscillate coherently. This is schematically pictured in Figure 1.6.

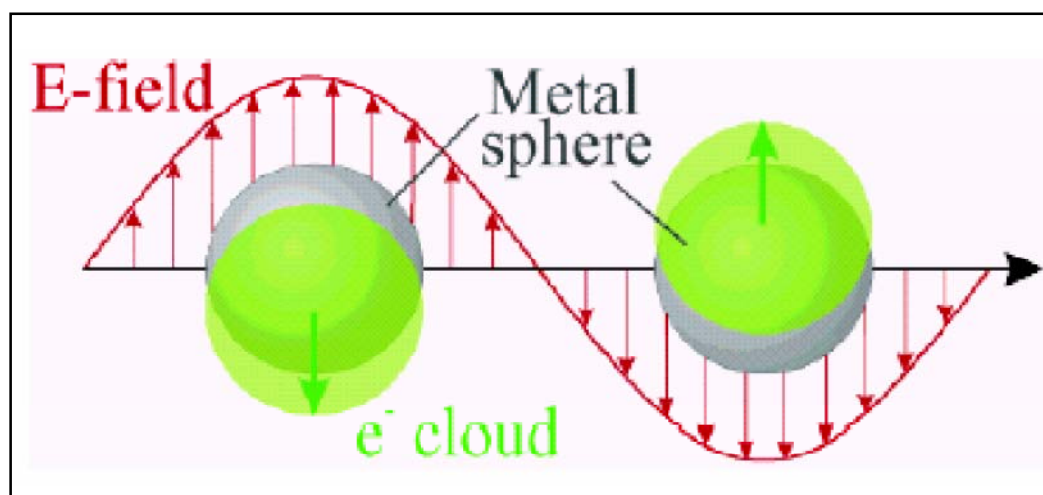


**Figure 1.6** Polarization of a spherical metal particle by the electrical field vector of the incoming light (Henglein 1993)

When the electron cloud is displaced relative to the nuclei, a restoring force arises from Coulomb attraction between electrons and nuclei that results in oscillation of the electron cloud relative to the nuclear framework. The oscillation frequency is determined by four factors, the density of electrons, the effective electron mass, and the shape and size of the charge distribution. The collective oscillation of the electrons is called the dipole plasmon resonance of the particle. Thus the electron density within a surface layer, the thickness of which is about equal to the screening length of a few angstroms, oscillates, whereas the density in the interior of the particle remains constant ("surface plasmon"). Therefore, any changes in the electron density of this surface layer will lead to changes in the plasmon absorption. UV-Vis spectroscopy measurements of all the samples in the present case were performed on Shimadzu UV-Visible spectrophotometer UV-1601 PC model.

### **1.8.2 Fourier transforms infrared spectroscopy (FT-IR)**

The electromagnetic radiation range between  $400\text{ cm}^{-1}$  to  $4000\text{ cm}^{-1}$  falls under infra red region. This range of electromagnetic radiations causes vibrational transitions in the bond. This happens when the frequency of incident IR radiation matches with the difference between vibrational levels belonging to the bonds.

FT-IR is useful to confirm presence of ligand and their structural changes on nanoparticles surface. Chen and Kimura (1999) reported that FT-IR spectra of gold particles stabilized with mercaptosuccinic acid (MSA) and that of pure MSA. The spectrum of MSA was similar to the standard one. The peak at  $2548\text{ cm}^{-1}$ , which corresponds to the S-H stretching mode, disappeared when MSA was adsorbed on the gold particle surface, giving strong evidence that MSA anchors on the gold surface through Au-S bond.

### **1.8.3 Transmission electron microscopy (TEM)**

Transmission electron microscopy is a very useful technique to observe the size, shape, and morphology of the particles at nanoscale. It gives image of atomic distribution of nanoparticles, also it can provide atomic resolution lattice images at resolution of 1 nm or less than that.

### **1.8.4 Atomic force microscopy (AFM)**

AFM is also known as scanning force microscopy (SFM). AFM is a basic technique and inevitable for all nanoscopic research.

### **1.8.5 Thermo gravimetric analysis (TGA)**

Thermal gravimetric technique is used to determine the thermal stability of given compound. It provides a quantitative measurement of weight loss associated with a temperature. In TGA, the sample is continuously weighed as it is heated to elevated temperatures. Along with polymer stability, in order to calculate the percentage of gold and polymer for graft density on nanoparticles surface TGA is most useful method. In present thesis TA universal analysis thermal analyser were used.

### **1.8.6 X-ray photoelectron spectroscopy (XPS)**

X-ray photoelectron spectroscopy is well known characterization technique which is basically used for obtaining chemical information of various material surfaces. It is

also known as electron spectroscopy for chemical analysis (ESCA). XPS help determine the gold oxidation state of the nanoparticles.

### 1.9 Ligand-protected AuNPs

Ligands play an important role in governing nanoparticle size, shape, and interparticle spacing (Figure 1.7). While the atomic composition of nanoparticles is most important in determining their physical properties, it is the chemical nature of the capping ligands that determine size, distribution and stability of nanoparticles.

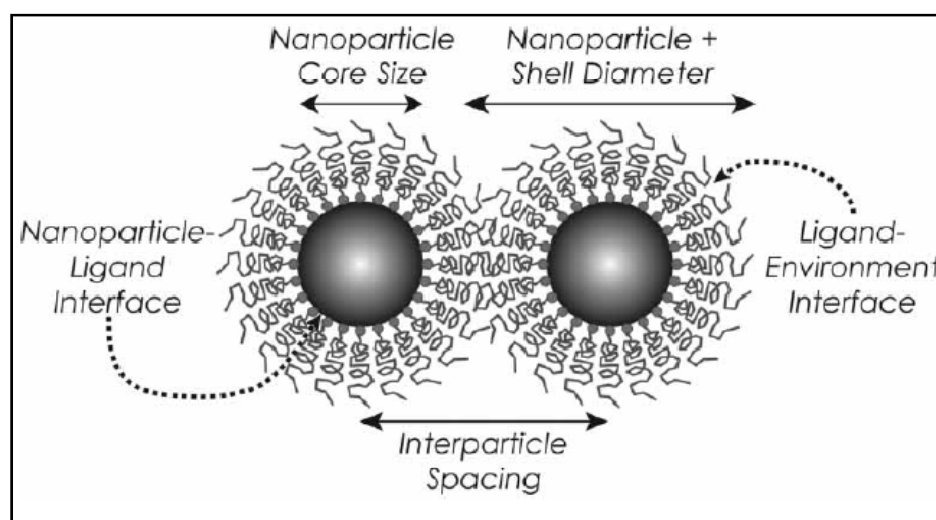


**Figure 1.7** Ligand stabilized gold nanoparticles (Grubbs 2007)

The use of stronger ligands can improve handling of gold nanoparticles. The citrate stabilized nanoparticles can be exchanged and are not very stable during handling. Phosphanes and thiols turned out to be excellent stabilizers because of strong Au-P bond and even better Au-S bond. These molecules allow the isolation of gold nanoparticles as solid materials that can be redispersed in appropriate solvents.

Phosphines have been used to stabilize gold nanoparticles. For instance,  $\text{P}(\text{C}_6\text{H}_4\text{SO}_3\text{Na})_3$  stabilises 15-20 nm gold nanoparticles which can be isolated and redispersed easily. There are very few reports on phosphines for stabilization of gold nanoparticles. Thiolates are most extensively investigated because of the strong binding characteristics of thiol to gold compared to that between phosphines, amines

and the citrate. Thiols in various forms have been used for stabilization and these are discussed in following section.

Frenkel et al (2005) reported synthesis of AuNPs using dodecanethiol as stabilizer. Dodecanethiol was added under vigorous stirring to a solution of hydrogen tetrachloroaurate III trihydrate ( $\text{HAuCl}_4 \cdot 3\text{H}_2\text{O}$ ) in 30 mL of freshly distilled, anhydrous tetrahydrofuran (THF). The mixture was stirred for about 20 min at room temperature. 20 mL 1.0 M solution of lithium triethyl borohydride in THF was added slowly. The mixture turned dark purple immediately indicating formation of nanoparticles. The particle size could be tuned using various thiols to gold ratio from 1: 6 to 6 : 1. TEM of these AuNPs showed size in the range 2.5 nm to 4.3 nm.

Dendron thiols were preferred for stabilize gold nanoparticles in view of steric stabilization and stability provided to the nanoparticles. Kim et al (2001) reported, first, second and third generation dendron-thiols ( $\text{D}_1$ ,  $\text{D}_2$ , and  $\text{D}_3$ , Figure 1.8) prepared by the reaction of the corresponding Fréchet-type dendron-bromides with thioacetic acid, followed by reduction with Lithium aluminium hydride ( $\text{LiAlH}_4$ ). The resultant dendrons were used to stabilize gold nanoparticles by the two-phase method. The  $\text{HAuCl}_4$  in water and tetraoctylammonium bromide in toluene was stirred, the toluene layer separated and treated with dendron-thiol and finally allowed to stir vigorously with an aqueous solution of  $\text{NaBH}_4$ . The TEMs of these dendron stabilized nanoparticles showed particle sizes in the range 2.4–3.1 nm with narrow size distribution and remarkably high stability. In particular, the nanoparticles synthesized with the second generation dendron ( $\text{D}_2$ ) had an almost monodisperse core ( $2.4 \pm 0.2$  nm). Also AuNPs prepared using these dendrons were smaller in size compared to the nanoparticles prepared by alkane and arene thiols.

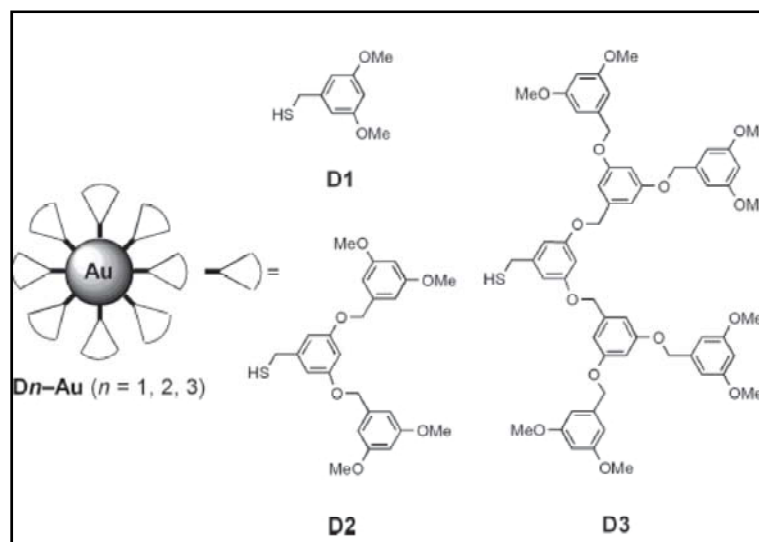


**Figure 1.8** Schematic of dendron-stabilized AuNPs (Kim et al 2001)

Other sulfur-containing ligands, such as xanthates (Porter et al 1999) and disulfides, (Manna et al 2003, Torigoe and Esumai 1999) di- and trithiols, (Resch et al 1999, Felidj et al 2003) and resorcinarene tetrathiols, (Balasubramanian et al 2002) thioacetates (Zhang et al 2009), dithiocarbamates (Vickers et al 2006) benzenesulfonate (SDBS) (Wang et al 2009), and thioctic acid (Volkert et al 2011) have been used to stabilize AuNPs. An approach that uses tailor-made multidentate thiols was introduced for stabilization of nanoparticles. The basic idea is that a large multidentate ligand might favour well-defined particle sizes by enwrapping the whole particle. Zhang et al (2008) reported that amongst a series of Hexadecanethiol (*n*-C16), 2,2-dimethylhexadecane-1-thiol (DMC16), and the multidentate thiol based ligands 2-tetradecylpropane-1,3-dithiol (C16C2), 2-methyl-2-tetradecylpropane-1,3-dithiol (C16C3), and 1,1,1-tris(mercaptomethyl)pentadecane (t-C16) (Figure 1.9) were evaluated to stabilize large gold nanoparticles in organic solution (20-50 nm). The bidentate ligands (C16C2 and C16C3) and particularly the tridentate ligand (t-C16) showed enhanced abilities to inhibit the aggregation of large gold nanoparticles in organic solution.

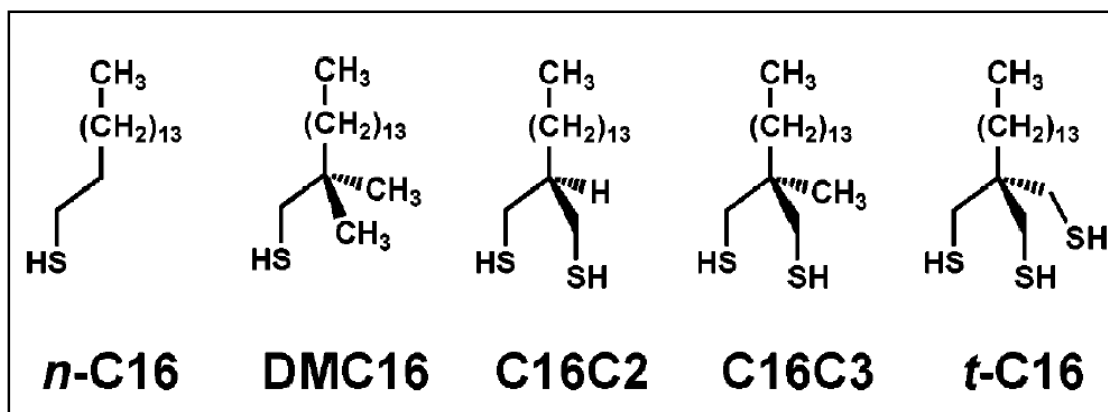


**Figure 1.9** Structures of alkane thiols (Zhang et al 2008)

Sakata et al (2007) also designed and synthesized mono thiol and tripodal thiol derivatives for stable immobilization of oligonucleotide probes on a gold surface. (Figure 1.10) When this substrate was exposed to temperatures, the tripodal interface molecules were attached to the gold surface more stable than the mono thiol derivative molecules.

The synthesis of ligands containing disulfide is a better choice since during the formation of the nanoparticles, the disulfide would be reduced to form thiols. This is easier than working with thiol based substrates which readily oxidize during the work up of the reaction products. Roux et al (2005) demonstrated that thioctic acid (Figure 1.11) can be reduced *in situ* to produce dihydrolipoic acid (DHLLA) which binds on AuNPs surface. The ionizable carboxylic acid groups ensure the water solubility of DHLLA-capped gold nanoparticles and enhance the stability of the resulting colloid by electrostatic repulsions.

Love et al (2004) explored lysine based dendrimers containing disulfide ligand (Figures 1.13) for the stabilization of gold nanoparticles in the range 1.8 to 2.9 nm, since the synthesis of nano particles on dendrimer-branches containing thiol resulted in oxidation. It was also reported that dendrimers thiol and disulfides on 2 D surfaces yielded films which had virtually identical properties.



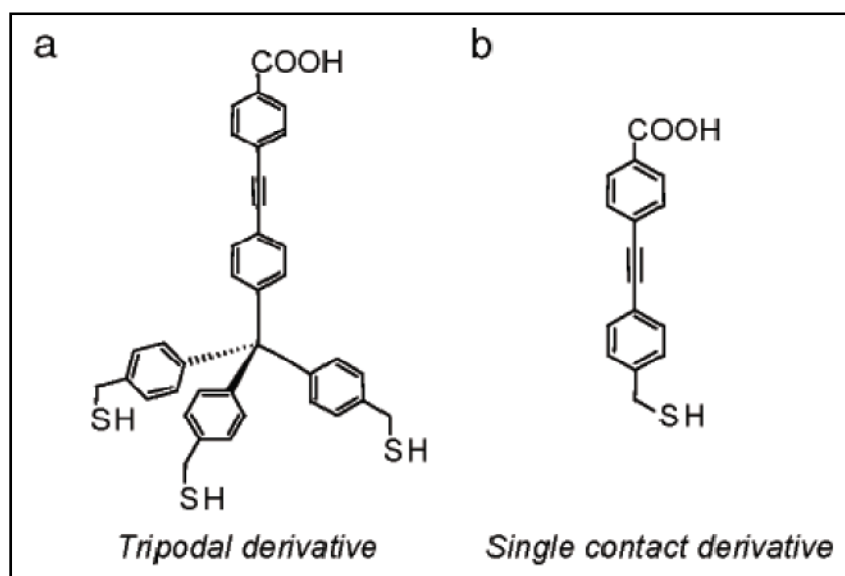


**Figure 1.10** Structure of Monothiol and trithiol ligand (Sakata et al 2007)

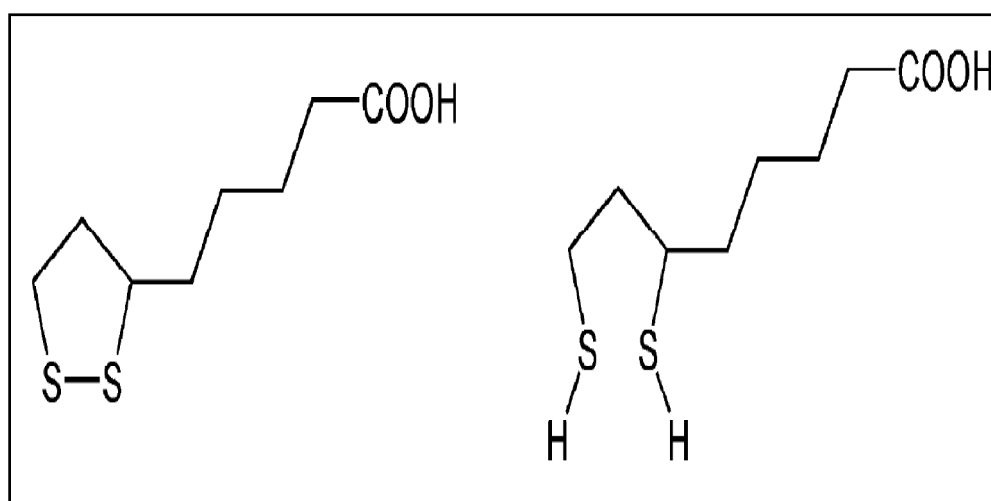


**Figure 1.11** Structure of thioctic acid and dihydrolipoic acid (Roux et al 2005)

Yonezawa et al (2001) synthesized 4 chain disulfide ligand viz. (4,4-dithiobis-(*N*-propyl-*O,O*-ditetradecanoyl-*L*-glutamate), as a stabilizer for AuNPs. During the preparation of the AuNPs the compound (4,4-dithiobis-(*N*-propyl-*O,O*-ditetradecanoyl-*L*-glutamate), was reduced to two double chain thiol derivatives (Figure 1.12) which stabilized the AuNPs of 2 nm, this particle size are smaller in size than AuNPs prepared by hexadecane and octadecane thiol stabilized AuNPs (2.5 nm and 2.7 nm).

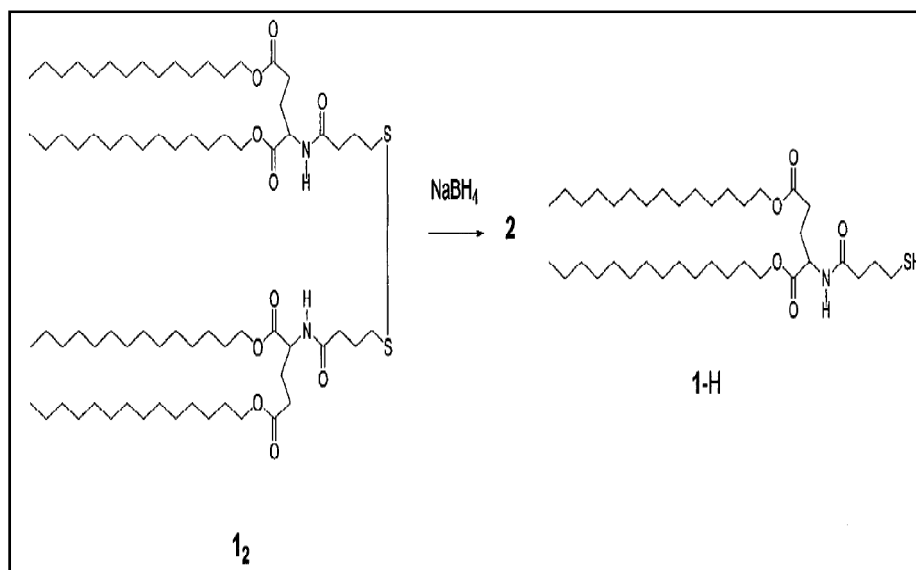


**Figure 1.12** Schematic for reduction of  $1_2$  by  $\text{NaBH}_4$  (Yonezawa et al 2001)

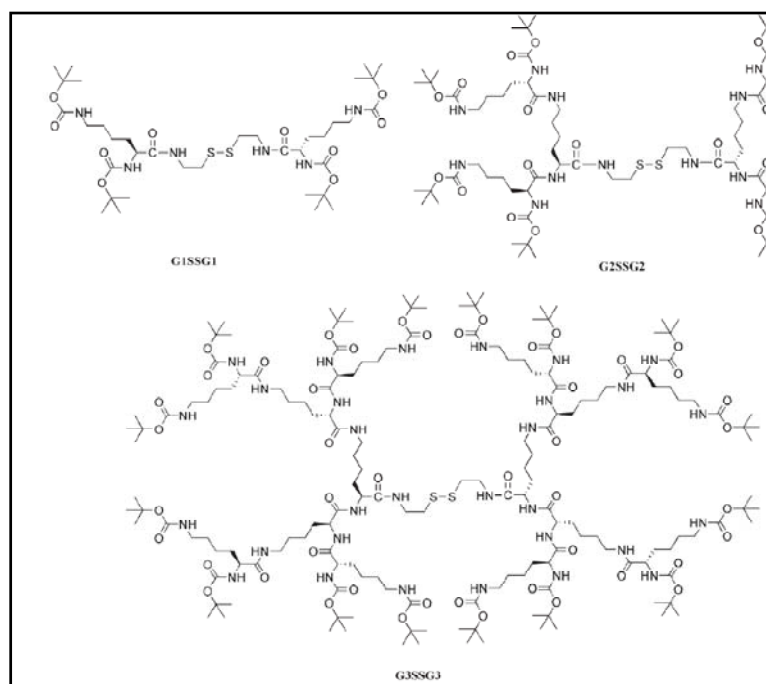


**Figure 1.13** Structures of dendrimers (Love et al 2004)

### 1.10 Role of polymer in stabilization of gold nanoparticles

Organic ligands have been used for the stabilization of gold at nanometer scale, while small molecules typically require very strong affinities for nanoparticle surface sites to ensure nanoparticle stability. Polymers have also played an important role in

stabilization of AuNPs. As reviewed by Shan and Tenhu (2007), use of polymers for AuNPs has several advantages: enhancement of long-term AuNPs stability, solubility adjustment of AuNPs, higher surface density of shell, tunable properties of AuNPs, processibility and compatibility.

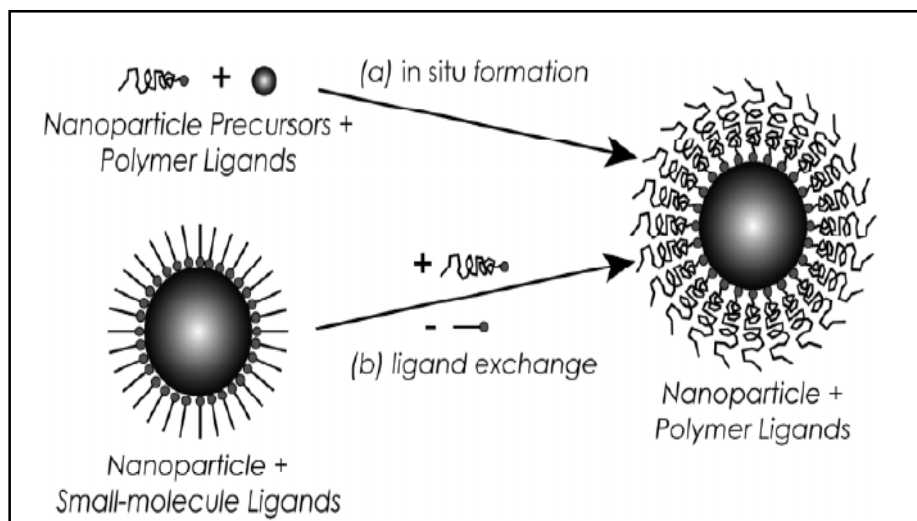


**Figure 1.14** Polymer stabilized AuNPs (Grubbs 2007)

The two major synthetic routes to polymer-stabilized AuNPs are the “grafting to” and “grafting from” techniques (Jordan et al 2006 Gries et al 2012, Li 2007). The latter method involves polymerization at the Au nanoparticle surface in the presence of various initiators. The “grafting to” method involves direct AuNP synthesis by attachment of polymers on the Au nanoparticles surface. There are two strategies for the “grafting to” method. The first one uses functionalized polymers with sulphur, nitrogen or other ligands at the end or in the middle of polymers to stabilize the AuNPs. This synthetic route is relevant to the Brust Schiffrin method or the ligand substitution reaction. For the Brust-Schiffrin route that is often used with polymers, the  $\text{HAuCl}_4$  solution is mixed with the functionalized polymers, and the reducing agent is added to form the AuNPs. Polymer ligands can be grouped into two general classes, those bearing a single stabilizing functional group, typically at either linear polymer chain terminals and those bearing a multiplicity of stabilizing functionality

(along the backbone or at the multiple chain ends of branched polymers). The polymeric ligands containing terminal thiols used for the stabilization of AuNPs are thiolate end-capped polystyrene (PS) (Figure 1.15), thiolate poly (ethylene glycol) (PEG), five-arm PEG-b-PCL star block copolymers, thiolate poly(*N*-isopropylacrylamide) (PNIPAM), thiolate poly (vinyl pyridine) (PVP), polypeptide with disulfide termini, poly(acryloylaminophenylarsonic acid) (PAAPHA) with amine and arsenic acid group, poly(ethylenimine) (PEI) with amine groups, thioether-functionalized polymer ligands (DDT–PVAc and PTMP–PVAc).

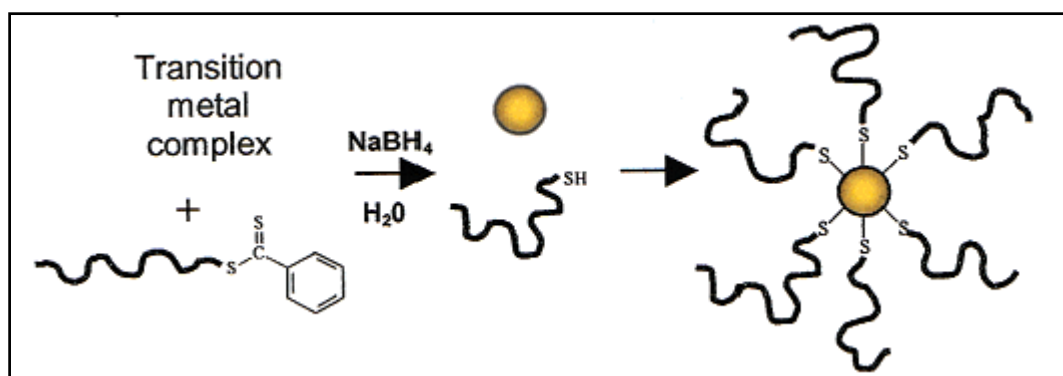


**Figure 1.15** Schematic for preparation polymer-stabilized transition metal nanoparticles (Lowe et al 2002)

The other linear polymer containing terminal thiol is discussed below in details. Aryal et al (2006) synthesized polymer terminated by 2-(2,4-dinitrophenylsulfanyl) ethanol by ring opening bulk polymerization of Caprolactone initiated by the reaction product of aluminium isopropoxide and 2-(2,4-dinitrophenylsulfenyl) ethanol. The corresponding thiolated poly(Caprolactone) (PCL) was obtained after removal of protecting group under slightly basic condition. Structure of the thiolated PCL (PCL-SH) was characterized by  $^1\text{H}$  NMR. Thiolated polymer was successfully used to stabilize AuNPs in the range 30-40 nm.

Gold nanoparticles stabilized by thiol-terminated poly(ethylene glycol) monomethyl ethers with molecular weights ranging from 350 to 2000 were prepared at thiol-to-

gold molar ratios ranging from 3:1 to 1:8 Shimmin et al (2004). Particle size distributions have been measured for these particles from TEM images. The mean diameters of these gold nanoparticles are in the range of 1.5 to 3.2 nm.

Natural polymers have also been used for the stabilization of AuNPs. Polymers containing carboxyl, carbonyl, hydroxyl and phenol groups, the natural source extracts reduce Au-III and stabilize the AuNPs with these groups.

Linear polymer ligands with backbone functionality have largely been polymers that can be prepared by the direct polymerization of vinyl monomers (e.g., poly(vinylpyridine) (PVP), poly(N-vinylpyrrolidone) (PVPy). The multivalency of polymer ligands enables the use of ligating species (e.g., pyridines or alkylpyrrolidones with gold nanoparticles) that are not as strongly bound. Therefore polymers which contain terminal multiple thiols were used for stabilization of AuNPs. Wang et al (2007) synthesized highly monodisperse gold nanoparticles with diameters below 5 nm using thioether and thiol-functionalized mono di and trithiol polymeric ligands (Figure 1.16). The particle size and size distribution was controlled by variation of the polymer structure.

Although thiols have been more extensively investigated than disulfides for binding AuNPs, working with disulfide is desirable since during the formation of the AuNPs the disulfide is reduced to thiol. In comparison, thiols are readily oxidized during the work-up of the reaction products and need handling under inert conditions.

In order to realize the potential of the functional polymer approach for nanoparticle synthesis, a better insight into the relationship between polymer characteristics and particle formation is required. Such fundamental information will enable rational design of polymers to meet specific needs, particularly for achieving size-controlled synthesis of nanoparticle, stability of AuNPs against, higher temperature and etching.

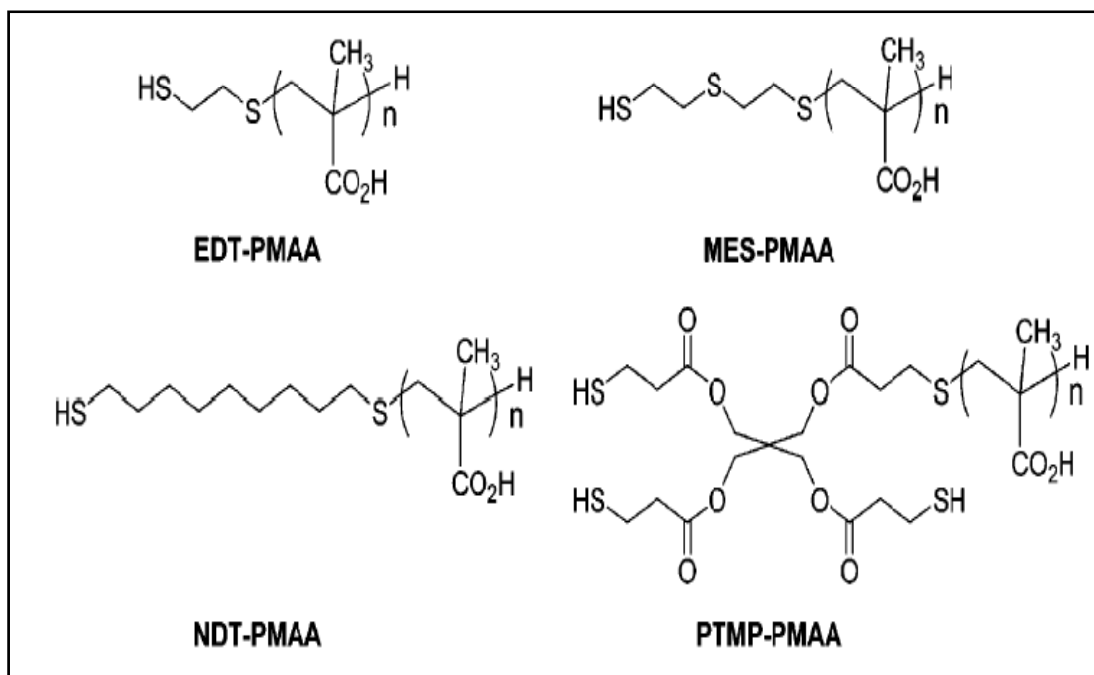


**Figure 1.16** Multidentate ligands for stabilization of AuNPs (Wang et al 2007)

### 1.11 Stability of AuNPs

Monomer bearing disulfide ligand and terminal unsaturation (Koenig and Chechik 2006), dendrimers bearing disulfide core and peripheral unsaturation, (Love et al 2007) and diblock copolymer bearing thiol ligand for binding to AuNPs and functional groups which could be photo crosslinked, (Boyer et al 2010), have been used for enhancing the stability of AuNPs. Thermally stable AuNPs have been explored for applications in photonic bandgap materials, nanostructure solar cells, light-emitting diodes, and memory devices.

Love et al (2007) synthesized dendritic polymers containing disulfide core lysine (Figure 1.17) and aromatic branched alkene groups at the periphery (Figure 1.18), to stabilise 1.9 to 3.4 nm AuNPs. The particle size decreased with increasing generation of the dendrimers. Interparticle crosslinking of the alkene groups by Grubbs catalyst resulted in insoluble product. However, intraparticle crosslinking in dilute solution resulted in soluble product. The size and morphology of the gold nanoparticles was not affected by crosslinking as evidenced by UV-Visible spectra and TEM analysis of

nanoparticles before and after crosslinking. Disulfides were preferred since thiol functionalised ligand would be susceptible to oxidation during synthesis. Intraparticle crosslinking led to soluble dendrimers which showed completion of the crosslinking as evidenced by the disappearance of the NMR peaks corresponding to alkene group at 4.8 and 5.8 ppm. Thermal stability of the dendrimers was evaluated in DMF at 130 °C. After 25 min SPR peak shifted and the duration increased by 25 to 35 minute on crosslinking. In all cases the crosslinked particles showed shift in peak after 75 minute. This was also accompanied by an increase in size of the AuNPs and aggregation of gold cores. The results indicated that crosslinking of the alkene groups on the surface did not inhibit growth of AuNPs.

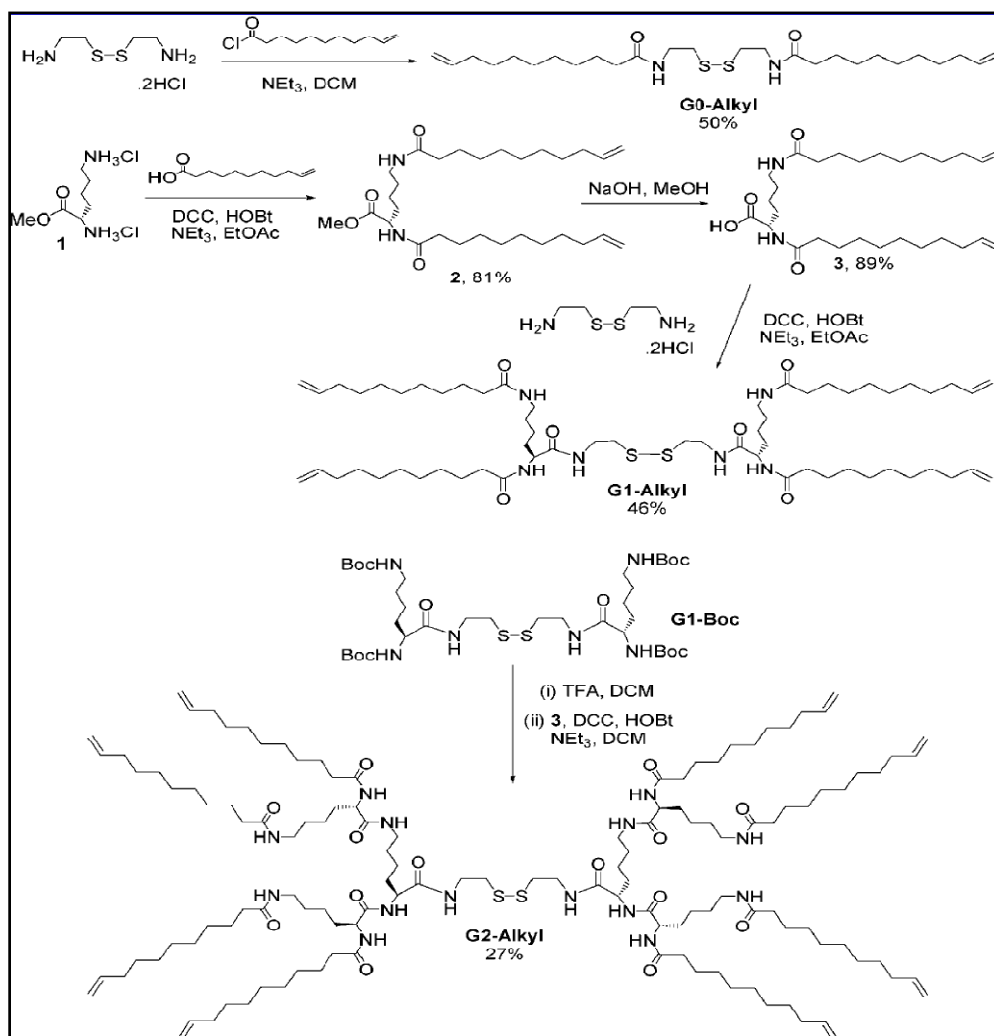


**Figure 1.17** G2 alkyl dendrimer (Love et al 2007)

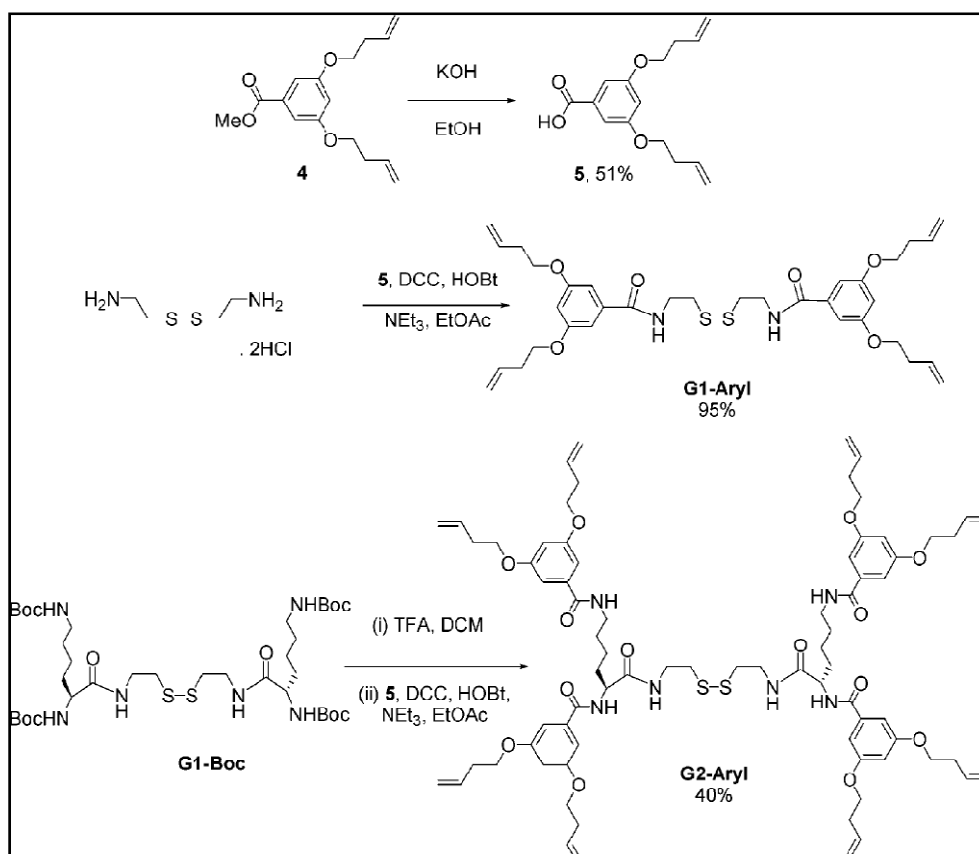


**Figure 1.18** G2 aromatic dendrimer (Love et al 2007)

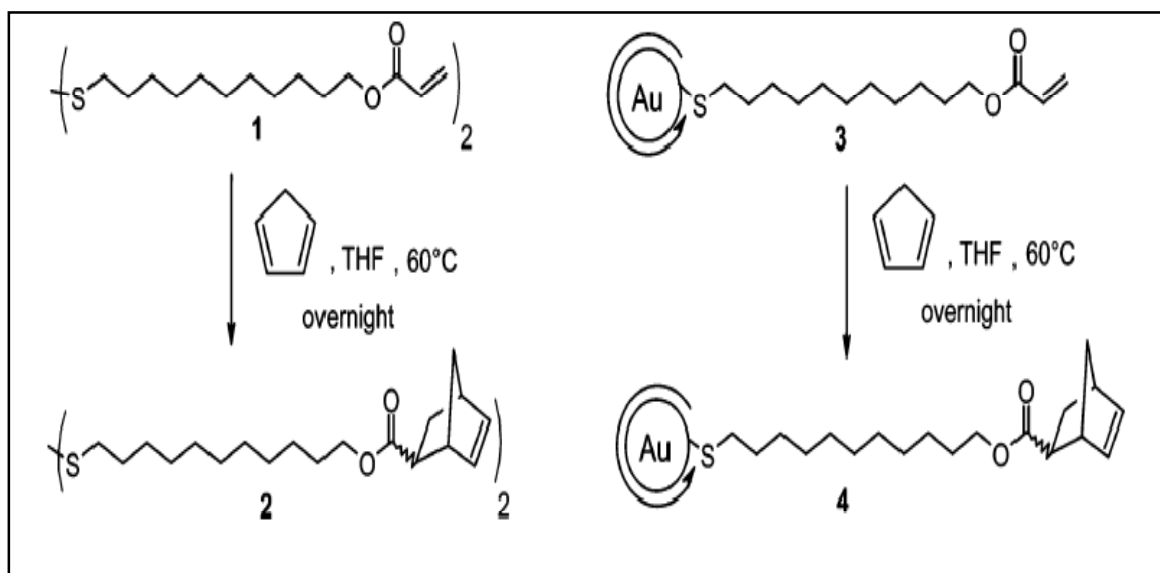


**Figure 1.19** Norbornene functionalized AuNPs (Koenig and Chechik 2006).

Koenig and Chechik (2006) prepared 3 nm AuNPs using acrylate as well as norbornene based disulfide derivative (Figure 1.19 and 1.20). Aggregation of the nanoparticles based on norbornene ligand could be avoided by effecting intra particle



crosslinking and reducing the catalyst concentration. The solubility of the nanoparticles after cross linking was lowered because of the rigid norbornene ligand structure. These nanoparticles were stable up to 75 °C whereas cross linking of the norbornene copolymers increased the stability up to 110 °C.

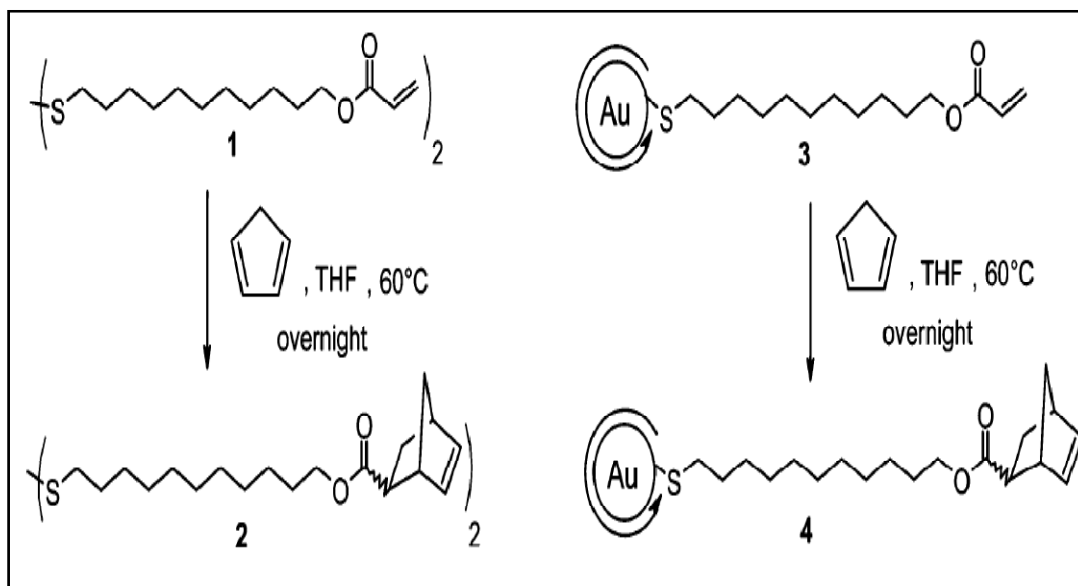


**Figure 1.20** Polyamine crosslinked AuNPs (Koenig and Chechik 2006)

### 1.12 Nanocapsules synthesis

There is growing interest in the synthesis of hollow nanocapsules in view of their applications in drug delivery, targeting and bioimaging. Such nanocapsules would also find application as nanoreactors and in extractions. Various approaches have been used for their synthesis of nanocapsules.

Ali et al (2011) synthesized 165 nm nanocapsules by starved feed emulsion polymerization (Figure 1.21). In aqueous solution of RAFT copolymer of t-butyl acrylate and acrylic acid, (Dimethyldioctadecylammonium bromide) DODAB cationic vesicle was added dropwise along with initiator V-501. The solution was heated to 70 °C using an oil bath followed by the addition of deoxygenated monomer mixture of (MMA/t-BA/EGDMA). The reaction mixture was kept stirring at 70 °C for another two hours. The obtained crosslinked latex was re-dispersed in dioxane and

trifluoroacetic acid and was allowed to stir for 24 hours under nitrogen to form nanocapsules.

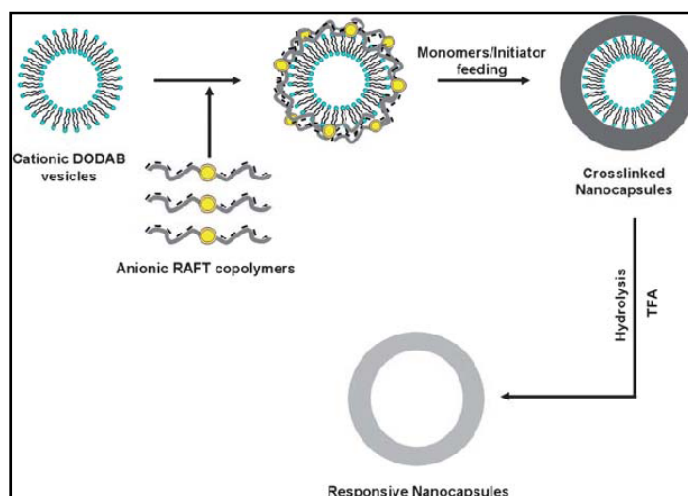


**Figure 1.21:** Schematic representation of the synthesis of vesicle-templated nanocapsules (Ali et al 2011)

Liu et al (2010) developed a strategy for the crosslinked polymeric nanocapsules of size 120 nm with controllable structure via the ‘self-templating’ approach (Figure 1.22). PVAc lattices were synthesized by the emulsion polymerization of vinyl acetate (VAc) followed by surface hydrolysis of the PVAc lattices, crosslinking of the PVAc segments on the surface of the surface-hydrolyzed PVAc lattices and eventually removal of the PVAc core of the core-shell structures by addition of methanol. Etching was completed within a week. Core-etching procedure needed a long time because of the high crosslinking degree of the crosslinked PVAc. The resultant size of capsules was confirmed by TEM.

The sacrificial template approach which involves encapsulation of nanoparticles in a polymer followed by the crosslinking of the latter and leaching out the core by treatment with etchant has been attempted by various researchers. This approach has yielded various levels of success as discussed in the preceding section. It has been noted that successful encapsulation of nanoparticles by polymers and crosslinking does not always yield nanocavities on etching. For instance crosslinking of dendritic

ligand based on disulfide cores and alkenes on the periphery by Grubbs catalyst reported by Love et al (2007) enhanced the thermal stability of AuNPs and also resistance to cyanide etching. Insoluble organic residues resulted on etching. However the presence or otherwise of nanocavities could not be established. Thus while Grubbs catalyst resulted in crosslinking of surface alkene groups which enhanced thermal and etchant stability of AuNPs, soluble nanoparticles containing cavities could not be obtained.

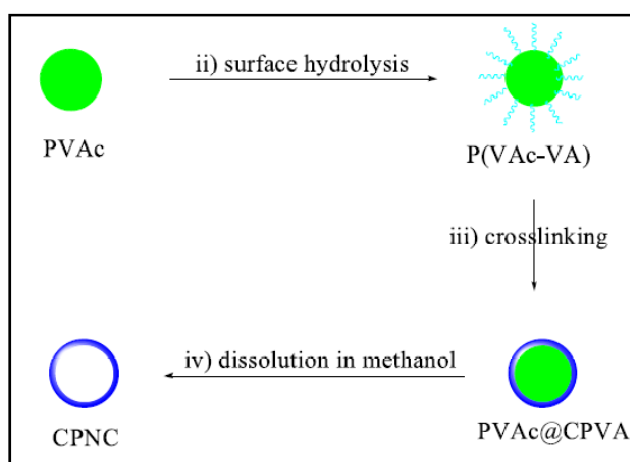


**Figure 1.22** Schematic of nanocapsules by self-temple. (Liu et al 2010)

Koenig and Chechik (2006) reported that monomer having disulfide cores and acrylate as well as norbornene double bonds at the periphery, could be used to synthesize AuNPs. Crosslinking of acrylate with polyamines and of norbornene by ring opening metathesis polymerization resulted in higher thermal stability and resistance to etching by methyl iodide. However etching with iodine resulted in insoluble products and the formation of nanocavities could not be demonstrated.

Yet some approaches using gold as sacrificial templates for nanocapsules synthesis have been successful. However, synthesis of nanocapsules required multiple steps. Boyer et al (2010) reported synthesis of hollow polymer nanocapsules of size 30 nm (Figure 1.23). Two different functional diblock polymers were used for the stabilization. The block polymers consisted either (poly (oligoethylene glycol)

acrylate, P(OEG-A), or poly(hydroxylpropylacrylamide), P(HPMA) and a cross-linkable segment comprised of an alternating copolymer of styrene and maleic anhydride. The gold cores were removed using aqua regia. The resultant hollow capsules were characterized by TEM.

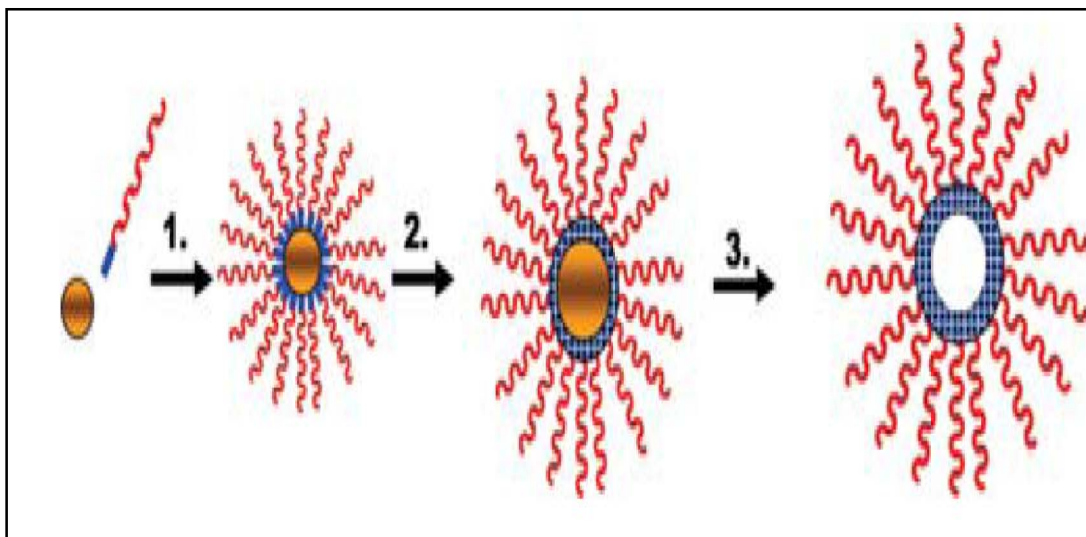


**Figure 1.23.** Synthesis of nanocapsules using AuNPs as sacrificial templates (Boyer et al 2010)

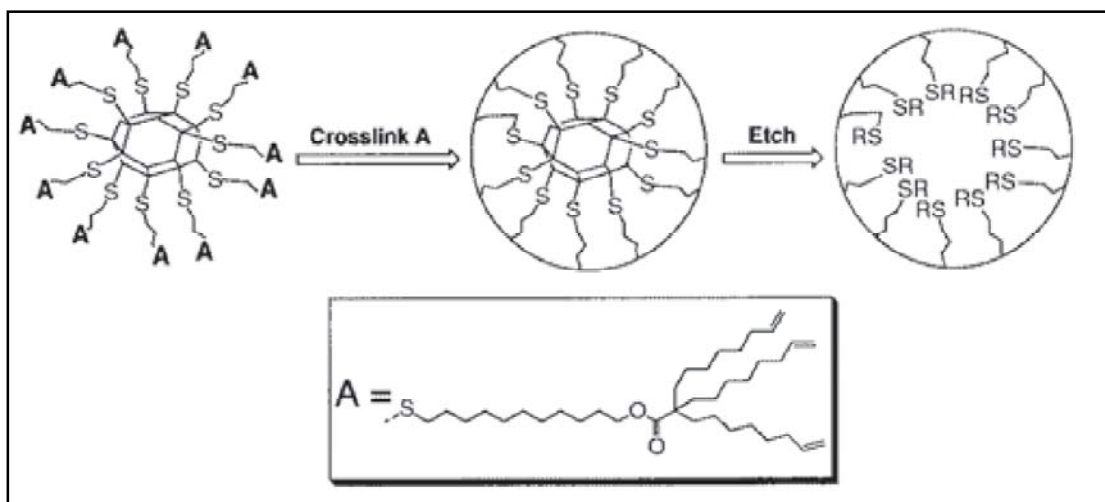


**Figure 1.24** Schematic of nanocapsules synthesis (Wu et al 2000)

Nanoparticle assembly; (2) Crosslinking (3) AuNPs core removal (Boyer et al 2010)

Sun et al (2006) reported synthesis of hollow polymer nanocapsules of size 10 nm (Figure 1.24). A tripodal alkylthiolate ligand was synthesized in seven steps and assembled on gold nanoparticles of 5 nm, which upon metathesis polymerization

(Intramolecular) and etching of the nanoparticles by sonicating a tetrahydrofuran – water solution containing KCN and  $K_3[Fe_2(CN)_3]$  followed by treatment with hydrogen peroxide resulted in  $10.47 \pm 2.54$  nm capsules. However, the role of sulfur in the ligand was not elucidated.

### **1.13 Synthesis of gold nanochains**

Synthesis of Au nanochains is important because of their potential applications in optoelectronics, as single electron transistors, as interconnects in electronic and sensing devices in biomedical applications, wave guides, as well as miniaturized photonic devices (Pissuwan et al 2006, Bae et al 2005, Dimitrakopoulos and Malenfant 2002, Rezaee et al 2010, Yang and Kim 2002, Gunawidjaja et al 2009, Biswas and Wang 2010). Many methods are available for the synthesis of Gold nanochains, although they require harsh conditions such as reducing agent or higher temperature and multistep synthesis. Also the stability has been primary concern. This has motivated researchers to design new strategies for the synthesis of robust nanochains.

Number of research groups reported physical interaction and chemical linkages approach for synthesis of Au nanochains. Wu et al (2008) reported a one pot method for the synthesis of linear assembly of AuNPs at  $125\text{ }^{\circ}\text{C}$  using a biocompatible, water-soluble, lower molecular weight Chitosan. Chitosan acts as reducing and stabilizing agent. The nanochains could be tuned by increase in concentration of Chitosan and formation of nanochains monitored by UV and TEM. Stability of nanochains was not reported.

Murugadoss and Chattopadhyay (2008) reported two stage approach for synthesis of nanochains in which citrate stabilized AuNPs were synthesized first and then addition of acetanilide at pH 3.5 nanochains were formed because of negatively charged

AuNPs and protonated acetanilide. The chain length was dependent on the concentration of acetanilide. Increase in acetanilide concentration chain length increases at higher concentration 13 mM and 19.4 mM branching of the assembly occurred instead of an increase in the length of the assembly.

Wang et al (2002) also reported two stage approach for the formation gold nanochains from alkane thiol and pyrrole functionalized alkane thiol AuNPs by the oxidative polymerization of pyrrole.

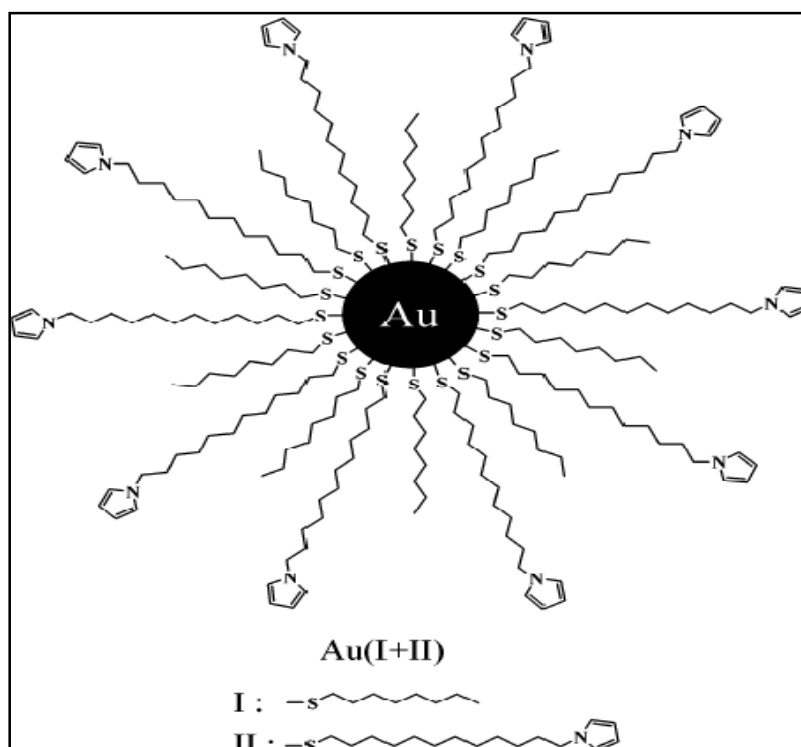


**Figure 1.25** Octanethiol and 12-(*N*-Pyrrolyl)dodecanethiol stabilized AuNPs (Wang et al 2002)

Lai et al (2011) synthesized gold nanochains in aqueous medium by the UV light triggered photolysis of light responsive *o*-nitro benzyl derivative thioctic acid 3-3 (3-hydroxymethyl -4-nitro phenoxy) – propyl ester functionalized AuNPs, which leads to condensation with (thioctic acid 4-amino methyl benzyl amide) functionalized AuNPs resulting in indazolone linkages (Figure 1.26).

More recently, Lee et al (2011) demonstrated synthesis of gold nanochains by the interaction of carboxylates on the citrate stabilized AuNPs with the imine in N-ethyl-N' (dimethyl amino propyl) carbodiimide (EDC) (Figure 1.27). Physicochemical properties of the nanochains were characterized by UV-Vis, TEM and FT-IR spectrophotometers

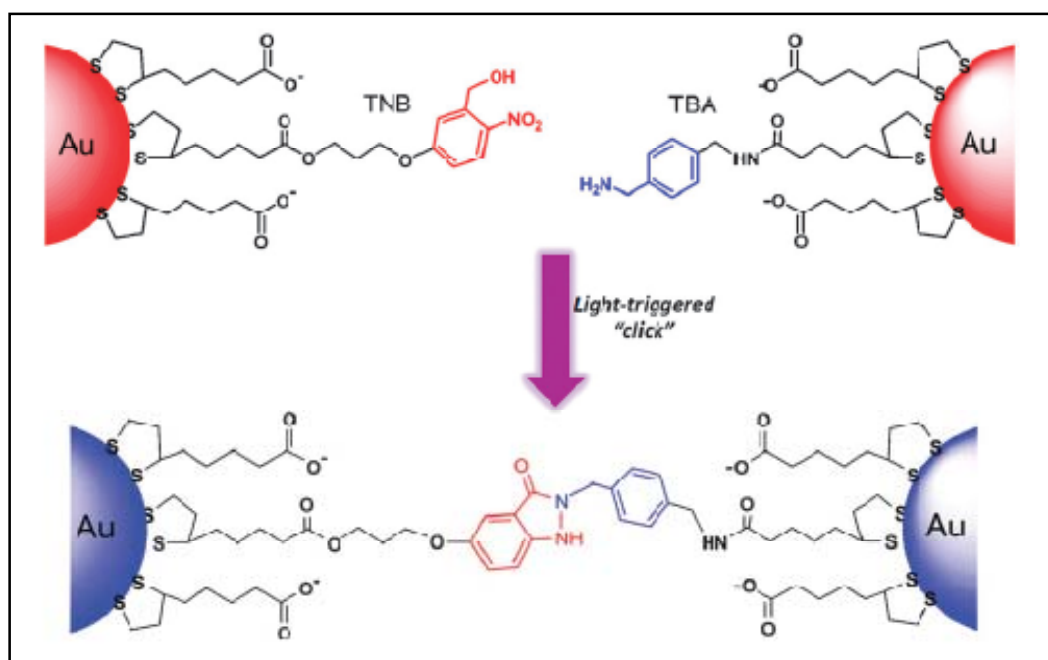


**Figure 1.26** Schematic of light triggered Covalent assembling of AuNPs.  
(Lai et al 2011)

Apart from the synthesis of gold nanochains, efforts have been made to enhance their stability by encapsulation in suitable matrix. Fernandes et al (2010) exploited the electric dipole dipole interaction resulting from ligand exchange between [(bis(p-sulfonato-phenyl)phenylphosphine (BSPP) or citrate] and AuNPs capped partially with [(46-mercapto-22,43-dioxo-3,6,9,12,15,18-hexaoxa-21,44-diazahexatetraconta-31,33-diyn-1-oiic Acid (DAPEG). These were destabilized by centrifugation to yield nanochains, which were then encapsulated in the polymer formed by UV induced photocrosslinking of DAPEG. Similarly the citrate capped AuNPs were exchanged with 2 mercapto ethanol and destabilized by incubation to yield nanochains which

were then encapsulated in a silica layer formed by the polycondensation of mercapto propyl triethoxysilane and tetra ethyl orthosilicate. However, during the process  $\lambda_{\max}$  blue shifted by 34 nm to 668 nm (Figure 1.28).

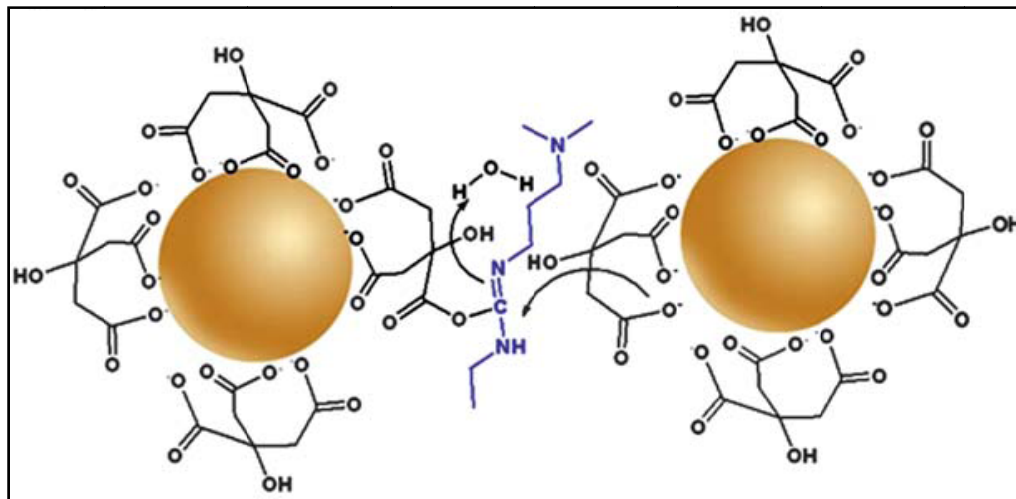


**Figure 1.27** Schematic for nanochains formation (Lee et al 2011)

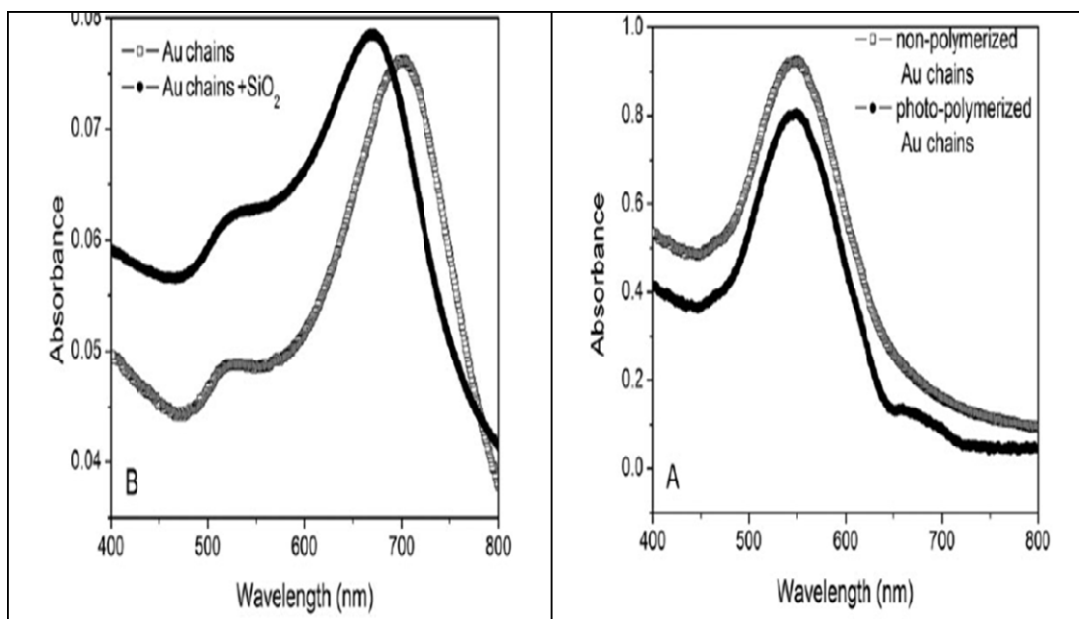


**Figure 1.28** UV-Visible spectra of (a) BSPP/DA-PEG stabilized AuNPs before and after photo-polymerization (b) citrate/MEA-stabilized AuNPs chains before and after silica coating (Fernandes et al 2010)



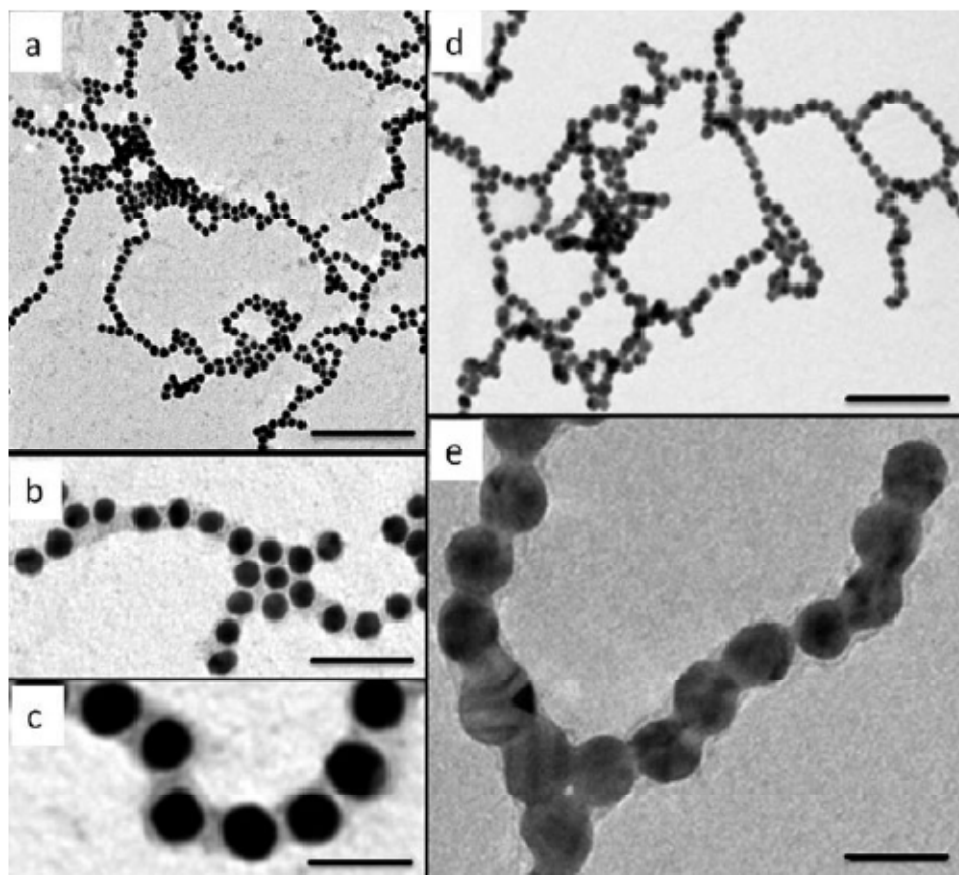


**Figure 1.29** TEM images of photo-polymerized DA-PEG (a-c) and silica coated AuNPs chains (d-e). (Fernandes et al 2010)

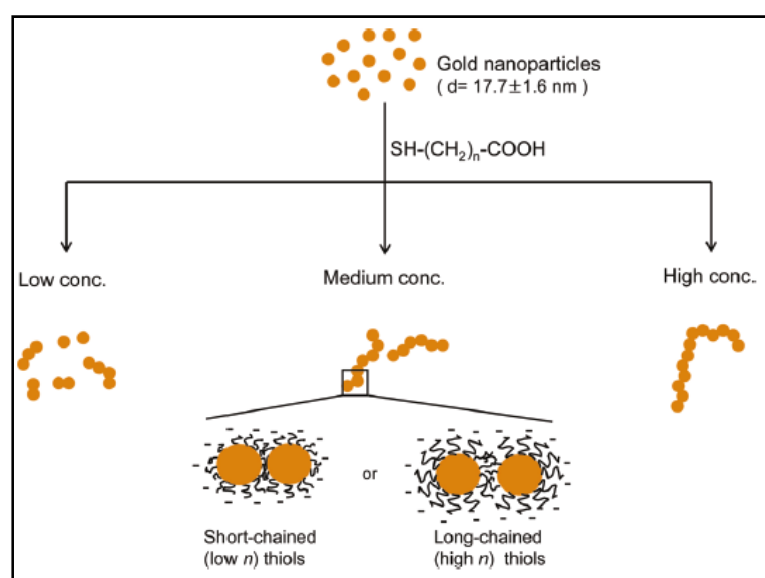


**Figure 1.30.** Schematic for preparation of chainlike assemblies of Au NPs. (Cho et al 2010)

Cho et al (2010) reported linear assemblies from AuNPs by adding alkane thiol carboxylic acids in the mixture of water/ethanol (Figure 1.30). The chain length was governed by the ligand concentration and the inter particle separation by the number of alkane groups in the ligand. The stability of chains was enhanced by encapsulating in silica or gelatin (Figure 1.31).

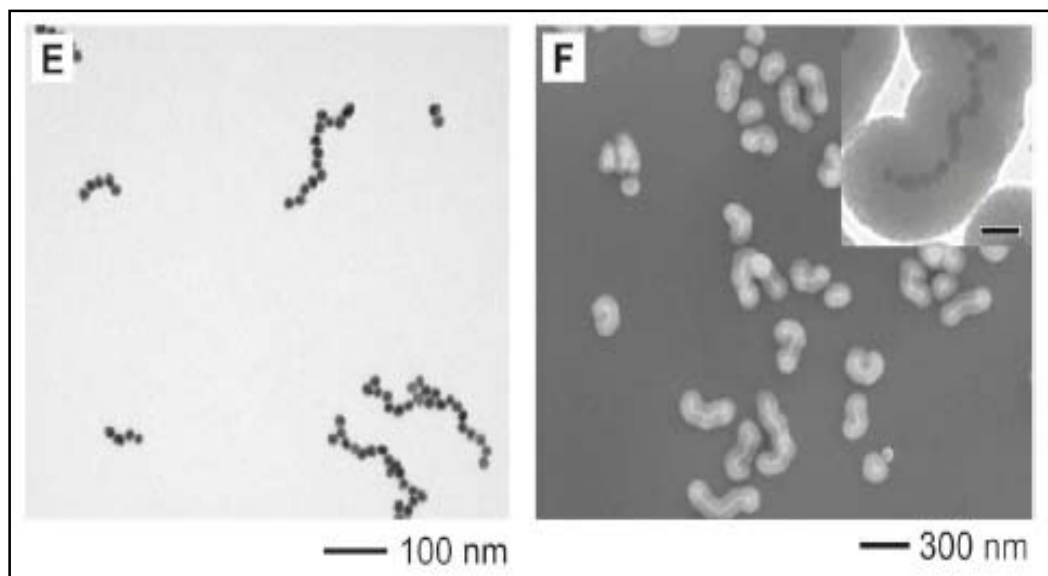


**Figure 1.31.** TEM before and after silica-coated nanochains (Cho et al 2010)

Zhang et al (2008) reported synthesis of isolated AgNPs and AuNPs by in situ reduction and stabilization of hyperbranched, poly (amidoamine) with terminal dimethylamine groups (HPAMAM-N(CH<sub>3</sub>)<sub>2</sub>) in water, and these nanoparticles exhibited highly antimicrobial activity. As the molar ratio increased from 10 to 30, the average particle diameters decreased from 7.1 to 1.0 nm for AgNPs and from 7.7 to 3.9 nm for AuNPs, respectively. Similarly linear poly amidoamine reduce auric and silver salt but resultant nanoparticles precipitated out due to chain entanglement.

Although poly(ethylene glycol) (PEG), poly-(amidoamine) (PAMAM) dendrimers, poly(propyleneimine) (PPI) dendrimers, PEG-[poly(2-(N,N-dimethylamino)ethyl methacrylate)] block copolymers, and poly(ethylene oxide)- poly(propylene oxide)-

poly(ethylene oxide) block copolymer (PEO-PPO-PEO) are known to form isolated nanoparticles at room temperature but not nanochains.

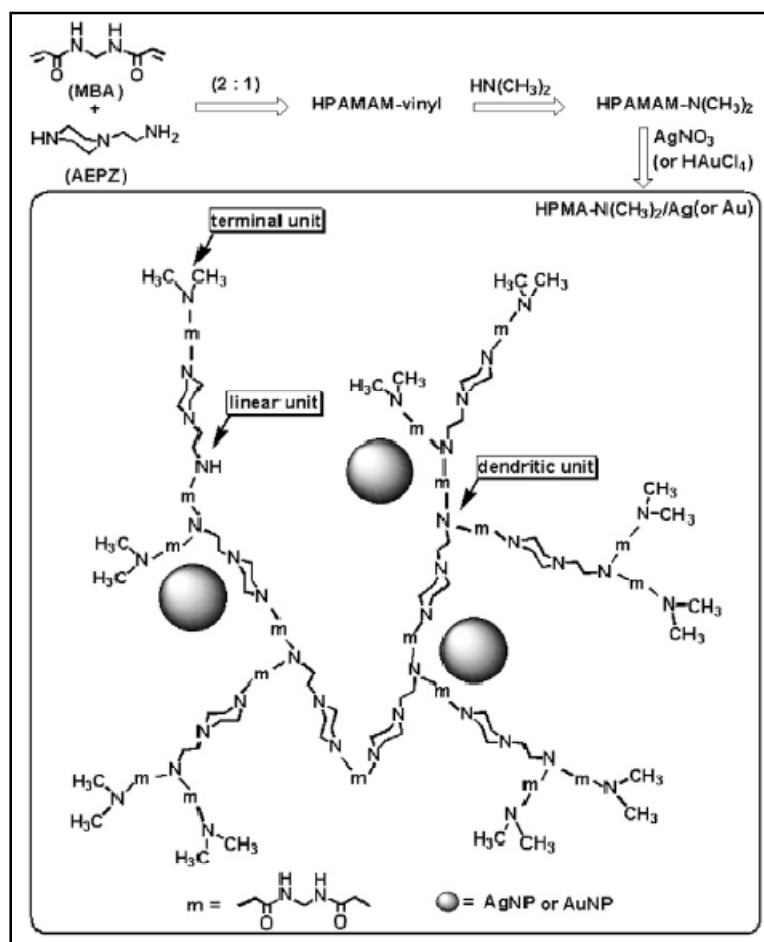


**Figure 1.32.** Schematic for the preparation of the HPAMAM- $\text{N}(\text{CH}_3)_2/\text{AuNPs}$  composite. (Zhang et al 2008)

In summary the review of the literature presents the current efforts on synthesis of 1) AuNPs and their stability against temperature and etching, which reveals that the success has been limited. Polymeric ligands containing multiple thiols should enhance the stability further. However synthesis of such a ligand has not been reported.

2) Synthesis of Au nanochains involves multiple steps and also needs encapsulation in polymeric matrices enhance the stability of nanochains. However, there is no report on synthesis of gold nanochains at room temperature and stability of as stabilized nanochains.

### 1.14 Our approach

In this work, we demonstrate a new approach for the synthesis and stabilization of AuNPs which involves the use of polydentate ligand as well as crosslinking. We show that the disulfide monomer DSDMA can be used for the stabilization of AuNPs, but subsequent polymerization of DSDMA was unsuccessful. In order to overcome this limitation, we stabilized AuNPs on poly(DSDMA) containing pendent vinyl unsaturation synthesized by selective polymerization technique. The use of this stabilizer resulted in AuNPs of smaller size compared to those obtained by DSDMA under identical conditions. The crosslinking of the vinyl groups resulted in enhanced thermal stability of AuNPs vis a vis DSDMA. Etching of AuNPs from poly(DSDMA) by methyl iodide resulted in nanocavities. These would find application in drug/ gene delivery and bioimaging.

Subsequently we demonstrate that the low molecular weight poly(amidoamine) acts as both reducing and stabilizing substrate during the synthesis of AuNPs at room temperature. With decreasing ratio of poly(amidoamine) to auric chloride, there is a transition from isolated nanoparticles to linear chain, which suggests that the linear morphology probably results from non uniform distribution of the stabilizer. However, a more systematic analysis reveals that the pH of the medium plays a more critical role than the stabilizer concentration. Under both conditions the binding between the nanoparticles and amine group in the main chain of the polymer is so strong that the nanochains are stable towards change in pH, temperature and salt concentration.

**References**

- 1 Ali S. I., Heuts J. P. A., Herk A. M., *Soft Matter*, 7, **2011**, 5382–5390.
- 2 Alkilany A.M., Nagaria P.K., Wyatt M.D., Murphy C.J., *Langmuir*, 26, **2010** 9328-9333.
- 3 Ayers J., Camusso L., Bortone S., *Ceramics of the World: From 4000 BC to the Present*, eds. New York, **1992**, 284.
- 4 Aryal S., Remant B.K., Dharmaraj N., Bhattarai N., Kim C. H., Kim H.Y., *Spectrochimica Acta Part A.*, 63, **2006**, 160–163.
- 5 Balasubramanian R., Kim B., Tripp S. L., Wang, X., Lieberman M., Wei, A., *Langmuir*, 18, **2002**, 3676-3681.
- 6 Bae A. H., Numata M., Hasegawa T., Li C., Kaneko K., Sakurai K., Shinkai S., *Angew. Chem., Int. Ed.*, 44, **2005**, 2030.
- 7 Biswas A., Wang T., Biris A. S., *Nanoscale*, 2, **2010**, 1516.
- 8 Bhat S., Maitra. C., *J. Chem. Sci.* 120, **2008**, 507–513.
- 9 Bakeeva I. V., Kolesnikova Yu. A., Kataeva N. A., Zaustinskaya K. S., Gubin S. P., and Zubova V. P., *Russian Chemical Bulletin, International Edition*, 57 **2008**, 337-344.
- 10 Brust M., Walker M., Bethell D., Schiffrin D.J., Whyman R.J., *J. Chem. Soc., Chem. Commun.* **1994**, 801-802.
- 11 Boyer C., Whittaker M. R., Nouvel C., Davis T. P., *Macromolecules*, 43, **2010** 1792–1799.
- 12 Chen S., Kimura K., *Langmuir*, 15, **1999**, 1075-1082.
- 13 Cho E. C., Choi S.W., Camargo H. C., Xia Y., *Langmuir*, 26, **2010**, 10005-10012.

- 14 Choofong S., Suwanmala P., Pasanphan W., *18th international conference on composite materials* Bangkok, Thailand **2010**.
- 15 Contreras-Caceres R., Sanchez-Iglesias A., Karg M., Pastoriza-Santos I., Perez-Juste J., Pacifico J., Hellweg T., Fernandez-Barbero A., Liz-Marzan L. M., *Adv. Mater*, 20, **2008**, 1666-1670.
- 16 Dimitrakopoulos C. D., Malenfant P. R. L., *Adv. Mater.*, 14, **2002**, 99.
- 17 Daniel M.C., D. Astruc, *Chem. Rev.*, 104, **2004**, 293-346.
- 18 Faraday M., *Phil. Trans.* 147, **1857**, 145.
- 19 Felidj, N., Aubard, J., Le'vi, G., Krenn, J. R., Hohenau, A., Schider, G., Leitner, A., Aussenegg, F. R., *Appl. Phys. Lett.* 82, **2003**, 3095-3097.
- 20 Frenkel A.I., Nemzer S., Pister I., Soussan L and Harris T., Sun Y. and Rafailovich M.H., *J. of chem.. phy.*, 123, **2005**, 184701.
- 21 Fernandes R., Mei L., Dujardin E., Mann S., Kanaras A. G., *Chem. Commun.*, 46, **2010**, 7602–7604.
- 22 Fenger R., Fertitta E., Kirmse H., Thunemann A. F., Rademann K., *Phys. Chem. Chem. Phys.*, 14, **2012**, 9343–9349.
- 23 Frens G., *Nature: Phys. Sci.* 241, **1973**, 20-22.
- 24 Freestone I., Meeks N., Sax M., Higgitt C., *Gold Bulletin* 40, **2007**, 270.
- 25 Gries K., M. El Helou., G. Witte., Agarwal S., A. Greiner, *Polymer*, 53, **2012**, 1632-1639.
- 26 Giljohann D. A., Seferos D.S., Daniel W. L., Massich M. D., Patel P. C., Mirkin C. A., *Angew. Chem. Int. Ed.* 49, **2010**, 3280 – 329.
- 27 Grubbs R. B., *Polymer Reviews*, 47, **2007**, 197–215.
- 28 Gunawidjaja R., Kharlampieva E., Choi I., Tsukruk V. V., *Small*, 5, **2009**, 2460.

- 29 Han G., You C.C., Kim B. J., Turingan R.S., Forbes N.S., Martin C.T., Rotello V.M., *Angew. Chem., Int. Ed.* 45, **2006**, 3165–3169.
- 30 Henglein A., *J. Phys. Chem.*, 97, **1993**, 5457.
- 31 Herring C., *Structure and Properties of Solid Surfaces*, University of Chicago, Chicago, IL, **1952**.
- 32 Hong R., Han G., Fernandez J.M., Kim B.J, Forbes N.S., Rotello V.M., *J. Am. Chem. Soc.*, 128, **2006**, 1078–1079.
- 33 Hussain S. T., Iqbal M., Mazhar M., *J Nano. Res.*, 11, **2009**, 1383–1391.
- 34 Jin Y., Wang P., Yin D., Liu J., Qin L., Yu N. Xie G., Li B., *Colloids and Surfaces A: Physicochem. Eng. Aspects*, 302, **2007**, 366–370.
- 35 Jordan R., *Adv. Polym. Sci.*, **2006**, 198.
- 36 Kim M., Jeon Y. M., Jeon W., Kim H-J., Hong S. G., Park C. G., Kim K., *Chem. Commun.*, **2001**, 667–668.
- 37 Kim D.J., Kang S.M., Kong B., Kim W.J., Paik H.J., Choi H., Choi I.S., *Macromol. Chem. Phys.*, 206, **2005**, 1941-1946.
- 38 Koenig S., Chechik V., *Langmuir*, 22, **2006**, 5168-5173.
- 39 Kruger C., Agarwal S., Greiner A., *J. Am. Chem. Soc.*, 130, **2008**, 2710-2711.
- 40 Kelly, K. L., Coronado, E., Zhao, L.L., Schatz, G. C., *J. Phys. Chem. B*, 107, **2003**, 668-672.
- 41 Li D., He Q., Cui Y., Wang K., Zhang X., Li J., *Chem. Eur., J.* 13, **2007**, 2224- 2229.
- 42 Li D., He, Q. Cui Y., Li J., *Chem. Mater.*, 19, **2007**, 412-417.
- 43 Lieber, M., *MRS Bull.*, 28, **2003**, 486.
- 44 Liu P., Liu G., Zhang W., Jiang F., *Nanotechnology* 21, **2010**, 15603.

- 45 Lowe A. B., Sumerlin B. S., Donovan M. S., McCormick C. L., *J. Am. Chem. Soc.*, 124, **2002**, 11562-11563.
- 46 Love C. S., Ashworth I., Brennan C., Chechik V., Smith D. K., *Langmuir*, 23, **2007**, 5787-5794.
- 47 Lai J., Xu Y., Mu X., Wu X., Li C., Zheng J., Wu C., Chen J., Zhao Y. *Chem. Commun.*, 47, **2011**, 3822–3824.
- 48 Lee J., Zhou H., Lee J., *J. Mater. Chem.*, 21, **2011**, 16935.
- 49 Male K.B., Li J., Bun C.C., Ng Siu-choon, and Luong J.H.T., *J. Phys. Chem. C*, 112, 2008,443-451.
- 50 Mafune F., Kohno J., Takeda Y., Kondow T., *J. Phys. Chem. B*, 105, 2001, 5114-5120.
- 51 Murugadoss A., Chattopadhyay A., *J. Phys. Chem. C.*, 112, **2008**, 11265–11271.
- 52 Manna, A., Chen, P.-L. Akiyama H., Wei, T.-X., Tamada K., Knoll W., *Chem. Mater.* **2003**, 15, 20-28.
- 53 Mullins W.W., *Metal Surfaces: Structure Energetics and Kinetics*, The American Society for Metals, Metals Park, OH, **1963**.
- 54 Ozin, G. A., Arsenault, A. C., *Nanochemistry, A Chemical Approach to Nanomaterials*, RSC Publishing, **2005**.
- 55 Porter, L. A., Ji D., Westcott S. L.; Graupe M., Czernuszewicz R. S., Halas N. J., Lee T. R., *Langmuir*, 14, **1998**, 7378-7386.
- 56 Polizzi M.A., Stasko N.A., Schoenfisch M.H., *Langmuir*, 23, **2007**, 4938–4943.
- 57 Poole, C.P., Owens, F. J., *Introduction to Nanotechnology*, Wiley - Interscience, Hoboken, NJ, **2003**.



- 58 Prathna T.C., Mathew L., Chandrasekaran N., Raichur A. M. and Mukherjee A. Biomimetic Synthesis of Nanoparticles: *Science, Technology & Applicability* **1999**.
- 59 Parab H. C., Jung M.A., Woo H.G., *J. Nanopart. Res.*, 13, **2011**, 2173-2180.
- 60 Polte J., Ahner, T. T., Delissen F., *J. Am. Chem. Soc.*, 132, **2010**, 1296–1301.
- 61 Rezaee A., Aliganga A. K., Pavelka L. C., Mittler S., *Phys. Chem. Chem. Phys.*, 12, **2010**, 4104.
- 62 Resch, R. Baur C., Bugacov A., Koel B. E., Echternach P. M., Madhukar A., Montoya N., Requicha A. A., *J. Phys. Chem. B* **1999**, 103, 3647-3650
- 63 Sakata T., Maruyama S., Ueda A., Otsuka H., Miyahara Y., *Langmuir*, 23, **2007**, 2269-2272.
- 64 Shimmin R.G., Schoch A.B., and Braun P.V., *Langmuir*, 20, **2004**, 5613-5620.
- 65 Sau T. K., Pal A., Jana N.R, Wang Z.L., Pal, T. *J. Nano. Res.*, 3, **2001**. 257–261.
- 66 Sayed I. H., Huang X. H., Sayed M. A., *Nano Lett.*, 5, **2005**, 829 Faraday M., *Phil. Trans.* 147, **1857**, 145.
- 67 Sastry M., Swami A., Kumar A., *Langmuir*, 19, **2003**, 1168-1172.
- 68 Tsunoyama H., Sakurai H., Ichikuni N., Negishi Y., Tsukuda T., *Langmuir*, 20, **2004**, 11293-11296.
- 69 Torchilin V. P., *Adv. Drug Delivery Rev.* 58, **2006**, 1532.
- 70 Torigoe, K.; Esumi, K. *J. Phys. Chem. B* 103, **1999**, 2862-2866.
- 71 Turkevich J., Stevenson P.C, Hillier J., *Discuss. Faraday. Soc.* 11, **1951**, 55-75.
- 72 Nguyn D. T., Kim D.J., Kim K.S., *Micron*, 42, **2011**, 207-227.
- 73 Verhoeven, J. D., Pendray A. H., Dauksch W. E., *Journal of the Minerals, Metals and Materials Society* 50, **1998**, 58.

- 74 Vickers M.S., Cookson J., Beer P.D., Bishop P.T., Thiebaut B., *J. Mater. Chem.* **2006**, 16, 209-215.
- 75 Volkert A.A., Subramaniam V., Ivanov M.R., Goodman A.M., Haes A.J, *ACS Nano*, 5, **2011**, 4570-4580.
- 76 Wang Z., Tan B., Hussain I., Schaeffer N., Wyatt M. F., Brust M., Cooper A. I., *Langmuir*, 23, **2007**, 885–895.
- 77 Wang T., Zhang D., Xu W., Li S., Zhu D., *Langmuir*, 18, **2002**, 8655-8659.
- 78 Wang S., Qian K., Bi X., Huang W., *J. Phys. Chem. C*, 113, **2009**, 6505-6510.
- 79 Whitesides G. M., *Small* **2005**, 1, 172.
- 80 Wu L, Shi C., Tian L., Zhu J., *J. Phys. Chem. C Letters*, 112, **2008**, 319-323.
- 81 Yang P. D., Kim F., *ChemPhysChem*, 3, **2002**, 503.
- 82 Yonezawa T., Yasui K., Kimizuka N., *Langmuir*, 17, **2001**, 271-273.
- 83 Zhao P., Li N., Astruc D., *Coordination Chemistry Reviews* doi:10.1016/j.ccr.2012.09.002.
- 84 Zhao H., Ning Y., *Gold Bull.*, 33, **2000**, 103.
- 85 Zhang H., Fung K-H, Hartmann J., Chan C. T., Wang D., *J. Phys. Chem. C*, 112, **2008**, 16830–16839.
- 86 Zhang H., Wang D., *Angew. Chem. Int. Ed.*, 47, **2008**, 3984 –3987.
- 87 Zhang S., Leem G., Lee T.R., *Langmuir*, 25, 2009, 13855-13860.
- 88 Zhang Y., Peng H., Huang W., Zhou Y. , Yana D., *Journal of Colloid and Interface Science*, 325, **2008**, 371–376.
- 89 Schmid G., Pfeil R., Boese R., Bandermann F., Meyer S., *G. Chem. Ber.* 114 **1981**, 3634-3642.

---

---

**Chapter 2**  
**Objective and scope**

---

---

## 2.1 Introduction

The literature review presented in the first chapter has highlighted that the stability of gold nanoparticles and nanochains are major concerns. Polydentate ligands appear to be a better choice to enhance the stability. The present research work has been undertaken with a view to demonstrate the utility of polydentate ligands in enhancing stability of gold nanoparticles and nanochains.

The objective of the present research work is to investigate if a polydentate ligand used for the synthesis of gold nanoparticles, would lead to enhanced stability against solvent, temperature, thiol exchange and be exploited as potential root to form nanocapsules. Another objective of the investigation was to explore poly amidoamines for the synthesis of gold nanochains and if so evaluate their stability against salt, temperature and against pH switching. The objectives of the proposed research investigation are highlighted below.

## 2.2 Objectives

1. To synthesize Bis (2-methacryloylhydroxyethyl) disulfide (DSDMA) and poly(DSDMA) containing disulfides and pendent unsaturation using cyclodextrin host guest chemistry.
2. To characterize DSDMA and poly(DSDMA) for chemical composition and molecular weight by FT-IR, <sup>1</sup>H NMR and GPC.
3. To evaluate the monomer and the polymer for the stabilization of gold nanoparticles using borohydride reduction method, and shell crosslinking.
4. To characterize gold nanoparticles for size, polydispersity and thermal stability by UV-Vis spectroscopy and TEM, and compare gold nanoparticles stabilized with DSDMA and poly(DSDMA).

5. Investigate the possibility of correlating thermal stability of gold nanoparticles on DSDMA and poly(DSDMA) on the basis of the graft density.
6. To characterize size dependent properties of gold nanoparticles by DPV and EPR.
7. To explore the possibility of preparing nanocavities/ nanocapsules by etching with methyl iodide and characterize the nanocapsules if formed by TEM and AFM.
8. To explore the possibility if low molecular weight linear poly amidoamines can stabilize gold nanochains and if so explore the mechanism of chain formation.
9. To evaluate the effect of concentration and pH on the morphology of gold nanoparticles.
10. To monitor AuNP formation by UV-Vis spectroscopy and morphology by TEM.
11. To evaluate the effect of temperature, salt and thiol concentration on the stability of gold nanochains.

---

---

**Chapter 3**  
**Shell crosslinked AuNPs for enhanced thermal stability**

---

---

### 3.1 Introduction

Metal nanoparticles in particular gold nanoparticles (AuNPs) are of particular interest because of their potential applications in optics, electronics, catalysis, and magnetic materials (Ghosh and Pal 2007, Liu et al 2008, Rastogi et al 2012, Yoo et al 2010). Active interaction of Au with various ligands, especially those bearing the sulphur, nitrogen and other heteroatoms is reported (Bakeeva et al 2008). Thiol stabilized AuNPs are of greater interest because of their relative stability and ease of functionalization which makes them ideal candidates for the preparation of functional materials. Number of efforts have been made for the synthesis of AuNPs and control particle size distribution and shape. Comparatively less attention has been paid to enhance stability of AuNPs. Koenig and Chechik (2006) prepared 3 nm AuNPs using acrylate as well as norbornene derivatives. Aggregation of nanoparticles based on norbornene ligand could be avoided by effecting intra particle crosslinking and reducing the catalyst concentration. The norbornene based nanoparticles were stable up to 75 °C whereas crosslinking of the copolymers with norbornene increased the stability up to 110 °C. Love et al (2007) synthesized dendritic monomers containing disulfide core lysine and aromatic branching and alkene at the periphery to stabilise 1.9-3.4 nm AuNPs, depending on composition. The particle size decreased with increasing generation of the dendrimers. Interparticle crosslinking of the alkene groups by Grubbs catalyst resulted in insoluble product. However intraparticle crosslinking in dilute solution resulted in soluble product. The size and morphology of the AuNPs was not affected by crosslinking as evidenced by UV-Visible spectra and TEM analysis of AuNPs before and after crosslinking. Intraparticle crosslinking led to soluble dendrimers which showed complete crosslinking as evidenced by the disappearance of the proton NMR peaks corresponding to alkene group at 4.8 and 5.8

ppm. Thermal stability of the dendrimers was evaluated in DMF at 130 °C. In all cases the crosslinked particles showed shift in peak after 75 minute. This was accompanied by an increase in size of the AuNPs and aggregation of Au cores. The results indicated that crosslinking of the alkene groups on the surface did not inhibit growth of AuNPs. Thus, crosslinking of long chain and dendritic alkenes on AuNP surfaces has had limited success. The impact of crosslinking is more significant in lower generation dendrimers or when crosslinking site is closer to AuNP surface.

In this chapter, we show that the disulfide monomer Bis (2-methacryloylhydroxyethyl) disulfide (DSDMA) can be used for the stabilization of AuNPs. While the AuNPs up to 4.4 nm could be synthesized, subsequent polymerization of the stabilized DSDMA using AIBN at 60 °C was unsuccessful. In order to overcome this limitation, we photo polymerized the monomer at room temperature using hydroxy cyclohexyl phenyl ketone using the irradiation intensity of 1 mW / cm<sup>2</sup> for 30 mins. IR analysis showed a decrease in the intensity of peak at 1640 cm<sup>-1</sup>. Thus while crosslinking did take place, it was not complete. UV and TEM analysis showed no change in the size of AuNPs following polymerization. The AuNPs were stable in DMF at 140°C upto 60 min. as monitored by UV-Vis spectroscopy and TEM analysis.

## 3.2. Experimental section

### 3.2.1. Materials

Bis (2-hydroxy ethyl) disulfide (Technical grade), Hydrogen tetrachloroaurate trihydrate (HAuCl<sub>4</sub>.3H<sub>2</sub>O) (99.9%), Deuterated chloroform (CDCl<sub>3</sub>) (99.9 atom % D), Azobisisobutyronitrile (AIBN) (98%), Dithiothreitol (DTT) (Minimum 99%) and Hydroxy cyclohexyl phenyl ketone (Irgacure 184) (99%), were purchased from Aldrich (USA), Sodium borohydride (NaBH<sub>4</sub>) (95%), N, N' Dimethylformamide



(DMF) (GR grade), Chloroform ( $\text{CHCl}_3$ ) (GR grade), Dichloromethane (DCM) (GR grade), were purchased from SD fine chemicals, India.

### **3.2.2. Measurements**

#### **3.2.2.1. UV-Vis spectrophotometry**

UV-Vis absorption spectra were recorded on Shimadzu UV-Visible spectrophotometer UV-1601PC model, in the wavelength range 200 to 1000 nm.

#### **3.2.2.2 Fourier transform infrared spectroscopy (FT-IR)**

The FT-IR studies were carried out using Perkin Elmer Spectrometer, UK in diffused reflectance mode. The samples were milled with KBr. The spectra were recorded over the frequency range  $3500 - 500 \text{ cm}^{-1}$  at resolution  $4 \text{ cm}^{-1}$ .

#### **3.2.2.3. Nuclear magnetic resonance spectroscopy (NMR)**

$^1\text{H}$  NMR measurements were carried out on DRX -200 spectrometer, operating at a proton frequency of 200 MHz.

#### **3.2.2.4 Transmission electron microscopy (TEM)**

FEI Technai, Transmission electron microscope was operated at accelerating voltage 200 kV and 80 kV. The samples were prepared by drop casting on carbon coated grid and dried at room temperature overnight.

### **3.2.3. Synthesis of DSDMA**

The procedure reported by Li and Armes (2005) was slightly modified. Bis (2-hydroxyethyl) disulfide (DSDMA) 5 g (1equivalent) and triethyl amine (35 ml, 8 equivalents) were dissolved in 100 ml DCM. The flask containing the solution was then immersed in ice bath, and methacryloyl chloride (13 ml, 4 equivalents) was added drop wise to DCM solution and stirred for 24 h. The reaction mixture was then filtered to remove triethylamine salt precipitated. The product was purified by column chromatography (yield 80%).

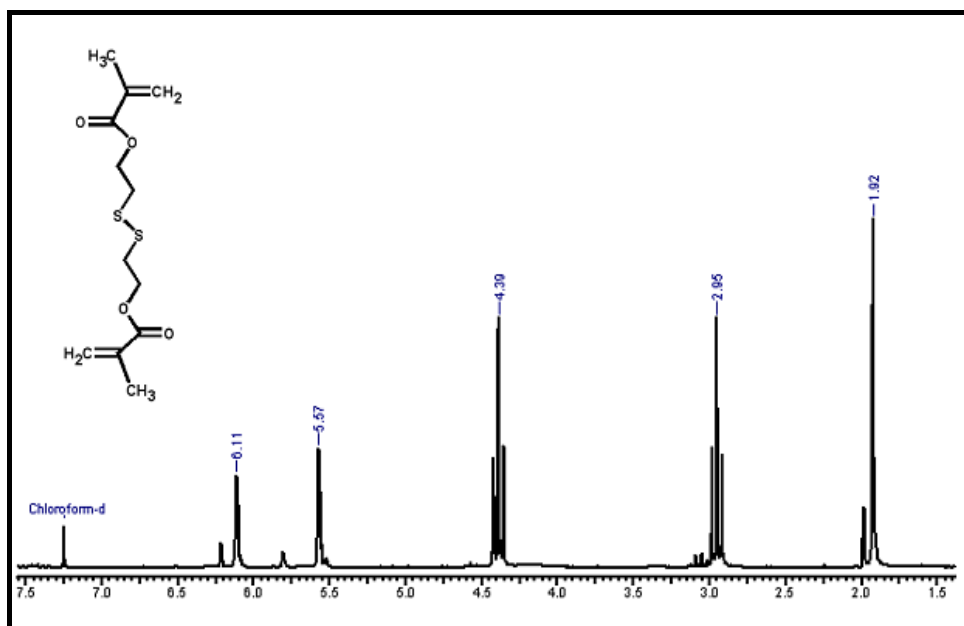


**Figure 3.1**  $^1\text{H}$  NMR spectrum of DSDMA

$^1\text{H}$  NMR (200 MHz,  $\text{CdCl}_3$ ): 5.57  $\delta$  and 6.11  $\delta$  (4H, singlet, terminal olefin proton)

4.30  $\delta$  (4H,  $-\text{OCH}_2-$ ), 2.96  $\delta$  (4H,  $-\text{SCH}_2-$ ) and 1.92  $\delta$  (6H, 2- $\text{CH}_3$  of DSDMA)

### 3.2.4. Synthesis of AuNPs

4 mg ( $2.03 \times 10^{-5}$  mole) of  $\text{HAuCl}_4 \cdot 3\text{H}_2\text{O}$  in 20 ml DMF and 5.8 mg ( $2.03 \times 10^{-5}$  mole) of DSDMA in 20 ml DMF were mixed in a 100 ml round bottom flask. Freshly prepared 8 mg ( $2.11 \times 10^{-4}$  mole) of  $\text{NaBH}_4$  in 4 ml DMF was added immediately with vigorous stirring. The solution which turned dark brown immediately, was stirred for 12 h. The disulfide: Au ratio was 1:1. For the synthesis of AuNPs using disulfide: Au ratio 10:1 and 25:1, 40 mg ( $20.3 \times 10^{-5}$  mole) and 100 mg ( $5.07 \times 10^{-4}$  mole) of DSDMA were dissolved in 20 ml DMF. For the synthesis of AuNPs using disulfide: Au ratio 1: 5 and 1: 10, 4 mg ( $2.03 \times 10^{-5}$  mole) of DSDMA, 20 mg ( $1 \times 10^{-4}$  mole) and 40 mg ( $2 \times 10^{-4}$  mole) of  $\text{HAuCl}_4 \cdot 3\text{H}_2\text{O}$  in 20 ml DMF were used. The AuNPs formed were purified by dialysis in DMF for 48 h using cellulose membrane, approximate molecular weight cut off 2000 for DSDMA stabilized AuNPs. All experiments were carried out at ambient temperature ( $27^\circ\text{C}$ ).

### 3.3. Results and discussion

Disulfide monomer was preferred over thiol since thiol functionalised ligand would be susceptible to oxidation during synthesis. Yonezawa et al (2001) synthesized four chain disulfide ligand viz. (4,4-dithiobis-(*N*-propyl-*O,O*-ditetradecanoyl-L-glutamate), as a stabilizer for AuNPs. During the preparation of the AuNPs the compound (4,4-dithiobis-(*N*-propyl-*O,O*-ditetradecanoyl-L-glutamate), was reduced to two double chain thiol derivatives which stabilized the AuNPs. Apart from choice of the ligand, its disposition on the backbone is critical in governing the properties of the nanoparticles formed. Love et al (2007) reported the synthesis of dendritic disulfide ligand containing alkene groups on the periphery for the stabilization of the AuNPs. Intraparticle crosslinking had no effect on the size or morphology of the nanoparticles formed but enhanced thermal stability at 130 °C and also during etching. The enhancement in stability was greater when the crosslinking was closer to nanoparticle surface. Thus, lower generation dendrimers were more effective. We chose DSDMA as a stabilizer which contains a disulfide core. The molecule is linear, the crosslinking site is closer to the functional group as compared to that in the case of the dendrimers reported by Love et al (2007). In view of these we expect the AuNPs stabilized on crosslinked DSDMA to exhibit enhanced thermal stability as compared to those exhibited by cross linked dendrimers reported by Love et al (2007).

#### 3.3.1 Synthesis and characterization of AuNPs.

##### 3.3.1.1 UV, IR and TEM analysis

UV-Visible absorption spectra for AuNPs prepared at 1 mM concentration of auric chloride and DSDMA, 1 to 25 mM and 10 mM borohydride are shown in Figure 3.3. Higher borohydride concentration was used since it was reported by Roux et al (2005) that at same S/ Au ratio, ten times higher amount of borohydride was required in the

case of thioctic acid as compared to that in the case of dihydrolipoic acid. At 1 mM concentration of DSDMA, the absorption peak at 516 nm, characteristic of AuNPs was observed (Figure 3.3a). The particle size was  $4.4 \pm 0.2$  nm as confirmed by TEM (Figure 3.4a). At 10 mM and 25 mM concentration of DSDMA the absorption peak decreased in intensity and peak broadening occurred (Figure 3.3b and c). These results are consistent with observation and reported by Wang et al (2007) for DDT and PTMP terminated PMAA, The decrease in intensity of Surface Plasmon (SP) band of dodecane thiol stabilized gold nanoparticles was attributed to the onset of quantum size effect (Wuelfing et al 1998, Shan et al 2003, Hostetler et al 1998). The particle size further confirmed by TEM was  $3.2 \pm 0.2$  nm and  $2.8 \pm 0.2$  nm, as shown in Figure 3.4b and c. An FT-IR spectrum of DSDMA stabilized AuNPs also showed the double bond peak at  $1640 \text{ cm}^{-1}$  indicating that the unsaturation was intact (Figure 3.5). The increase in concentration of Au resulted in chain like structure as shown in Figure 3.6a and b.

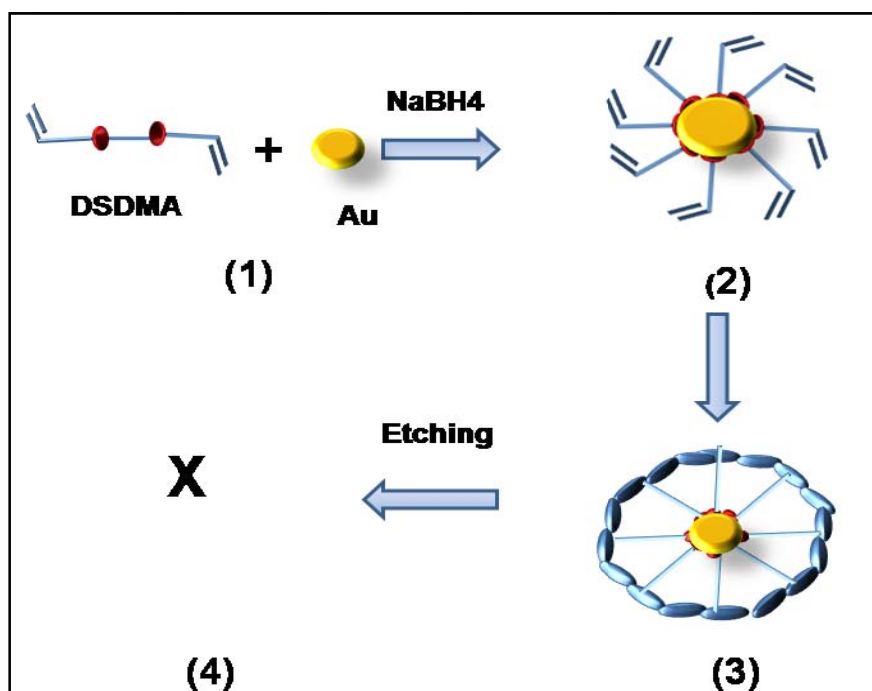


**Figure 3.2** schematic for DSDMA stabilization AuNPs

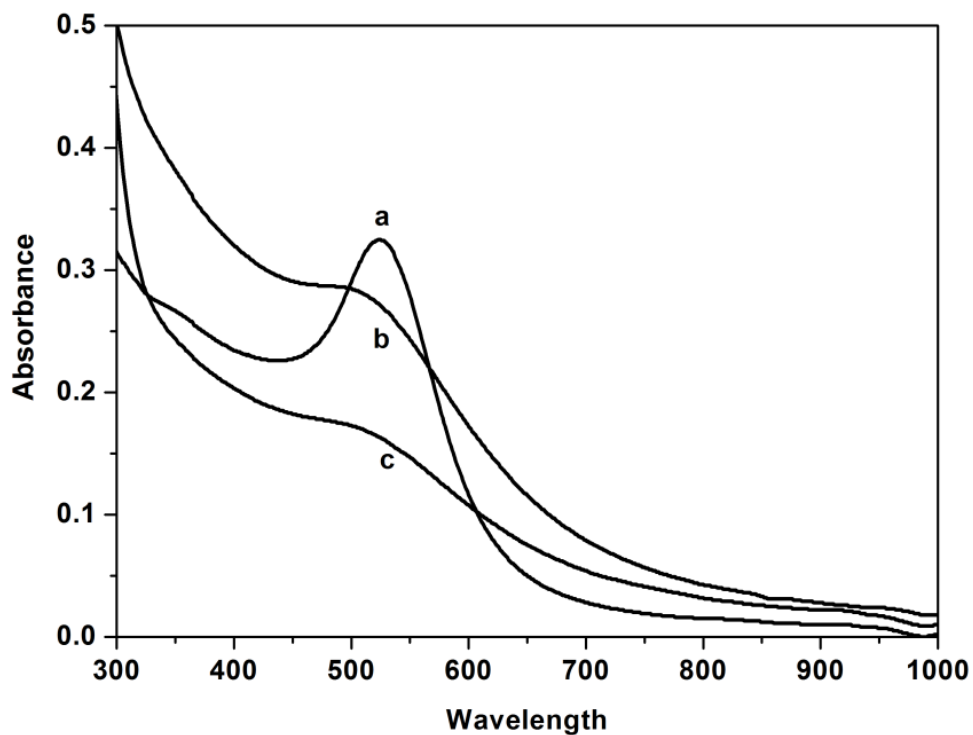


**Figure 3.3** UV-Visible spectra of AuNPs at disulfide to Au ratio a) 1 b) 10 c) 25 mM DSDMA concentration

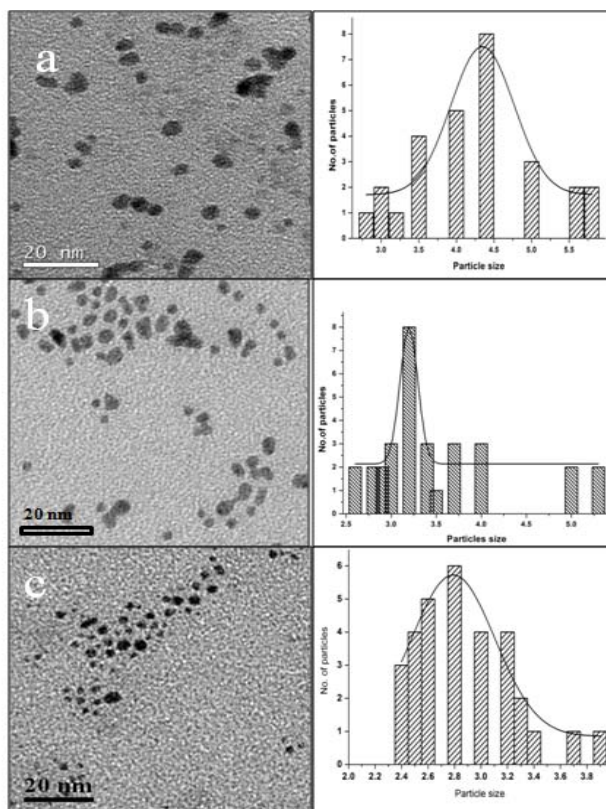


**Figure 3.4** TEM images of DSDMA AuNPs at a) 1 b) 10 c) 25 mM concentration

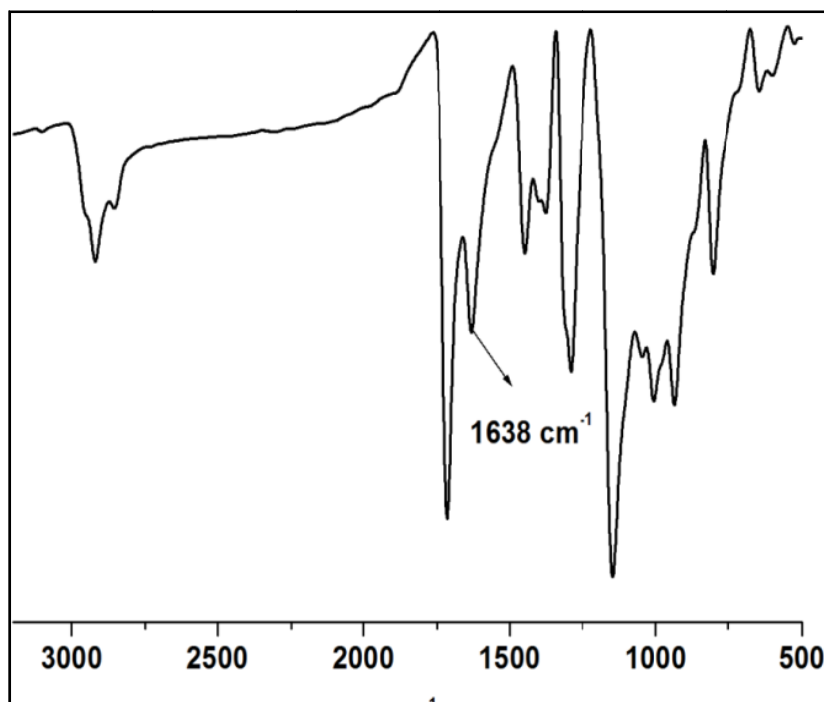


**Figure 3.5** IR Spectrum of DSDMA stabilized AuNPs

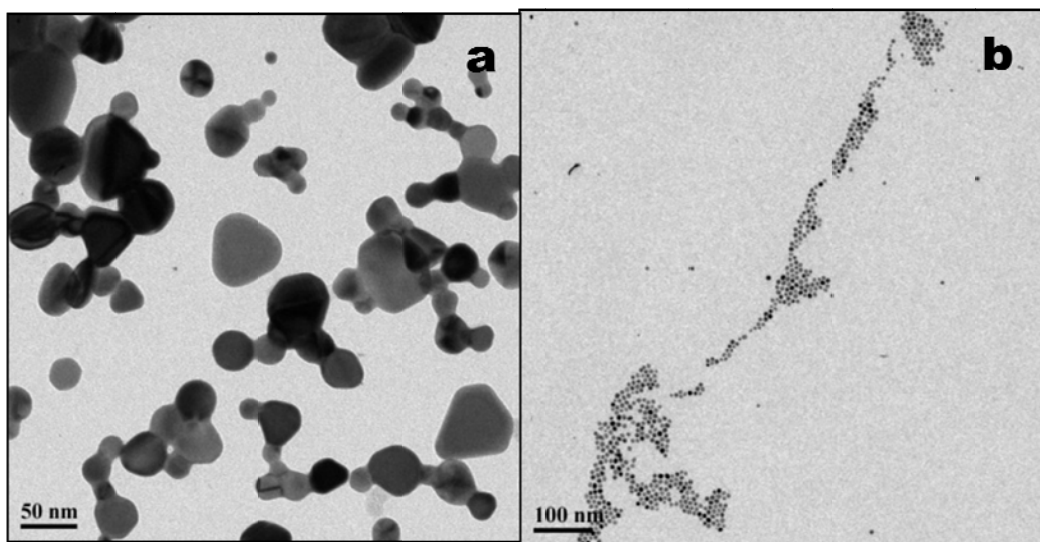


**Figure 3.6** TEM images of DSDMA AuNPs at disulfide: Au a) 1:5 b) 1: 10

### 3.3.1.2. Thermal - crosslinking of DSDMA stabilized AuNPs

We successfully synthesized AuNPs upto  $3.2 \pm 0.2$  nm using DSDMA as a stabilizer. To enhance the stability of DSDMA stabilized AuNPs, an attempt was made to crosslink the monomer by free radical polymerization at  $60^{\circ}\text{C}$  using AIBN as initiator. However, AuNPs precipitated due to desorption of the monomer because of

limited stability of thiolated AuNPs at 60 °C Yoo et al (2010). Koenig and Chechik (2006) reported that polymerization of acrylate bearing thiol ligands adsorbed on AuNPs was unsuccessful and attributed the same to chain transfer to thiolate ligands leading to nanoparticles aggregation.

### 3.3.1.3. Photo - crosslinking of DSDMA stabilized AuNPs

Crosslinking of DSDMA stabilized AuNPs (3.2 nm) using AIBN was unsuccessful due to desorption of monomer at 60 °C therefore an attempt was made to crosslink the DSDMA stabilized AuNPs by photoinitiator (Irgacure) with UV irradiation of intensity 1 mW / cm<sup>2</sup> for 30 min at room temperature. FT-IR analysis showed a decrease in the intensity of peak at 1640 cm<sup>-1</sup> which corresponds to C=C stretching. However, the peak did not disappear completely, indicating crosslinking was not quantitative. UV and TEM analysis showed no change in the size of AuNPs during polymerization (Figure 3.7 and 3.8).

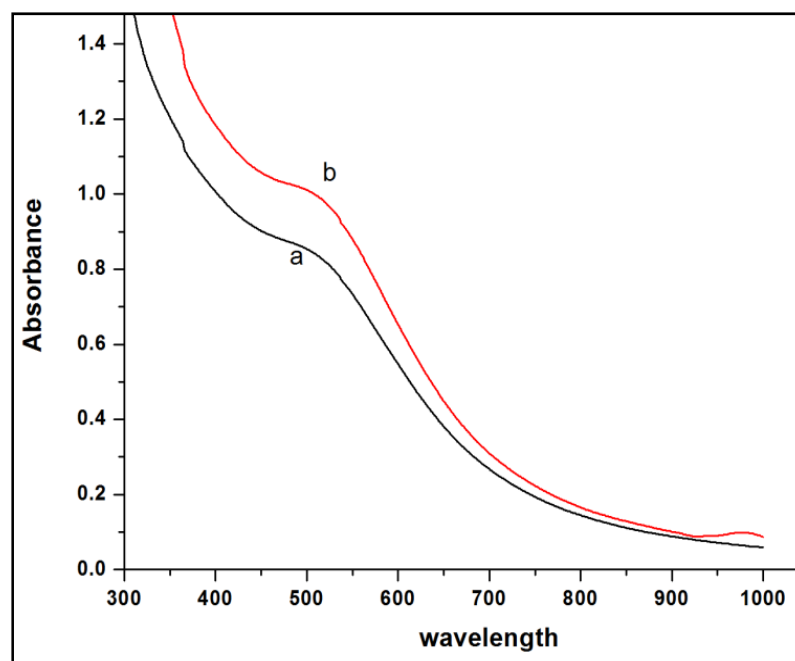


**Figure 3.7** UV-Visible spectra of DSDMA AuNPs after a) before b) after heating at 140 °C for 1 h

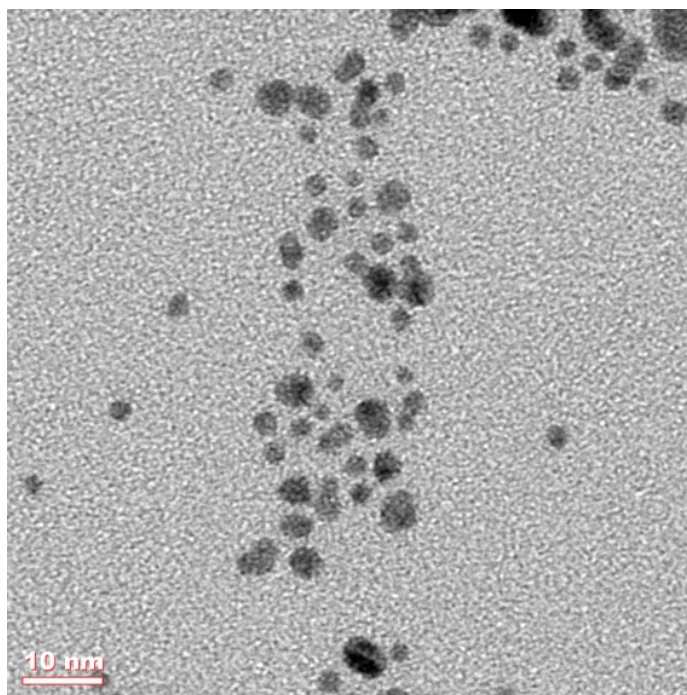


**Figure 3.8** TEM image of DSDMA stabilized AuNPs after heating at 140 °C for 1h.

### 3.3.2. Stability of AuNPs

The stability of AuNPs as a function of time and also against exchange with thiolated ligands especially in aqueous media is critical in biological application. In present case, although gold nanoparticles were in DMF, the effect of crosslinking on particle size with respect to time and against DTT exchange was evaluated.

#### 3.3.2.1 Solvent stability

The AuNPs stabilized on DSDMA (4.4 nm) were stored at room temperature. There was visually no change in color the particle even after several days. However in the case of DSDMA stabilized AuNPs UV-Visible spectra showed shift in the SPR band from 516 nm to 527 nm after 15 days (Figure 3.9) indicating particle size increase from 5 nm to 10 nm as confirmed by TEM (Figure 3.10). The particles after crosslinking with photoinitiator showed no change in UV peak position even after three months which indicates that crosslinking inhibit the growth of nanoparticles.



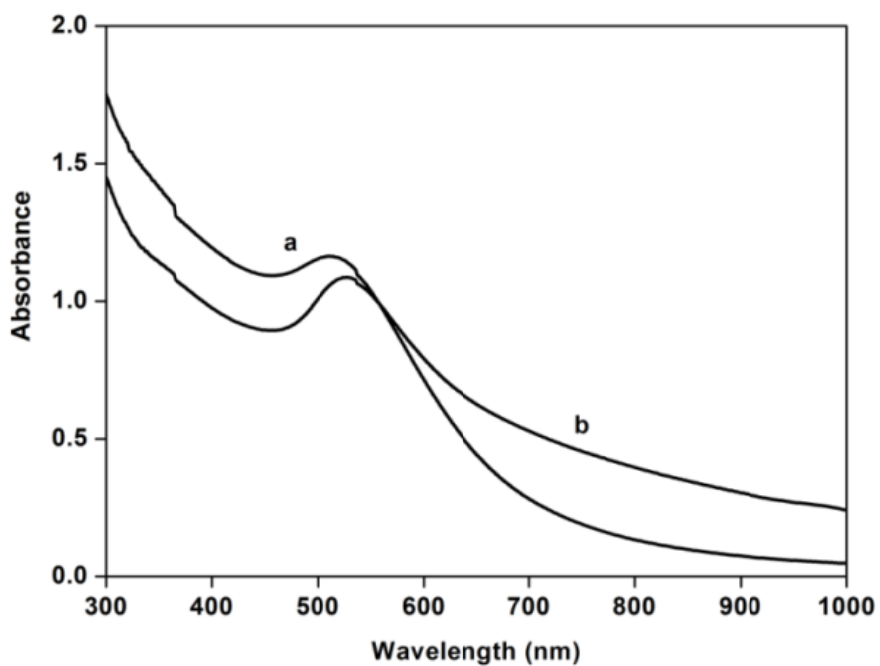


**Figure 3.9** UV-Visible spectra of DSDMA AuNPs after a) 1 day b) 15 days.

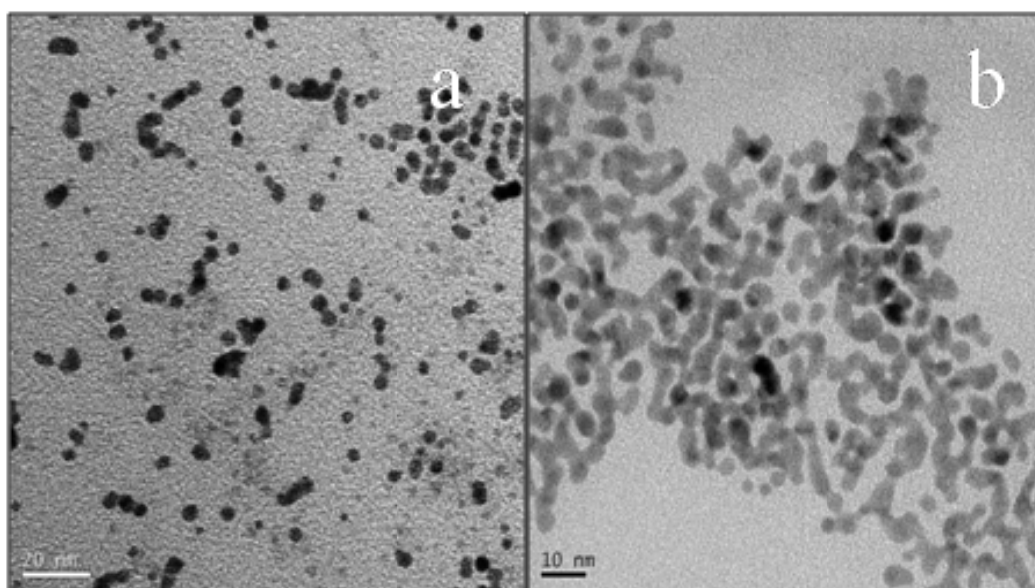


**Figure 3.10** TEM image of DSDMA stabilised AuNPs 1:1 molar ratio after a) 1 day  
b) 15 days.

### 3.3.2.2. Stability against DTT

The nanoparticles at 1mg /ml concentration were also evaluated for stability against DTT. Initially 10 mM DTT was used for ligand exchange. However, there was no

effect on particle size even after 7 days. Hence 100 mM DTT concentration for evaluating the stability, monitored by UV-Visible spectroscopy.

On addition of DTT to non crosslinked DSDMA stabilized AuNPs, SPR showed shift in peak after 24 h indicating particle aggregation (Figure 3.11). For crosslinked gold nanoparticles SPR peak remained unchanged for 39 h after addition of DTT which indicates that stability increased as a result of crosslinking of DSDMA.

### 3.3.2.3. Thermal stability

Stability of AuNPs is important because of their application in the field of photonic bandgap materials, nanostructure solar cells, light-emitting diodes, and memory devices. The stability of AuNPs could be enhanced using multidentate ligand or reticulated network. Love et al (2007) synthesized dendrimers bearing disulfide core and peripheral unsaturation and used for stabilization of AuNPs. Interparticle crosslinking of the alkene groups by Grubbs catalyst resulted in insoluble product.

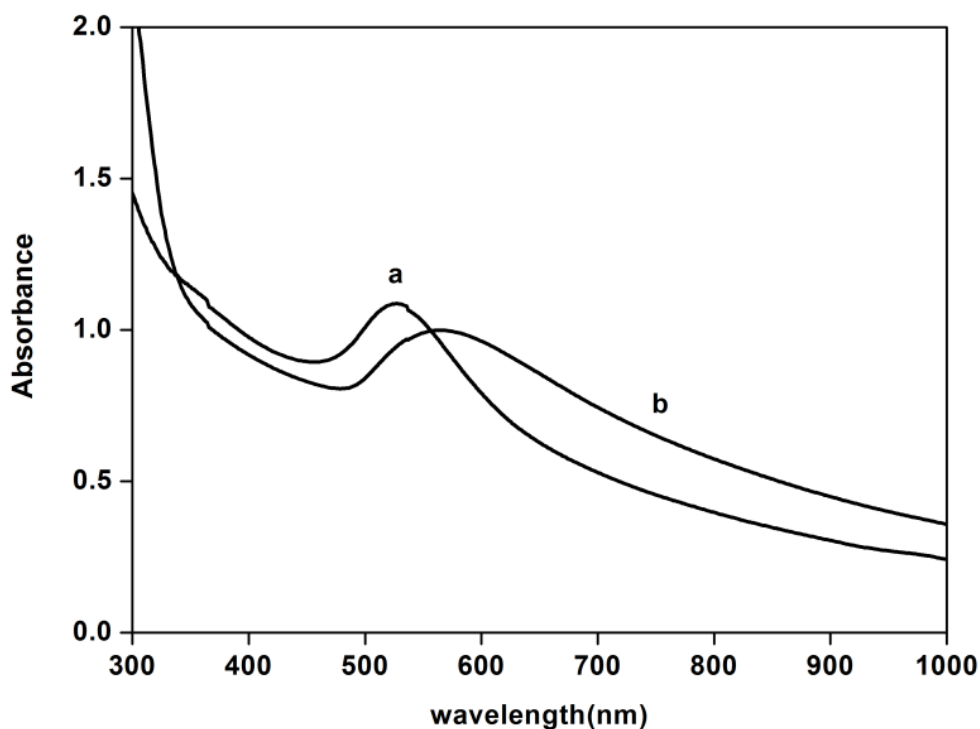


**Figure 3.11** UV-Visible spectra of DSDMA -AuNPs stability against DTT

However intraparticle crosslinking in dilute solution resulted in soluble product. The size and morphology of the gold nanoparticles was not affected by crosslinking as evidenced by UV-Visible spectra and TEM analysis of nanoparticles before and after crosslinking. Koenig and Chechik (2006) prepared AuNPs of 3 nm in diameter using acrylate based disulfide as well as based on norbornene derivative. While aggregation of the nanoparticles based on norbornene ligand could be avoided by effecting inter particle crosslinking and reducing the catalyst concentration. The solubility of the nanoparticles after cross linking was lowered because of the rigid norbornene ligand structure. The norbornene based nanoparticles were stable up to 75 °C whereas cross linking of the copolymers with norbornene increased the stability up to 110 °C.

In contrast to the dendritic structures reported above, DSDMA contains a disulfide group in the center and unsaturation at the periphery. The molecule is linear, the crosslinking site is closer to the functional group as compared to that in the case of the dendrimers reported by Love et al (2007). In view of these we expect the AuNPs stabilized on cross linked DSDMA to exhibit enhanced thermal stability as compared to those exhibited by cross linked dendrimers reported by Love et al (2007).

We monitored the SPR band in UV-Visible spectrum of AuNPs stabilized by DSDMA before and after crosslinking. This study revealed that the AuNPs stabilized on DSDMA before crosslinking were thermally stable up to 90 °C. Above this temperature SPR band shifted from 516 to 540 nm (Figure 3.12) which resulted in colour change from dark brown to pink and was followed by aggregation, as confirmed by TEM (Figure 3.14). In contrast, the cross linked AuNPs were stable upto 140 °C for upto 60 min as confirmed by UV and TEM as shown in Figure 3.13 and 3.15.

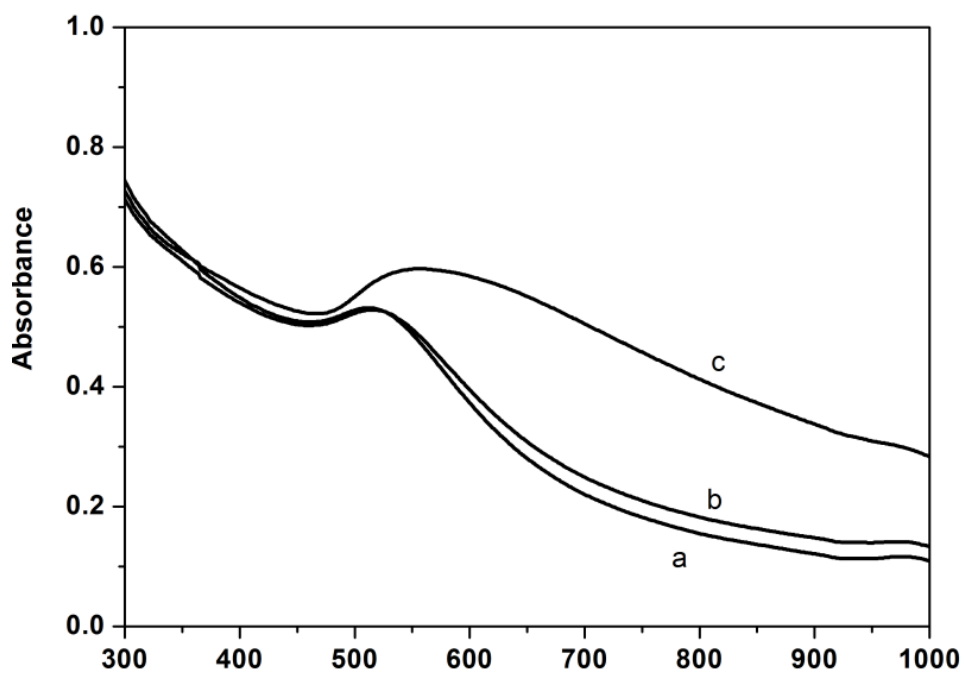


**Figure 3.12** UV-Vis spectra of DSDMA AuNPs at a) 50 b) 90 c) 100 °C

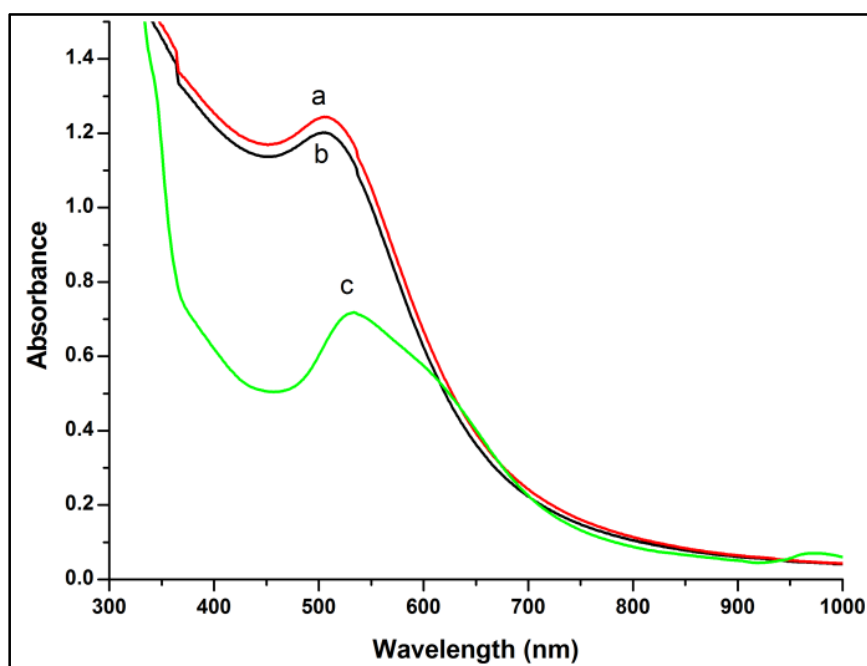


**Figure 3.13** UV-Vis spectra of crosslinked DSDMA stabilized AuNPs at a) room temperature b) 140 °C after 1 h c) 140 °C after 1.25 h

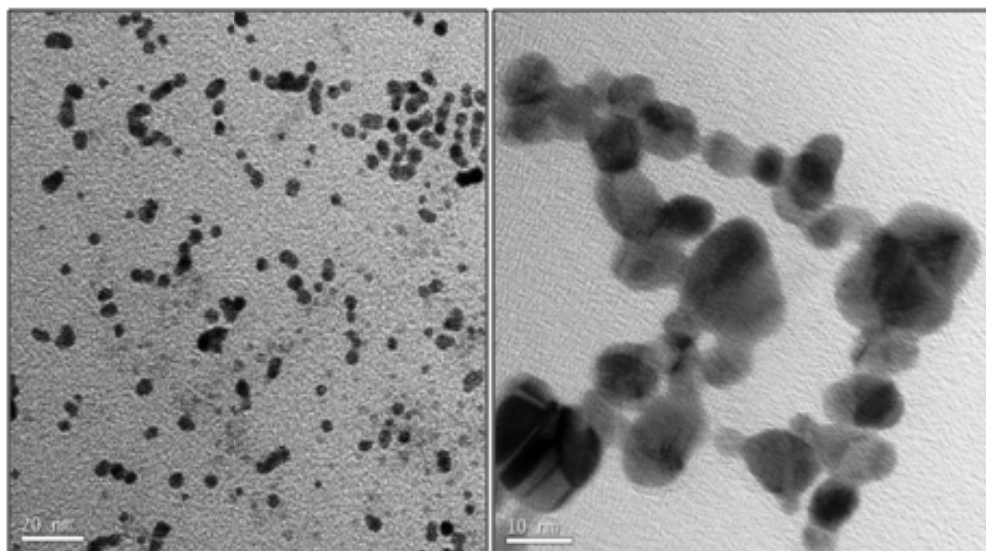


**Figure 3.14** AuNPs with 1:1 ratio of disulfide: Au at a) 40 °C b) 100 °C.

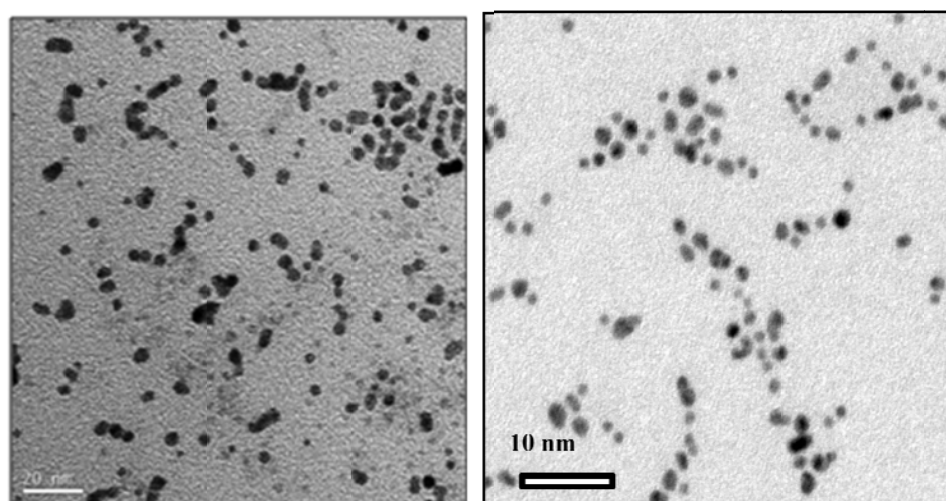


**Figure 3.15** AuNPs with 1:1 ratio of disulfide: Au a) 40 °C b) 140 °C after 1

#### 3.3.2.4 Nanocapsules synthesis

Thermal stability of DSDMA – AuNPs was enhanced because crosslinking results in multidentate poly DSDMA ligand. We therefore expected in situ formed poly DSDMA AuNPs to yield nanocavities on etching.

In order to form nanocapsules we etched these nanoparticles with methyl iodide for 24 h. No insoluble product or aggregates were observed at the end of the etching. Removal of gold from the nanoparticles was visually observed by change in colour

from brown to yellow. UV-Visible spectrum of the solution showed no peak at 516 nm. A peak at 362 nm appeared which could be attributed to Au<sup>+3</sup> species and at 270 nm which was attributed DSDMA. The peak at 362 nm disappeared on repeated extraction with methanol and dissolution in DMF while that at 270 nm was retained. TEM and AFM analysis of these etched crosslinked DSDMA showed no nanocapsules. This could be attributed to incomplete crosslinking which results in inadequate stabilization of nanoparticles during etching. Thus, stabilization of AuNPs on monodentate ligand followed by crosslinking does not lead to nanocapsules. These observations are consistent with those of Koenig and Chechik (2006) who prepared 3 nm AuNPs using acrylate as well as norbornene based disulfides. Aggregation of the AuNPs based on norbornene disulfide was avoided by effecting intra-particle crosslinking which enhanced thermal stability from 75 °C to 110 °C. But etching of AuNPs resulted in insoluble precipitates, which was attributed to rigid polymer structure, incomplete crosslinking and incompatibility with the solvent.

#### **3.4. Conclusions**

Bis (2-methacryloylhydroxyethyl) disulfide (DSDMA) could be successfully used to stabilize AuNPs in the range of  $2.8 \pm 0.2$  nm in size as confirmed by UV-Visible spectra and TEM. The particle size could be modulated by molar ratio of disulfide to Au. AuNPs stabilized on DSDMA were stable in DMF only up to 90 °C while those crosslinked AuNPs were stable up to 140 °C for one hour. Etching of AuNPs did not lead to nanocapsules due to incomplete crosslinking.

**References**

1. Bakeeva I. V., Kolesnikova Y. A., Kataeva N. A., Zaustinskaya K. S., Gubin S. P., and Zubova V. P., *Russian Chemical Bulletin, International Edition*, 57, **2008**, 337-344.
2. Ghosh S. K., Pal T., *Chem. Rev.*, 107, **2007**, 4797-4862.
3. Hostetler M.J., Wingate J.E. and Murray R.W., *Langmuir*, 14, **1998**, 17-30.
4. Koenig S., Chechik V., *Langmuir*, 22, **2006**, 5168-5173.
5. Liu X., Li C., Xu J., Lv J., Zhu M., Guo Y., Cui S., Liu H., Wang S., and Li Y., *J. Phys. Chem. C*, 112, **2008**, 10778-10783.
6. Li Y. and S.P. Armes, *Macromolecules*, 38, **2005**, 8155-8162.
7. Love C. S., Ashworth I., Brennan C., Chechik V., Smith D. K., *Langmuir*, 23, **2007**, 5787-5794.
8. Love C.S., Chechik V., Smith D.K., and Brennan C., *Journal Material Chemistry*, 14, **2004**, 919.
9. Rastogi S. K., Denn B. D., Branen A. L., *J. Nano. Res.*, 14, **2012**, 673.
10. Shan J., Nuopponen M., Jiang H., Kappinen E., Tenhu H., *Macromolecules*, 36, **2003**, 4526 – 4533.
11. Shimmin R.G., Schoch A.B. and Braun P.V., *Langmuir*, 20, **2004**, 5613-5620.
12. Wuelfing W. P., Gross S. M., Miles D. T., Murray R. W., *Journal of American Chemical Society*, 120, **1998**, 12696 – 12697.
13. Yonezawa T., Yasui K. and Kimizuka N., *Langmuir*, 17, **2001**, 271-273.
14. Yoo M., Kim S., Lim J., Kramer E.J., Hawker C. J., Kim B. J., Bang J., *Macromolecules*, 43, **2010**, 3570–3575.

---

---

**Chapter 4**  
**Polydentate disulfides for enhanced stability of AuNPs and facile  
nanocavity formation**

---

---



**4.1. Introduction**

There is growing interest in the synthesis of AuNPs and nanoclusters in view of their applications in diverse fields which are well documented. (Daniel and Astruc 2004, Gosh and Pal 2007, Liu et al 2008, and Rastogi et al 2012) AuNPs less than 5 nm diameter are of particular interest because of their size and shape-dependent properties and applications in single electron transistors, light-emitting diodes, data storage devices, super capacitors and chemical sensors (Pellegrino et al 2005, Roux et al 2005, Wang et al 2007, and Yoo et al 2010). However, for these diverse applications, it is critical that AuNPs be stable in different solvents, against competing ligands and also during processing, often at elevated temperatures. While a wide range of ligands has been investigated for the stabilization of AuNPs, thiols and disulfides have been found to be most effective. For example, Zhang et al (2001) reported that amongst a series of C<sub>16</sub>-C<sub>18</sub> based mono, di and tri thiols, the bidentate and tridentate thiols enhance the stability of 20-50 nm AuNPs in toluene, as a result of multidentate chelate effect, while the hydrocarbon chains enhance the solubility of AuNPs in 1:1 toluene / tetrahydrofuran. Sakata et al (2007) demonstrated that tripodal thiol derivatives bound to AuNPs exhibited higher solvent stability than the corresponding mono thiol, which was exploited for conjugation with oligonucleotide probes. A logical extension of these results implies that a polymeric ligand containing multiple thiol groups should enhance the stability further. However synthesis of such a ligand has not been reported. Instead, monomers containing disulfide groups have been used to stabilize AuNPs and subsequently crosslinked to yield AuNPs stabilized by multiple thiol groups. The approach has had limited success Koenig and Chechik (2006), Love et al (2007) and our own results discussed in the previous chapter. This is because at the stage of stabilization of AuNPs, the ligand is still monomeric with each monomer bearing a single thiol group. For example, Koenig and Chechik (2006)

prepared 3 nm AuNPs using acrylate as well as norbornene based disulfides. Aggregation of the AuNPs based on norbornene disulfide was avoided by effecting intra-particle crosslinking which enhanced thermal stability from 75 °C to 110 °C.

AuNPs have been also exploited as sacrificial templates for the synthesis of nanocavities. Etching of AuNPs as reported by Koenig and Chechik (2006) resulted in insoluble precipitates, which was attributed to rigid polymer structure, incomplete crosslinking and incompatibility with the solvent. Sun et al (2001) and Boyer et al (2010) reported 10-30 nm capsules obtained by etching of the AuNPs stabilized on thiolated  $\beta$ -cyclodextrin and P[(HPMA)-b-(St-alt-MA)] and P[(OEG-A)-b-(St-alt-MA)]. Wu et al (2000) synthesized a triene functionalized disulfide in seven steps and stabilized 5 nm AuNPs on the same. Intra-molecular polymerization of the alkene was achieved using Grubb's catalyst. The etching of the nanoparticles by sonicating a tetrahydrofuran / water solution containing KCN and  $K_3[Fe_2(CN)_3]$  followed by treatment with hydrogen peroxide resulted in  $10.47 \pm 2.54$  nm capsules. However, the role of sulfur in the ligand was not elucidated. Also in none of these cases, the thermal stability of AuNPs was evaluated. Thus, while it is recognized that multidentate thiols enhance the stability of AuNPs in solvents and against competitive ligand exchange, their thermal stability is limited due to the lack of polymerizable groups. In contrast, the polymerizable disulfides so far investigated, function only as monodentate ligands during the stabilization of AuNPs and suffer from the limited stability of the Au-S bond. There is, therefore, a need to synthesize a polymeric ligand containing pendent disulfide groups so that it acts as a truly polydentate ligand during the stabilization of AuNPs and overcomes the limitations of the prior approaches explored so far.

In this chapter, we report the synthesis of AuNPs using the polydentate ligand, poly(DSDMA) synthesized by selective polymerization of DSDMA:  $\beta$ -CD inclusion

complex. In previous chapter we showed that AuNPs stabilized on DSDMA exhibit modest increase in stability in solvent, against competing ligand and at elevated temperature. Etching of AuNPs does not lead to nanocapsules. In contrast, the AuNPs (2.2–3.2 nm) stabilized on poly(DSDMA) followed crosslinking results in enhanced thermal stability upto 4 h at 140 °C. The etching of AuNPs by methyl iodide results in 5 nm cavities. The polydentate ligand has been shown to stabilize the AuNPs, enhancing thermal stability and leading to the formation of nanocavities.

## **4.2. Experimental section**

### **4.2.1. Materials**

Bis(2-hydroxy ethyl) disulfide (Technical grade), Hydrogen tetrachloroaurate trihydrate (HAuCl<sub>4</sub>.3H<sub>2</sub>O) (99.9%), Deuterated chloroform (CDCl<sub>3</sub>) (99.9 atom % D), Deuterated Dimethyl sulfoxide (d<sub>6</sub>-DMSO) (99.8 atom % D), Azobisisobutyronitrile (AIBN) (98%), Dithiothreitol (DTT) (Minimum 99%) and Hydroxy cyclohexyl phenyl ketone (Irgacure 184) (99%), were purchased from Aldrich (USA), β-Cyclodextrin (β-CD) (minimum assay 98%) was from Himedia Laboratories India. Sodium borohydride (NaBH<sub>4</sub>) (95%), N, N' Dimethylformamide (DMF) (GR grade), Chloroform (CHCl<sub>3</sub>) (GR grade), Dichloromethane (DCM) (GR grade), were purchased from SD fine chemicals, India.

### **4.2.2. Measurements**

#### **4.2.2.1. UV-Vis spectrophotometry**

UV-Vis absorption spectra were recorded on Shimadzu UV-Visible spectrophotometer UV-1601PC model, in the wavelength range 200 to 1000 nm.

#### **4.2.2.2 Fourier transform infrared spectroscopy (FT-IR)**

The FT-IR studies were carried out using Perkin Elmer Spectrometer, UK in diffused

reflectance mode. The samples were milled with KBr. The spectra were recorded over the frequency range 3500 -500  $\text{cm}^{-1}$  at resolution 4  $\text{cm}^{-1}$ .

#### **4.2.2.3. Nuclear magnetic resonance spectroscopy (NMR)**

$^1\text{H}$  NMR measurements were carried out on DRX -200 spectrometer, operating at a proton frequency of 200 MHz.

#### **4.2.2.4. Gel permeation chromatography (GPC)**

Molecular weight of poly(DSDMA) was measured by GPC using polystyrene-DVB cross-linked gel column  $1 \times 60 \text{ cm}$   $100 \text{ \AA}$  from PSS GmbH using chloroform as eluent at a flow rate of  $1 \text{ ml min}^{-1}$ . The column were calibrated with poly methyl methacrylate standards.

#### **4.2.2.5. Dynamic light scattering (DLS)**

The particle size was measured on DLS on Malvern Brookhaven Instrument Corporation 90 plus particle size analyser at  $25 \text{ }^\circ\text{C}$  in DMF with the laser operating at 659 nm (DMF viscosity 0.80 centipoise and refractive index (1.427)). The scattered light intensity was measured at an angle of  $90^\circ$ . Samples were prepared in DMF at concentration  $1 \text{ mg / ml}$  and were filtered from  $0.2 \text{ }\mu$  hydrophobic filters.

#### **4.2.2.6 Transmission electron microscopy (TEM)**

FEI Technai, Transmission electron microscope was operated at accelerating voltage 200 kV and 80 kV. The samples were prepared by drop casting on carbon coated grid and dried at room temperature overnight.

### **4.2.3. Synthesis**

#### **4.2.3.1. Inclusion complex of DSDMA (Precipitation method)**

The inclusion complex of DSDMA was synthesized by the precipitation method reported by Satav et al (2006). 23.5 g (0.02 moles)  $\beta$ -cyclodextrin was dissolved in 1375 ml distilled water at room temperature. 6 g (0.02 moles) DSDMA was added in

one portion and the mixture was stirred using a magnetic stirrer for 72 h. The complex precipitated from the solution was filtered under vacuum. The precipitate was washed thoroughly with distilled water to remove uncomplexed  $\beta$ -cyclodextrin and with Petroleum ether to remove free DSDMA. The complex was dried at room temperature in desiccator under vacuum and its structure was confirmed by  $^1\text{H}$  NMR.

#### **4.2.3.2. Polymerization of DSDMA - $\beta$ CD inclusion complex**

In a single neck 100 ml round bottom flask 8 g ( $5.6 \times 10^{-3}$  mole) of DSDMA-  $\beta$ - CD inclusion complex was dissolved in 80 ml DMF. 80 mg ( $4.8 \times 10^{-4}$  mole) of AIBN was added. The flask was purged with nitrogen for 30 minutes and fitted with adaptor along with nitrogen balloon and immersed for 20 h in a water bath maintained at  $65^\circ\text{C}$ . DMF was subsequently evaporated off under vacuum at room temperature. Poly(DSDMA) was recovered from the complex by dissolving it in DCM, filtering out  $\beta$ -CD and concentrating the filtrate to dryness in a rota vapor at room temperature.

#### **4.2.3.3. Preparation of gold nanoparticles**

4 mg ( $2.03 \times 10^{-5}$  mole) of  $\text{HAuCl}_4 \cdot 3\text{H}_2\text{O}$  in 20 ml DMF and 5.8 mg ( $2.03 \times 10^{-5}$  mole) of poly (DSDMA) in 20 ml DMF were mixed in a 100 ml round bottom flask. Freshly prepared 8 mg ( $2.11 \times 10^{-4}$  mole)  $\text{NaBH}_4$  in 4 ml DMF was added immediately with vigorous stirring. The solution which turned dark brown immediately, was stirred for 12 h. The disulfide: Au ratio in this case was 1:1. For the synthesis of AuNPs using disulfide: Au ratio 10:1 and 25:1, 40 mg ( $20.3 \times 10^{-5}$  mole) and 100 mg ( $5.07 \times 10^{-4}$  mole) of poly(DSDMA) were dissolved in 20 ml DMF. For the synthesis of AuNPs using disulfide: Au ratio 1: 5 and 1: 10, 4 mg ( $2.03 \times 10^{-5}$  mole) of poly(DSDMA), 20 mg ( $1 \times 10^{-4}$  mole) and 40 mg ( $2 \times 10^{-4}$  mole) of  $\text{HAuCl}_4 \cdot 3\text{H}_2\text{O}$  in 20 ml DMF were used. The AuNPs formed were purified by dialysis

in DMF for 48 h using cellulose membrane, approximate molecular weight cut off 12000 for poly(DSDMA) stabilized AuNPs. All experiments were carried out at ambient temperature (27 °C)

#### 4.2.3.4 Thermal stability

AuNPs (1 mg/ml) dispersed in DMF were heated in oil bath from 30 °C to 140 °C, increasing temperature in steps of 10 °C / 5 min.

#### 4.2.3.5 Nanocapsules synthesis

1 mg stabilized AuNPs were dispersed in 1 ml DMF, 50 µl methyl iodide was added and the solution was allowed to stand for 24 h at room temperature. Methanol washings were given to remove dissolved gold salt completely.

### 4.3. Results and discussion

Amongst a wide range of ligands used for the synthesis of AuNPs, thiols, thiol compounds, disulfides, polymers bearing end functionalized alkyl thiol ether have been investigated as stabilizers. Polymethacrylic acid bearing thiol di and tetra dentate ligands ensured enhanced stability in salt solutions up to 1.5 M and in alkaline solutions up to pH 13 (Wang et al 2007). Roux et al (2005) demonstrated that both thiol groups on dihydrolipoic acid were bound to AuNPs. When thiol groups as in  $\alpha \omega$  dithiols were used for the synthesis of AuNPs only one of the thiols was bound. In poly(DSDMA) the disulfide functionalities are in juxta position and can be expected to bind to AuNPs as in the case of Dihydrolipoic acid. Yonezawa et al (2001) synthesized 4 chain disulfide ligand viz. (4,4-dithiobis-(*N*- propyl-*O,O*-ditetradecanoyl-L-glutamate), as a stabilizer for AuNPs. During the preparation of the AuNPs the compound (4,4-dithiobis-(*N*-propyl-*O,O*-ditetradecanoyl-L-glutamate), was reduced to two double chain thiol derivatives which stabilized the AuNPs.

Love et al (2004) explored lysine based dendrimers containing disulfide ligand for the stabilization of gold nanoparticles in the range 1.8 to 2.9 nm, since the synthesis of nanoparticles on dendrimer-branches containing thiol resulted in oxidation. It was also reported that dendrimers based on thiols and disulfides on 2 D surfaces yielded films which had virtually identical properties. The synthesis of ligands containing disulfide is a better choice since during the formation of the nanoparticles, the disulfide would be reduced to form thiols. This is easier than working with thiol based substrates which readily oxidize during the work up of the reaction products. Apart from the choice of the functional group, its disposition on the backbone is critical in governing the properties of the nanoparticles formed. Love et al (2007) reported the synthesis of dendritic disulfide ligand containing alkene groups on the periphery for the stabilization of the AuNPs. The cross linking had no effect on the size or morphology of the nanoparticles formed but enhanced stability of the nanoparticles towards etching and thermal treatments. The impact of cross linking on the nanoparticle stability was greater when the cross linking was closer to nanoparticle surface. Thus lower generation dendrimers were more effective.

In contrast to the dendritic structures investigated, the poly(DSDMA) has the advantage that the disulfide group density is very high, the molecule is linear, and the crosslinking site is closer to the functional group as compared to that in the case of the dendrimers reported by Love et al (2007). In view of these, we expect the AuNPs stabilized on cross linked poly(DSDMA) to exhibit better thermal stability as compared to those exhibited by cross linked dendrimers reported by Love et al (2007). In subsequent sections we discuss the synthesis of AuNPs using poly(DSDMA) containing pendent chain unsaturation as stabilizer for AuNPs. We have specifically

focused on the synthesis and characterization of AuNPs in the range of 8 - 2 nm by varying thiol to gold ratio from 1:10 to 25: 1.

We demonstrate that poly(DSDMA) encapsulated AuNPs are more stable *vis a vis* those obtained from the corresponding monomer and that stability is further enhanced as a result of crosslinking of the pendent chain. The etching of AuNPs by methyl iodide results in nanocavities depending on the size of the AuNPs, polymer content and crosslinking. The approach could be extended to water soluble monomers for the synthesis of nanocavities for biological applications

#### 4.3.1. Poly(DSDMA) characterization

While we could synthesize AuNPs upto  $3 \pm 0.2$  nm using DSDMA as a stabilizer the effort to enhance the stability of DSDMA AuNPs by free radical polymerization at 60 °C using AIBN as initiator did not succeed. Therefore DSDMA stabilized 3.2 nm AuNPs were photopolymerized. However, crosslinking was not quantitative as has been reported in the literature. The AuNPs were stable in DMF at 140 °C upto 1 h. The resultant particles subjected to methyl iodide etching were soluble although nanocavities could not be observed. Therefore we synthesized polydentate ligand containing disulfide and unsaturation in the pendent chain by the method reported earlier by Satav et al (2006) for the selective polymerization of ethylene glycol dimethacrylate (EGDMA) to yield a soluble polymer containing pendent unsaturation. Since, poly(EGDMA) has no binding site for the stabilization of AuNPs, we prepared inclusion complex of DSDMA and  $\beta$ -CD (Figure 4.1) Formation of 1 : 1 inclusion complex was determined by proton NMR spectroscopy (Figure 4.2). Selective polymerization of the same yielded a polymer containing disulfide group and vinyl unsaturation in the pendent chain (Figure 4.3). The polymer formed had a molecular weight 6000 and PDI 1.51, as confirmed by GPC. Poly(DSDMA) has a free vinyl



group in the pendent chain of every repeat unit (Figure 4.4) which can be exploited for crosslinking as will be shown later. Poly(DSDMA) at this stage is soluble in DMF, THF, DCM and  $\text{CHCl}_3$ . The presence of disulfide group in the repeat unit is expected to enhance binding with AuNPs since each chain now contains approximately 20 disulfides.

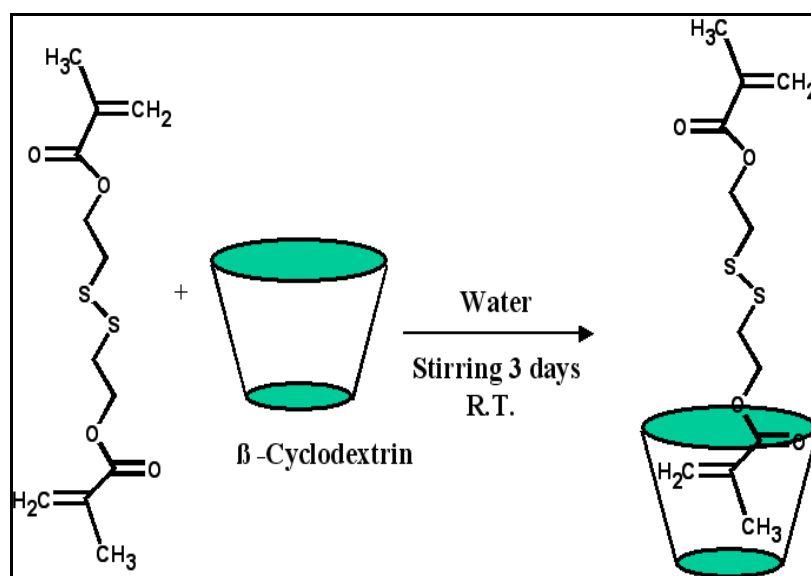


Figure 4.1 DSDMA inclusion complex synthesis

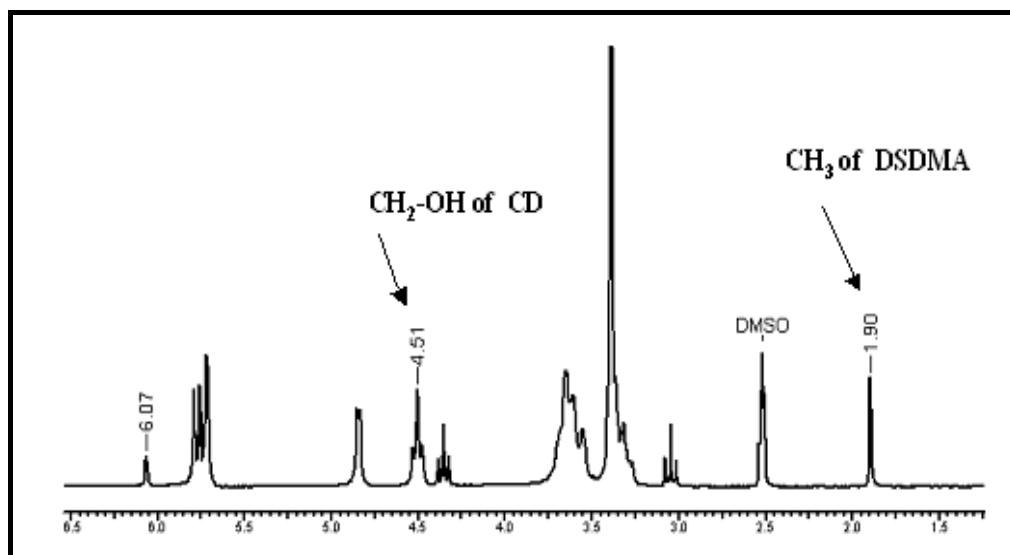
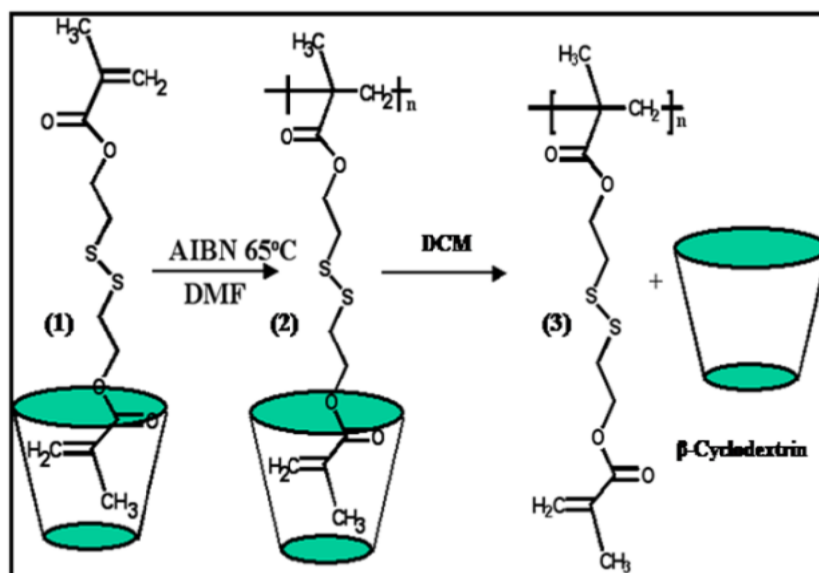
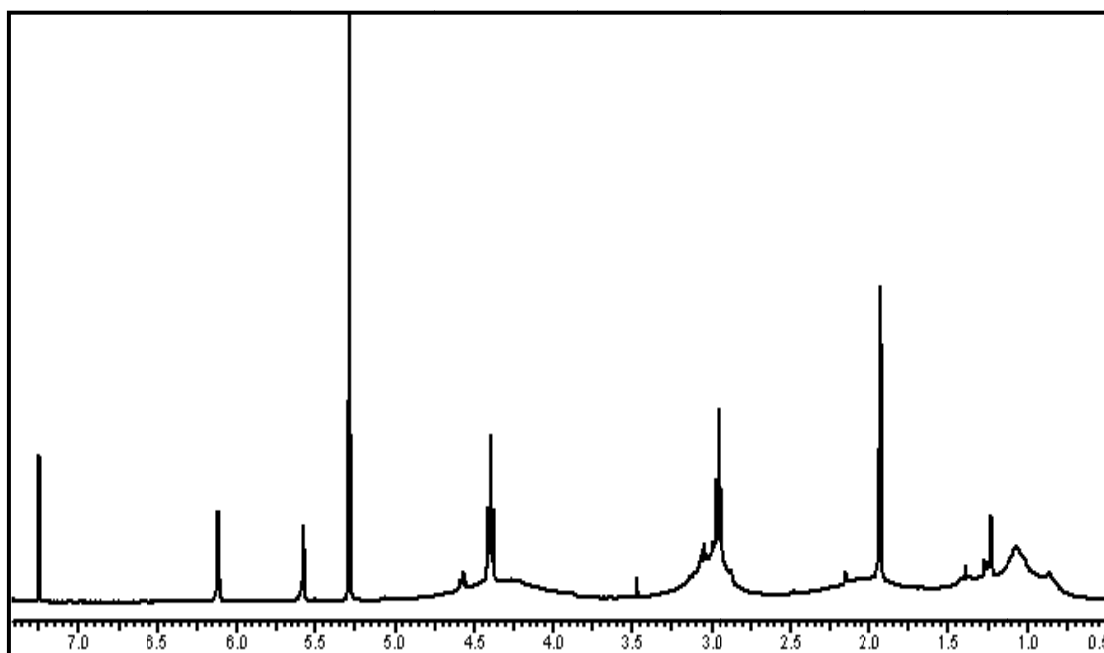


Figure 4.2  $^1\text{H}$  NMR spectrum of DSDMA –  $\beta$  CD inclusion complex

The 1:1 Stoichiometry of DSDMA- $\beta$ -CD inclusion complex was established by comparing the integration of peak at 4.51  $\delta$  corresponding to four methylene protons adjacent to ester of DSDMA and the peak at 1.90  $\delta$  for two methyl protons (6H, 2-CH<sub>3</sub> of DSDMA).



**Figure 4.3** Poly(DSDMA) synthesis 1) DSDMA;  $\beta$ -CD inclusion complex 2) Poly(DSDMA) with  $\beta$ -CD 3) Poly(DSDMA) with free vinyl group.



**Figure 4.4** <sup>1</sup>H NMR of poly(DSDMA)

$^1\text{H}$  NMR of poly(DSDMA) in  $\text{CDCl}_3$ . Peaks at 5.51 and 6.11 ppm confirm presence of free vinyl groups, peak at 4.30 and 2.95 ppm for methylene proton adjacent to ester and disulfide confirm the polymer structure.

### 4.3.2 Synthesis and characterization of poly(DSDMA) stabilized AuNPs

#### 4.3.2.1 UV, IR and TEM analysis

Synthesis of AuNPs under identical condition reported in the previous chapter was carried out using poly(DSDMA). At 1 mM concentration of poly(DSDMA) the absorption peak was observed at 505 nm (Figure 4.5a) *vis a vis* at 516 nm in the case of DSDMA. A TEM examination showed that the particle size was  $3.2 \pm 0.2$  nm and was nearly monodisperse in nature (Figure 4.6a). At 10 mM and 25 mM poly(DSDMA) concentration, peak at 505 nm broadened and decreased in intensity (Figure 4.5b and 4.5c) indicating a further decrease in particle size. The TEM analysis showed that the AuNPs were to  $2.8 \pm 0.2$  and  $2.2 \pm 0.2$  nm in size as shown in Figure 4.6b and 4.6c. While particle size of AuNPs can be modulated by varying disulfide : gold ratio,

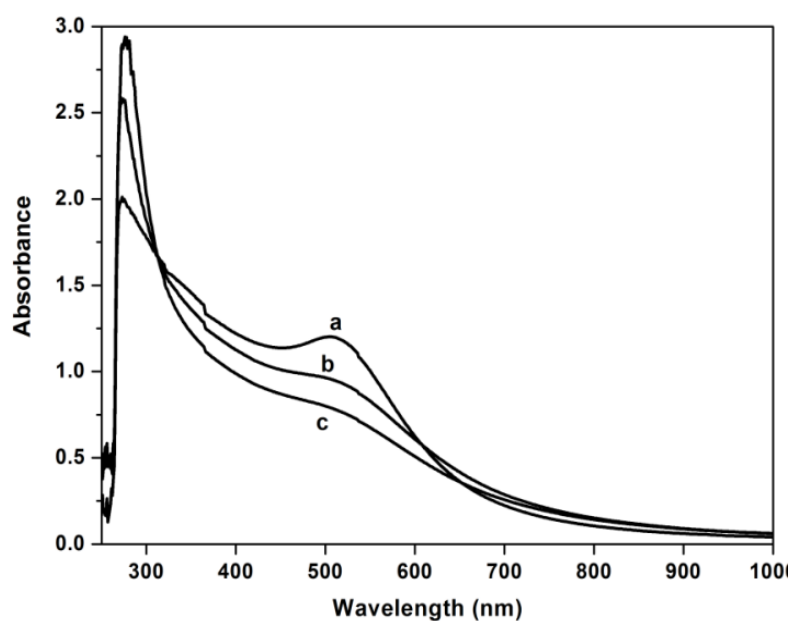


**Figure 4.5** UV-Vis spectra of poly(DSDMA) AuNPs at disulfide: Au ratio a) 1:1, b) 10:1, c) 25:1

at low disulfide to gold ratio (1:1 in present case) use of polymeric thiols results in lower particle size as compared to those obtained from alkane thiols (Wuelfing et al 1998, Shan et al 2003, Shimmin et al 2004). Polymeric thiols are considered to be more efficient in suppressing aggregation of nanoparticles as compared to lower molecular weight alkane thiols. Our results are not surprising in view of the fact that the molecular weight of the polymer is 6000 and the polydentate ligand would bind AuNPs more effectively and suppress aggregation more effectively. At disulfide: gold ratio 1:5 and 1:10, SPR peak appeared at 523 and 536 nm respectively (Figure 4.7a and 4.7b). TEM analysis showed particle sizes 6 and 8 nm (Figure 4.8a and b). Thus by varying thiol to gold ratio, AuNPs in the size range 2 to 8 nm were obtained.

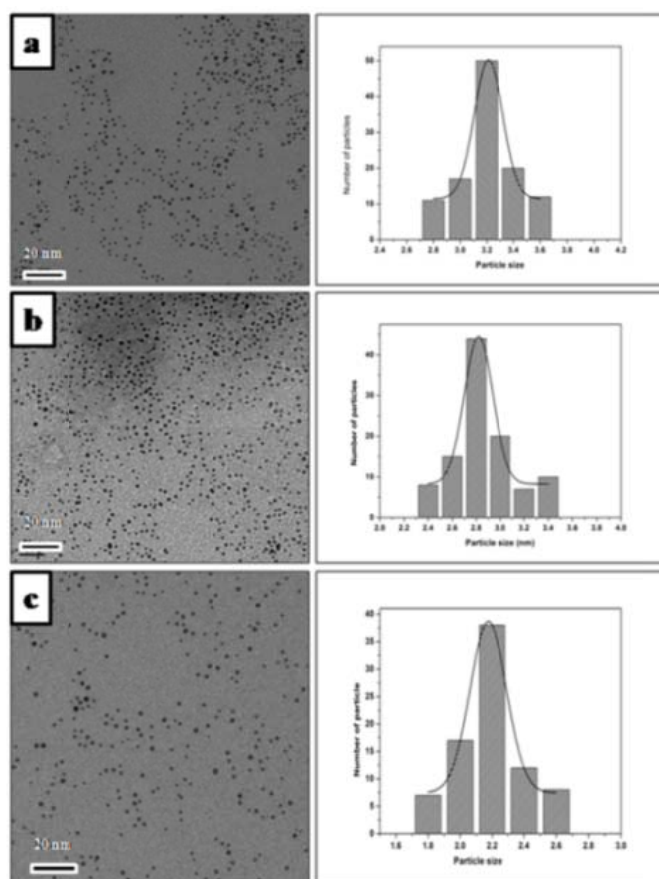


**Figure 4.6** TEM images of AuNPs stabilized on poly(DSDMA) at disulfide: Au ratio a) 1:1 b) 10:1 c) 25: 1 show particle size 3.2, 2.8 and 2.2 nm.

FT-IR spectral analysis of poly(DSDMA) stabilized AuNPs exhibited peak at  $1640\text{ cm}^{-1}$  indicating the presence of vinyl unsaturation (Figure 4.9). These can be further exploited for crosslinking to enhance the stability of the AuNPs as will be shown in subsequent section.

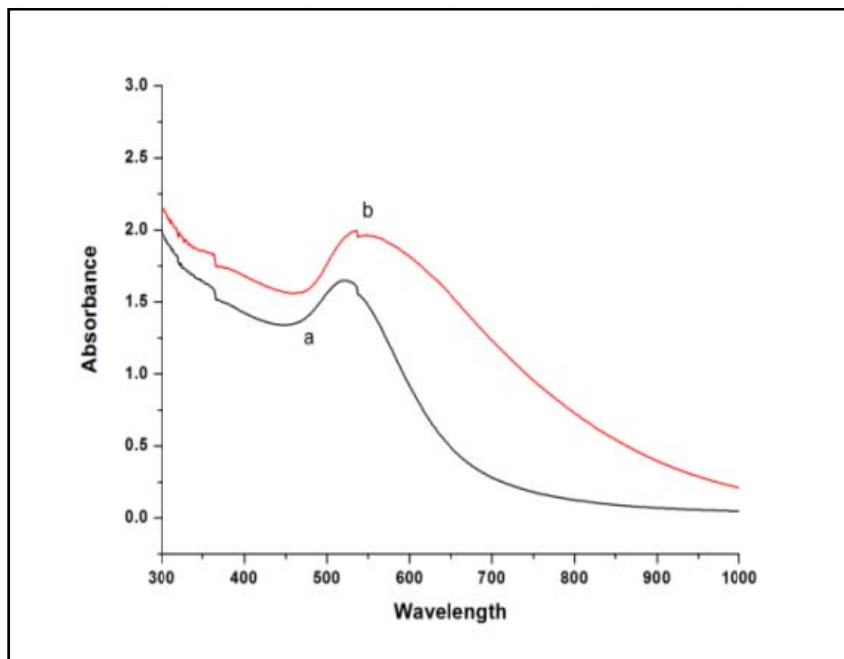


**Figure 4.7** UV-Visible spectra of AuNPs at disulfide : gold ratio a) 1:5 b) 1: 10

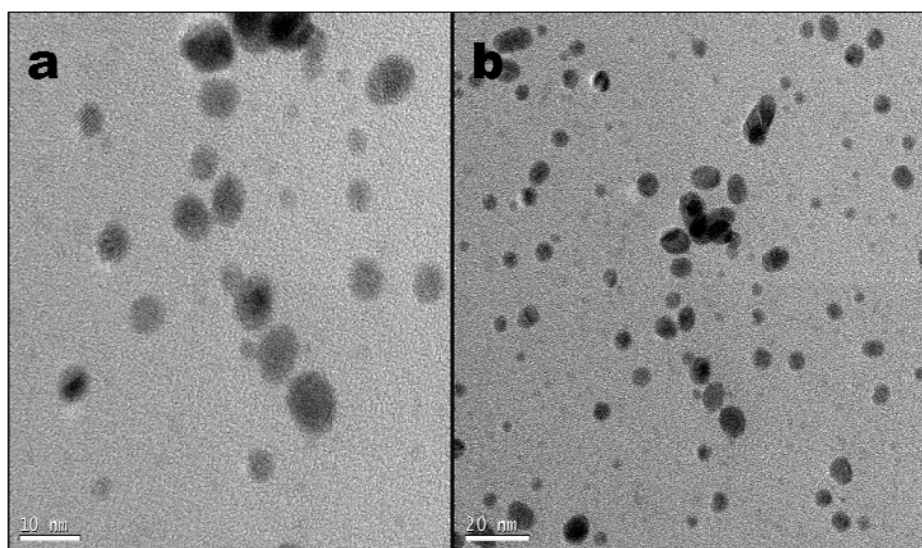


**Figure 4.8** TEM images AuNPs at disulfide: gold ratio a) 1: 5 b) 1: 10

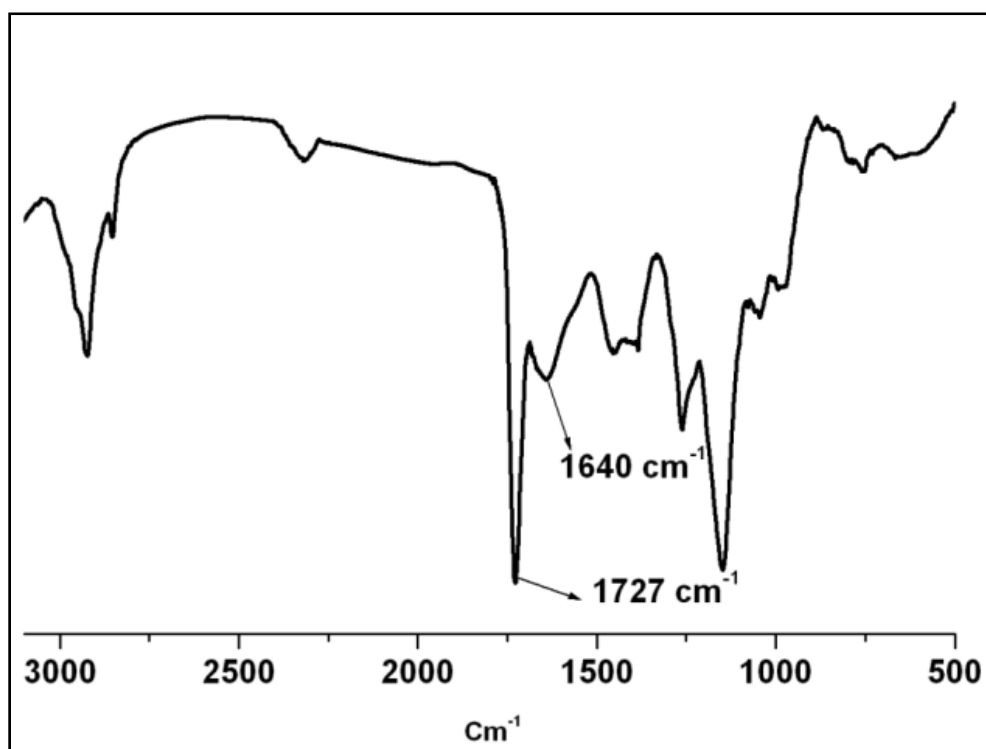


**Figure 4.9** IR Spectrum of poly(DSDMA) stabilized AuNPs

### 4.3.3 Stability of AuNPs

Poly(DSDMA) stabilized AuNPs were evaluated for stability in solvents, against competing ligands and at elevated temperature.

#### 4.3.3.1 Solvent stability

The stability of AuNPs as a function of time and also against exchange with other ligands especially in aqueous media is critical in biological application. The stability could be enhanced by increasing the binding between the AuNPs and the ligand by using substrate containing polydentate ligand. Alternatively the stability could also be enhanced by reticulation (Li et al 2002).

The AuNPs stabilized on DSDMA (4.4 nm) and poly(DSDMA) (3.2 nm) were stored at room temperature. Poly(DSDMA) stabilized AuNPs were stable for more than one year in solution as shown by UV analysis in Figure 4.10. The corresponding particle size obtained by TEM for the particles stored in solution is shown in Figure 4.11.

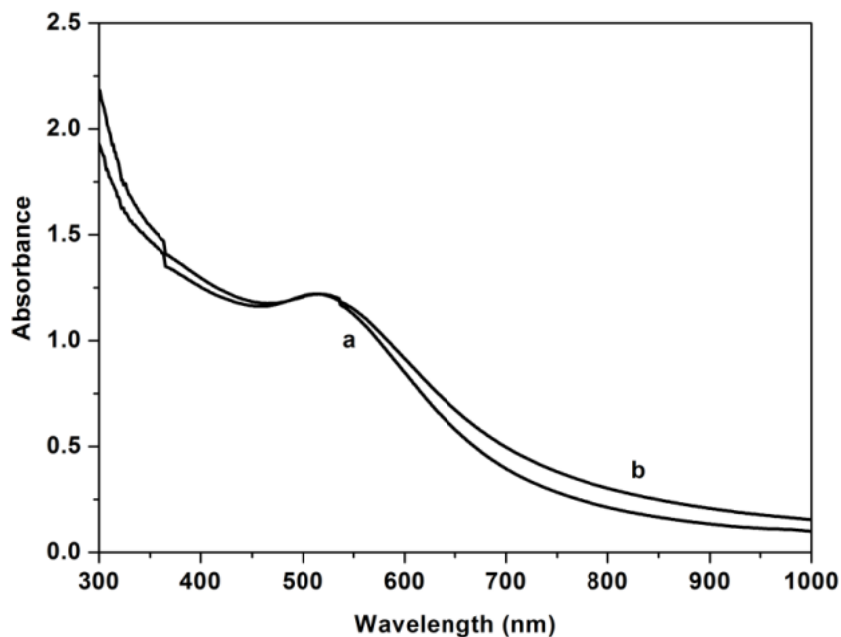


**Figure 4.10** UV-Visible spectra of poly (DSDMA) AuNPs in solution after a) 1 day  
b) 1 year

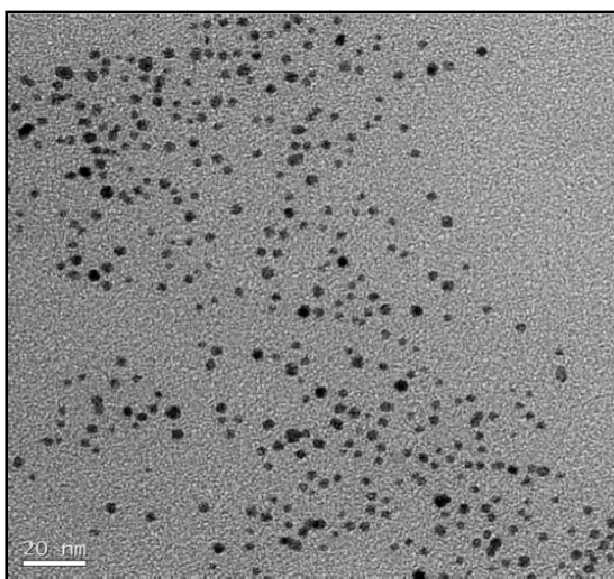


**Figure 4.11** TEM of poly(DSDMA) AuNPs in solution after 1 year.

#### 4.3.3.2 Stability against DTT

The nanoparticles at 1mg /ml concentration were also evaluated for stability against DTT. Initially 10 mM DTT was used however, there was no effect on particle size even after 7 days. Hence we used 100 mM DTT for evaluating the stability and monitored the same by UV-Visible spectroscopy.

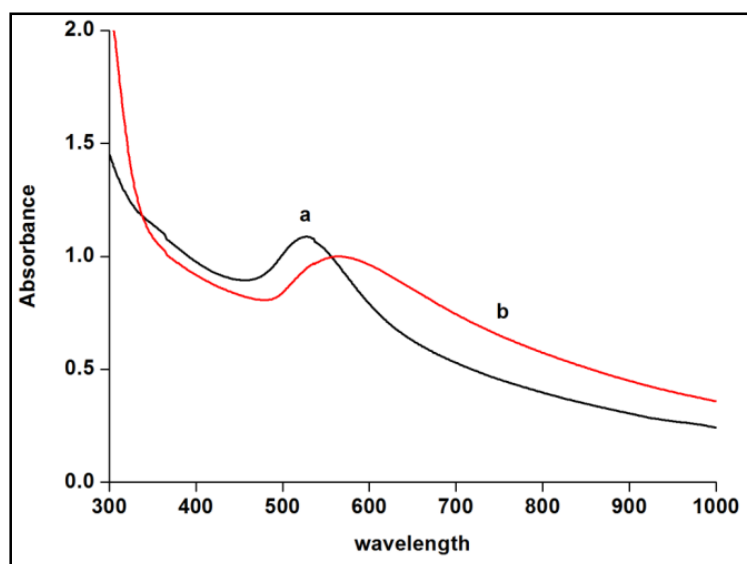


**Figure 4.12** UV-Visible spectra of DSDMA AuNPs stability against DTT.

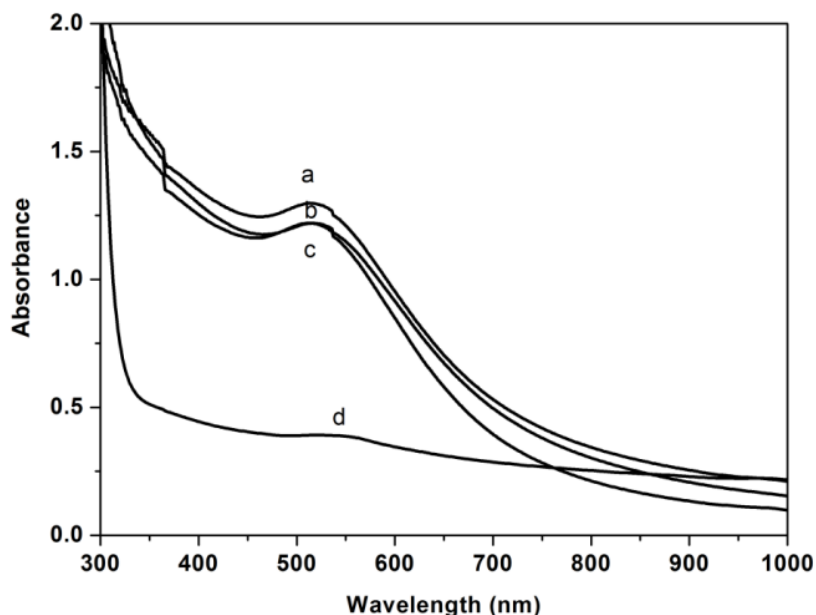


**Figure 4.13** Poly(DSDMA) AuNPs stability against DTT a) before and b) after addition 5 c) 72 d) 80 h.

DSDMA stabilized AuNPs were easily exchanged with DTT. Particles aggregated and showed the shift in SPR after 24 h (Figure 4.12). For poly(DSDMA) stabilized AuNPs, the particles were stable for 72 h (Figure 4.13) this clearly suggested that stability was increased due to polydentate nature of poly(DSDMA). The results demonstrate the additional stability imparted by the disulfide in the polymeric form. The same principle could be extended to other disulfide bearing water soluble



polydentate monomer such as cystine to develop of AuNPs which will be stable against DTT, glutathione in aqueous medium.

#### **4.3.3.3 Thermal stability**

In literature monomer bearing disulfide ligand and terminal unsaturation (Koenig and Chechik 2006), dendrimers bearing disulfide core and peripheral unsaturation, (Love et al 2007) and diblock copolymer bearing thiol ligand for binding to AuNPs and functional groups which could be photo crosslinked, (Boyer et al 2010), have been used for enhancing the stability of AuNPs. Thermally stable gold nanoparticles have been explored for applications in photonic bandgap materials, nanostructure solar cells, light-emitting diodes, and memory devices.

The thermal stability of polymer stabilized AuNPs depends on the choice of functional groups and their disposition along the polymer architecture. Love et al (2007) synthesized dendritic polymers containing disulfide core lysine and aromatic branches alkene groups at the periphery, to stabilise 1.9 to 3.4 nm AuNPs. The particle size decreased with increasing generation of the dendrimers. Interparticle crosslinking of the alkene groups by Grubbs catalyst resulted in insoluble product. However, intraparticle crosslinking in dilute solution resulted in soluble product. The size and morphology of the gold nanoparticles was not affected by crosslinking as evidenced by UV-Visible spectra and TEM analysis of nanoparticles before and after crosslinking. Disulfides were preferred since thiol functionalised ligand would be susceptible to oxidation during synthesis. Intraparticle crosslinking led to soluble dendrimers which showed completion of the crosslinking as evidenced by the disappearance of the NMR peaks corresponding to alkene group at 4.8 and 5.8 ppm. Thermal stability of the dendrimers was evaluated in DMF at 130 °C. After 25 min SPR peak shifted and the duration increased by 25 to 35 minute on crosslinking. In all

cases the crosslinked particles showed shift in peak after 75 minute. This was also accompanied by an increase in size of the AuNPs and aggregation of gold cores. The results indicated that crosslinking of the alkene groups on the surface did not inhibit growth of AuNPs.

Koenig and Chechik (2006) prepared 3 nm AuNPs using acrylate as well as norbornene based disulfide derivative. Aggregation of the nanoparticles based on norbornene ligand could be avoided by effecting intra particle crosslinking and reducing the catalyst concentration. The solubility of the nanoparticles after cross linking was lowered because of the rigid norbornene ligand structure. These nanoparticles were stable up to 75 °C whereas cross linking of the norbornene copolymers increased the stability up to 110 °C.

In contrast to the dendritic structures reported above, the poly(DSDMA) contains a disulfide group in every repeat unit. The molecule is linear, the crosslinking site is closer to the functional group as compared to that in the case of the dendrimers reported by Love et al (2007) and the crosslink density can be very high. In view of these we expect the AuNPs stabilized on cross linked poly(DSDMA) to exhibit enhanced thermal stability as compared to those exhibited by cross linked dendrimers reported by Love et al (2007). We monitored the SPR band in UV-Visible spectrum of AuNPs stabilized by poly(DSDMA). This study revealed the AuNPs stabilized on poly(DSDMA) using disulfide to gold ratio 10 :1 were stable up to 140 °C for 4 h as confirmed by no change in SPR peak position in Figure 4.14. TEM also reveals that the particle size of AuNPs stabilized on poly(DSDMA) was same after heating for 4 h in DMF (Figure 4.15b). Increase in thermal stability of poly(DSDMA) stabilized AuNPs synthesized using disulfide : gold ratio, 10 :1 can be attributed to crosslinking of the pendent unsaturation during heating of nanoparticles and was confirmed by FT-

IR. The absence of peak at  $1640\text{ cm}^{-1}$  which corresponds to unsaturation in poly(DSDMA) is shown in Figure 4.16. While nanoparticles synthesized using disulfide : gold, 1: 5 are stable up to 1.5 h as confirmed by UV- Visible spectra. The SPR peak at 523 nm was unaffected which indicates that there is no change in particle size. These results are comparable to the AuNPs stabilized on DSDMA which were stabilize up to 1 h. Crosslinking leads to the formation of additional multidentate ligand which increases thermal stability of AuNPs. SPR peak shift to 545 nm (Figure 4.17) could be attributed to increase in particles size. TEM analysis showed that particles are arranged in chain like structure (Figure 4.18). However, the chains were unstable. Hence this phenomenon was not investigated further.

The particle size of poly(DSDMA) stabilized AuNPs before (31 nm) and after thermal treatment which resulted in crosslinking of the unsaturated vinyl groups (31 nm) was measured by DLS (Figure 4.19). The result indicated that crosslinking had no effect on particle size.

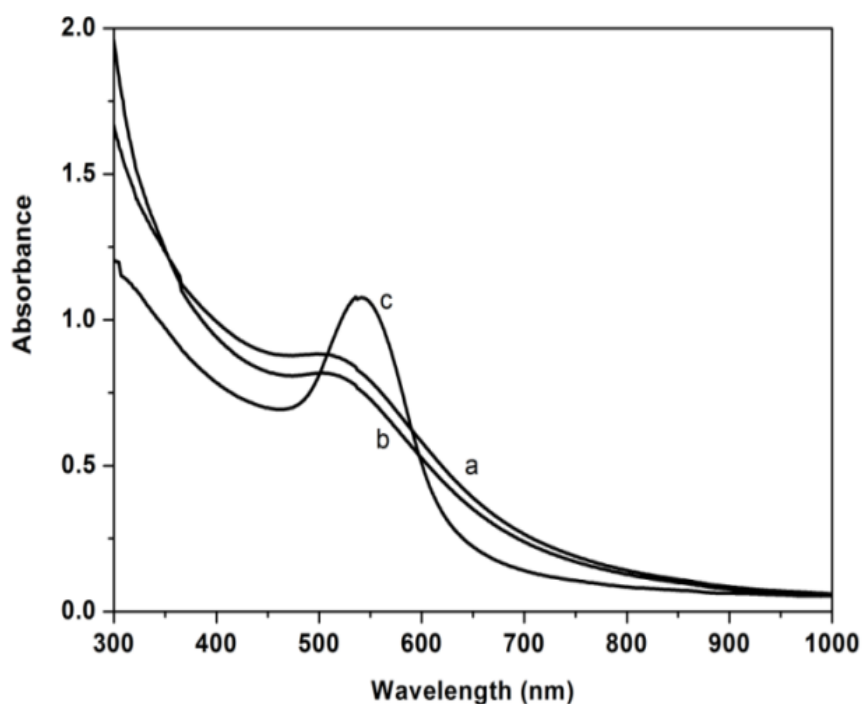


**Figure 4.14** UV-Vis spectra of poly(DSDMA) AuNPs at a)  $40\text{ }^{\circ}\text{C}$  b) at  $140\text{ }^{\circ}\text{C}$  after 4 h c) after 4.5 h.

More recently, Yoo et al (2010) used thiol terminated polystyrene (2000) azido polystyrene (900) block copolymers to stabilize 2.62 nm AuNPs. Thiol terminated polystyrene was also used as control (2.8 nm). The AuNPs were dispersed in chloroform and exposed to 254 nm UV irradiation for one hour. The thermal stability was evaluated at 150 °C in dibutyl phthalate. AuNPs stabilized on polystyrene thiols which do not crosslink, aggregated and precipitated on heating due to dissociation of gold thiol bonds. The SPR peak at 530 nm completely disappeared. The nanoparticles stabilized on polystyrene azido polystyrene block copolymers crosslinked on UV irradiation showed no change in colour after 3.5 h and an increase in size to 2.71 nm. Also there was no change in the peak at 530 nm. Thus polystyrene azido polystyrene block copolymer when crosslinked by UV irradiation, suppressed dissociation of gold thiol bonds because of the presence of the crosslinked shell. It may be noted that in this case each thiol terminated block copolymer chain behaves as monomeric ligand.

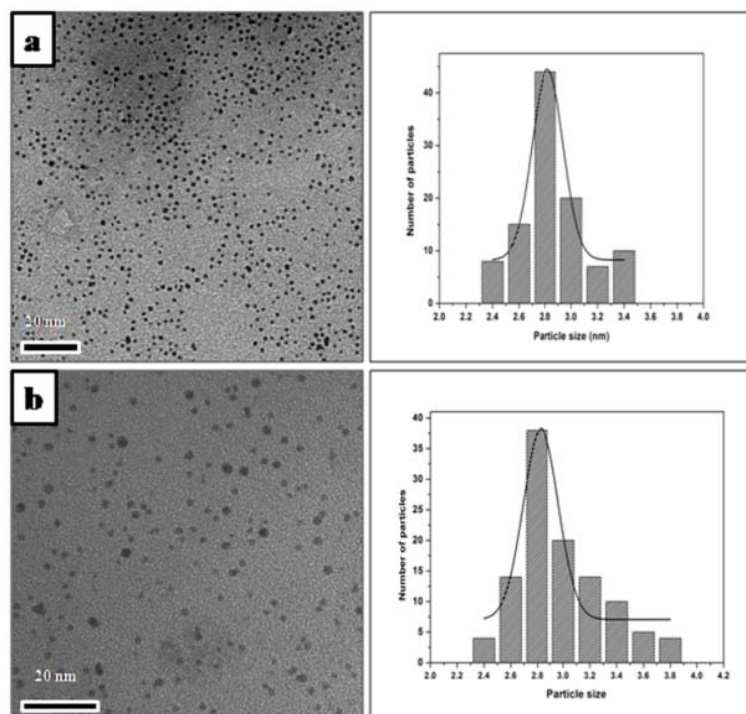


**Figure 4.15** AuNPs with 10:1 ratio of poly(DSDMA) and auric chloride a) room temperature b) 140 °C after 4 h.

High thermal stability of the photo cross linked nanoparticles results from room temperature cross linking which prevents desorption of the ligand and effects cross linking of the azido unit close to the surface of the gold nanoparticle. These results are comparable to the ones reported by us herein. Further, the synthesis of the polydentate ligand reported herein is much simpler than that of [Poly (Styrene-*b*-Styrene azide)-SH] and leads to higher graft density which imparts stability during etching as well (vide infra).

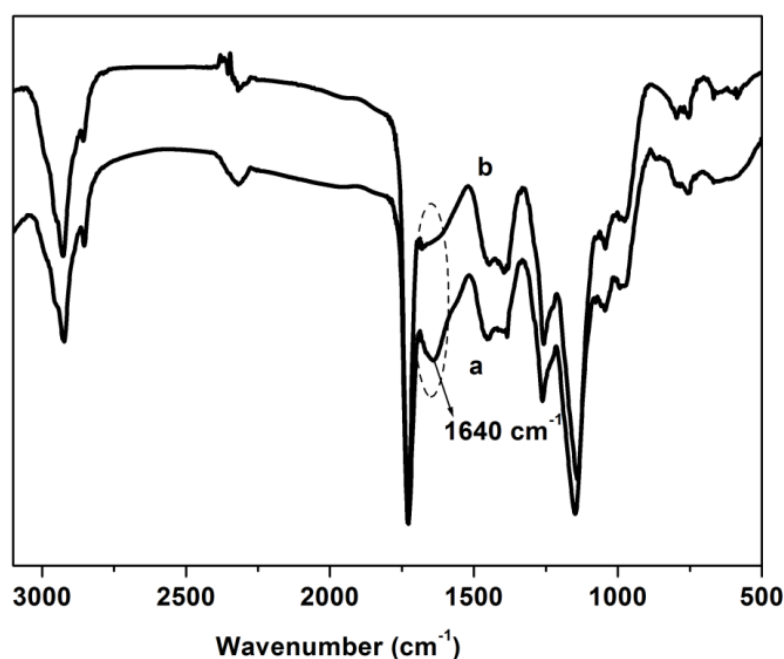


**Figure 4.16** IR spectrum of noncrosslinked and crosslinked poly(DSDMA) AuNPs.

Enhanced thermal stability of AuNPs stabilized by poly(DSDMA) could be explained on the basis of higher graft density, calculated from the weight percent of gold and polymer obtained by TGA (Figure 4.20). In the case of the DSDMA stabilized AuNPs, there are 9 DSDMA units / nm<sup>2</sup> whereas in the case of the poly(DSDMA) stabilized AuNPs there are 37 DSDMA units / nm<sup>2</sup>. In the latter case, the formation of the AuNPs results in the reduction of poly(DSDMA) to Poly Methacryloyl hydroxy ethyl thiol which has a DP of 20. This corresponds to a graft density of approximately

1.8 chains / nm<sup>2</sup>. Since the thiols are at the termini in the pendent chains, these could bind more effectively with AuNPs than in the case of linear polymers containing terminal thiols. Also it is not necessary that every thiol be bound to the AuNPs. Sun et al (2001) reported that binding of a minimum three thiols is sufficient to immobilize the chain on the AuNPs. This is reflected in the higher weight loss during thermo gravimetric analysis. The graft density of approximately 1.8 chains / nm<sup>2</sup> obtained by us is greater than that reported by Yoo et al (2010) (1.4 chains / nm<sup>2</sup>) for Poly (Styrene-b-Styrene azide)-SH stabilized 2.6 nm AuNPs and can be attributed to the polydentate nature of poly(DSDMA). Lim et al (2011) showed that the graft density (0.90 chains / nm<sup>2</sup>) on 2.5 nm (Au-PS-N<sub>3</sub>-b-PS 2) formed by conventional “grafting to” approach could be enhanced to 1.22 chains / nm<sup>2</sup> by adopting click chemistry (Au-PSN<sub>3</sub>-b-PS 1). In both cases the AuNPs are bound to the ligand by a single thiol group. In contrast, in the present case, graft density could be enhanced to 1.8 chains / nm<sup>2</sup> as a result of the polydentate nature of poly(DSDMA). The other

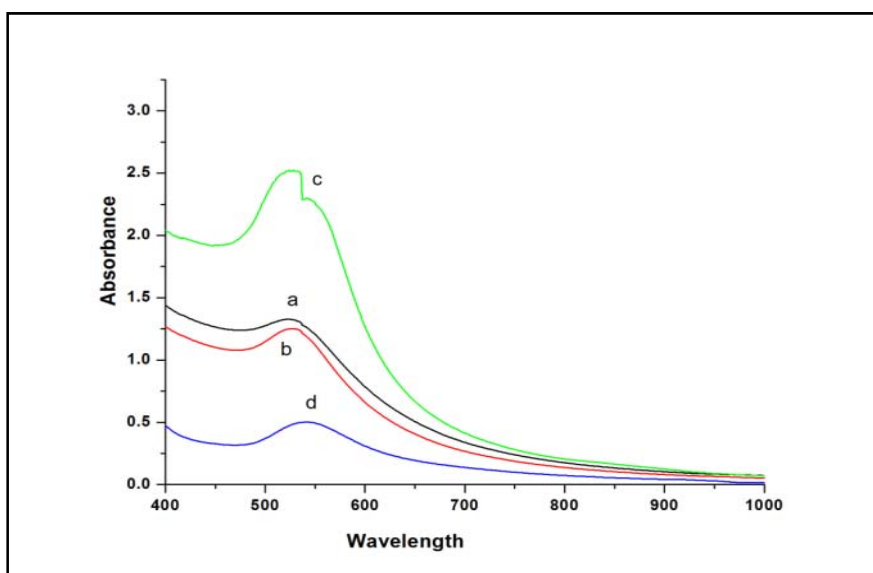


**Figure 4.17** UV-Vis spectra of poly (DSDMA) AuNPs at a) 40 °C b) at 140 °C after 1.5 h c) after 1.75.

fragment of reduction, Methacryloyl hydroxyl ethyl thiol is entrapped in the polymer chain enveloping the AuNP as reflected in the FT-IR spectrum and is further crosslinked during thermal treatment contributing to higher thermal stability. At 1:5 disulfide: Au ratio, graft density was 0.95 chain / nm<sup>2</sup>. The nanoparticles were stable upto 1.5 h which is still higher compared to DSDMA stabilized AuNPs.

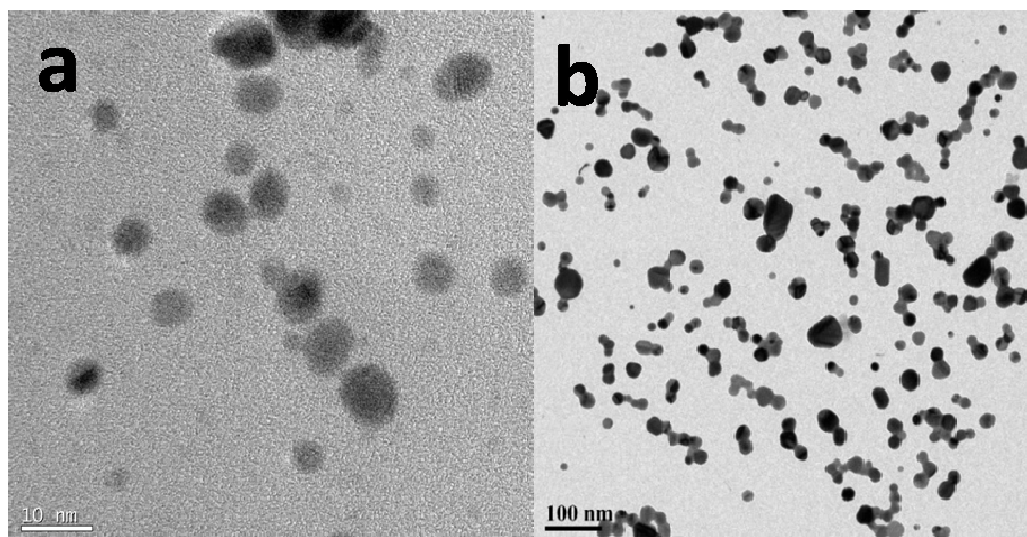


**Figure 4.18** AuNPs with 1:5 ratio of poly(DSDMA) and auric chloride a) room temperature b) 140 °C at 1.75 h.

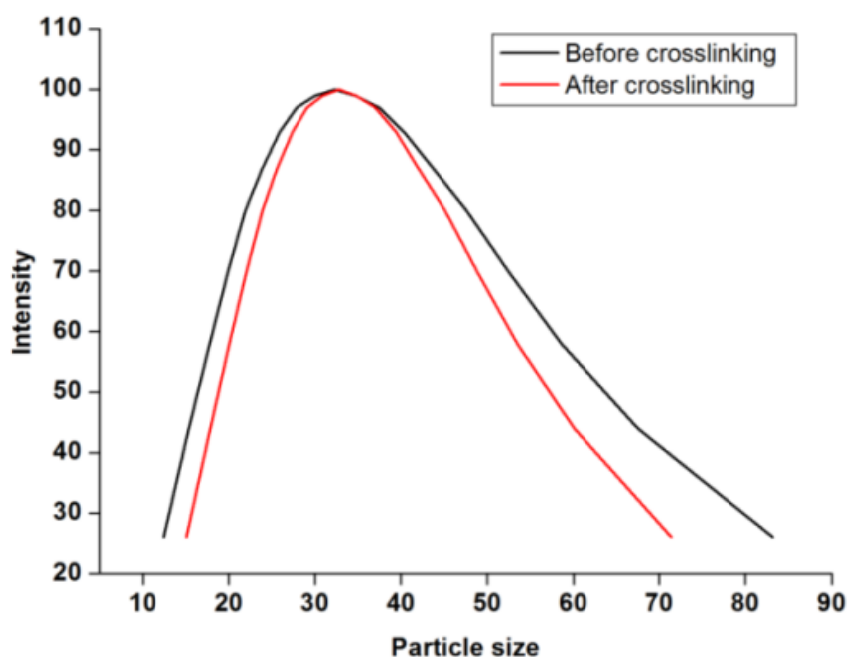


**Figure 4.19** DLS of poly(DSDMA) AuNPs before and after crosslinking.

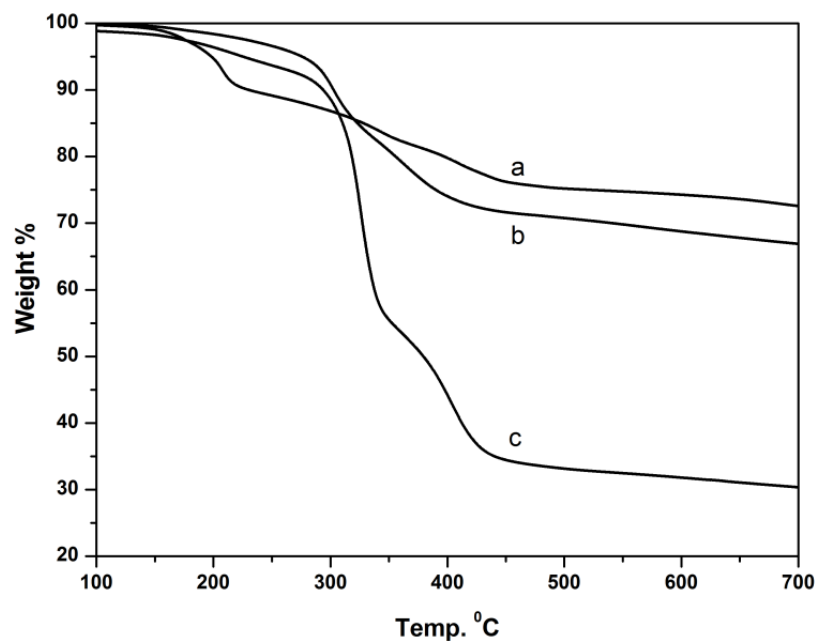


**Figure 4.20** TGA of AuNPs stabilized by a) DSDMA b) Poly(DSDMA) at 1: 10 c) 10: 1

#### 4.3.3.4 Nanocapsules

##### 4.3.3.4.1 Synthesis of nanocavities from 3.2 nm AuNPs

There is growing interest in the synthesis of hollow nanoparticles in view of their applications in drug delivery, targeting and bioimaging. Such nanocavities would also find application as nanoreactor and in extractions. The approaches used for their synthesis viz formation of assembled structures, crosslinking of micelles and emulsion polymerization have been enumerated by Boyer et al (2010).

The sacrificial template approach which involves encapsulation of nanoparticles in a polymer followed by the crosslinking of the latter and leaching out the core by treatment with etchant has been attempted by various researchers. This approach has yielded various levels of success as discussed in the preceding section. It has been noted that successful encapsulation of nanoparticles by polymers and crosslinking does not always yield nanocavities on etching. For instance crosslinking of dendritic ligand based on disulfide cores and alkenes on the periphery by Grubbs catalyst



reported by Love et al (2007) enhanced the thermal stability of AuNPs and also resistance to cyanide etching. Insoluble organic residues resulted on etching. However the presence or otherwise of nanocavities could not be established. Thus while Grubbs catalyst resulted in crosslinking of surface alkene groups which enhanced thermal and etchant stability of AuNPs, soluble nanoparticles containing cavities could not be obtained.

Koenig and Chechik (2006) reported that monomer having disulfide cores and acrylate as well as norbornene double bonds at the periphery, could be used to synthesize AuNPs. Crosslinking of acrylate with polyamines and of norbornene by ring opening metathesis polymerization resulted in higher thermal stability and resistance to etching by methyl iodide. However etching with iodine resulted in insoluble products and the formation of nanocavities could not be demonstrated.

In the preceding section we demonstrated enhancement in the thermal stability of poly(DSDMA) AuNPs as a result of concomitant crosslinking. The crosslinking of the polymer layer encapsulated AuNPs was established by the disappearance of the peak at  $1640\text{ cm}^{-1}$ . These nanoparticles were etched using methyl iodide for 24 h. No insoluble product or aggregates were observed at the end of etching. Removal of gold from the nanoparticles was visually observed by change in colour from brown to yellow. UV spectrum of the solution showed no peak at 505 nm. A peak at 362 nm appeared (Figure 4.21a) which could be attributed to  $\text{Au}^{+3}$  species and at 270 nm which could be attributed to poly(DSDMA). The peak at 362 nm disappeared on repeated extraction with methanol and dissolution in DMF while that at 270 nm was retained (Figure 4.21b). An IR analysis of the polymer showed that the characteristic peak at  $1716\text{ cm}^{-1}$  for ester and methylene stretching at  $2950\text{ cm}^{-1}$  were retained (Figure 4.22), indicating that poly(DSDMA) was not affected by etching with methyl

iodide. More specifically no CH<sub>3</sub>S peak was seen. This was consistent with the finding reported by Koenig and Chechik (2006). Analysis of the etched particles by TEM shown in Figure 4.23b clearly shows the presence of cavities of  $5 \pm 1$  nm.

Thus while crosslinked poly(DSDMA) enhances the thermal stability of the AuNPs, it also enables etching of gold to form nanocavities. We believe that the nanocavities are further stabilized by additional crosslinking between free thiols within the nanoparticles in a manner analogue to that described by Sun et al (2000) for AuNPs stabilized by thiolated cyclodextrin ligand. Using an approach similar to that reported by Yoo et al (2010), Boyer et al (2010) used block copolymer comprising poly oligoethylene glycol acrylate and styrene maleic anhydride bearing terminal thiol to stabilize 20 nm AuNPs. During the aminolysis process the RAFT end group was converted to thiol and the polymer chain was bound to the nanoparticles. Subsequent crosslinking of the anhydride with ethylene diamine resulted in crosslinked shell around gold nanoparticles. Subsequent leaching of gold by aqua regia resulted in nanocavities in 3-4 nm in size as demonstrated by TEM.

It appears that stabilization of the assembly prior to etching and high degree of crosslinking closer to the surface of the AuNPs help in the formation of nanocavities. It may be noted that in our case the AuNPs stabilized by poly(DSDMA) serve as polydentate ligand imparting enhanced stability to the assembly. Crosslinking of the unsaturated groups which are close to the surface of the AuNPs results in a structure which imparts high thermal stability and also enables retain the nanocavities formed during etching of AuNPs by methyl iodide. Further confirmation is provided by the AFM images of the etched poly(DSDMA) nanocapsules in tapping mode shown in Figure 4.24a. The height profile shown in Figure 4.24b confirms the presence of  $\sim 7$  nm capsules, which interestingly, retain the shape even after the removal of AuNPs as

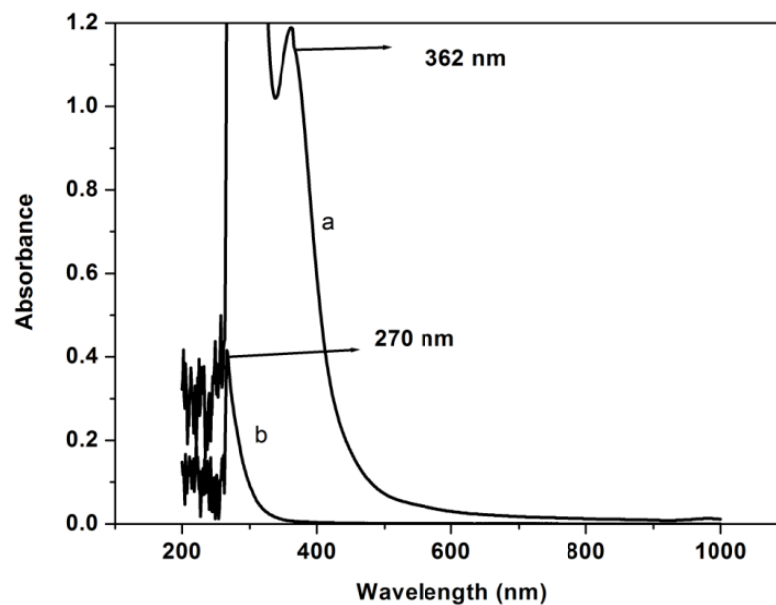


**Figure 4.21** UV-Visible spectra of etched poly(DSDMA) AuNPs a) before b) after washing

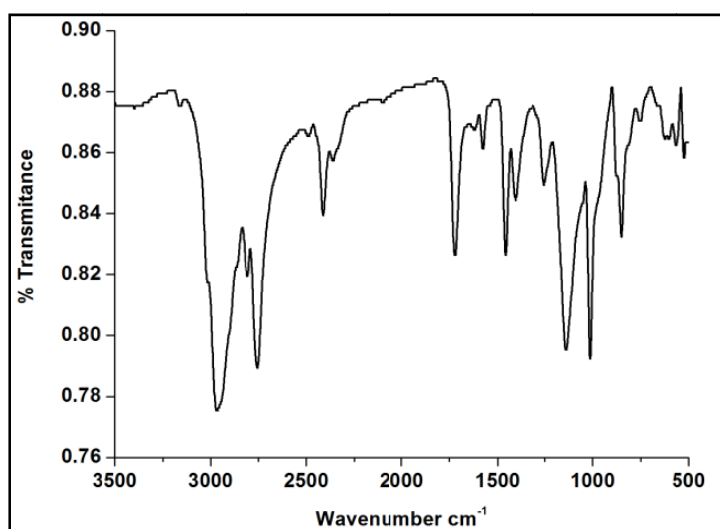


**Figure 4.22** IR spectrum of etched poly(DSDMA)

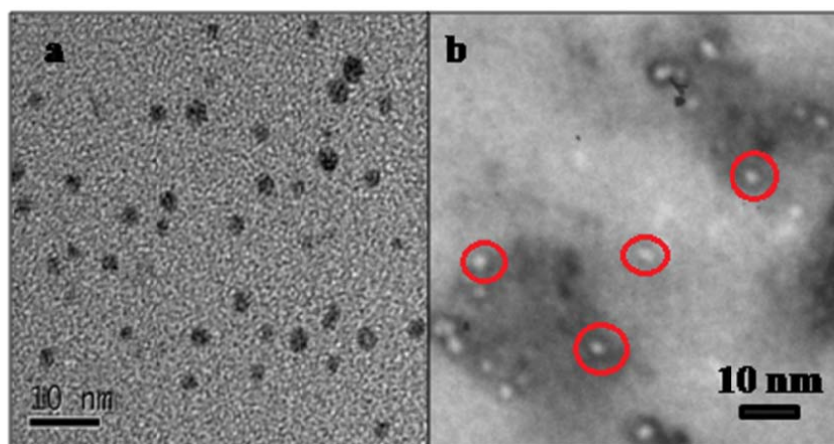


**Figure 4.23** TEM images of nanocavities from crosslinked poly(DSDMA).

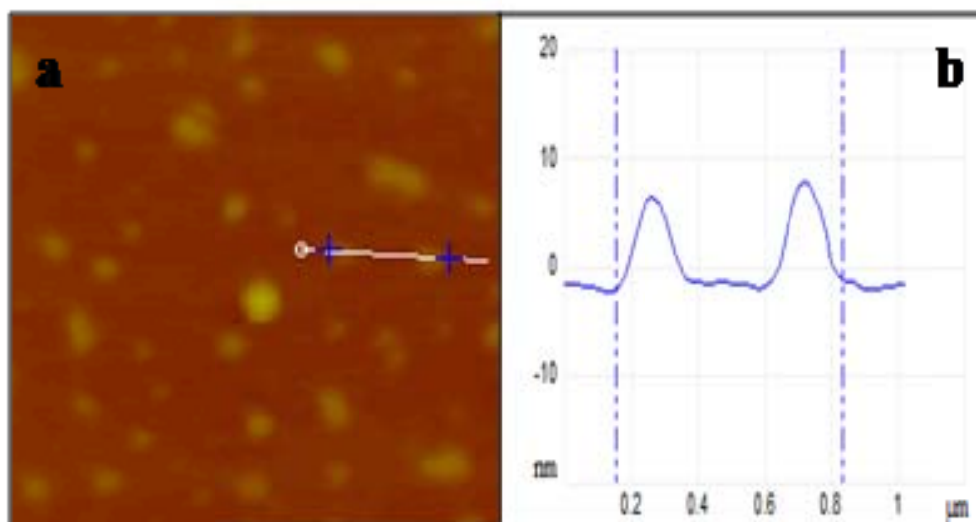


**Figure 4.24** AFM of a) Poly(DSDMA) nanocapsules b) height profiles of selected particles.

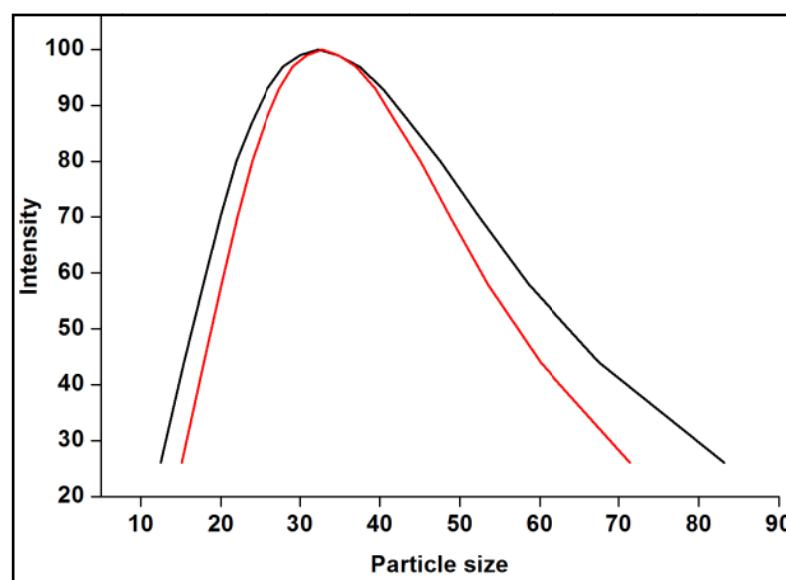


**Figure 4.25** DLS of gold etched from before crosslinking and after crosslinking of poly(DSDMA)

was reported by Wu et al (2000). The hydrodynamic size of the nanocapsules 31 nm as measured by DLS (Figure 4.25), is larger than that of the nanocavities obtained from TEM measurement (5 nm). This could be attributed to the swelling of polymer. Further the particle size obtained from DLS measurement is biased towards larger particle size (Li et al 2009 and Merican et al 2007). Interestingly the nanocapsules size remains unchanged after etching.

#### 4.3.3.4.2 Synthesis of nanocavities from 6 nm AuNPs

AuNPs prepared at disulfide to gold ratio 1: 5, resulted in particle size of 6 nm confirmed by TEM. These particles were heated at 140 °C in order to crosslink the polymer shell up to 1.25 h (before destabilization of gold nanoparticles). Thermally heated particles were treated with methyl iodide to form nanocavities. The TEM analysis showed cavities of 200 nm (Figure 4.26) which was quite larger compared to original particle size of AuNPs (6 nm). This was due to 25% capping of polymer as showed in TGA *vis a vis* 70 % in 3.2 nm particles (Figure 4.24). FT-IR also confirmed that during thermal treatment the polymer was not crosslinked and therefore did not stabilize nanocavities as in the case of nanocavities synthesized from nanocapsules obtained using disulfide: gold 10: 1. During etching of AuNPs thiols oxidised to disulfides and internally crosslinked and stabilize the nanocavities.

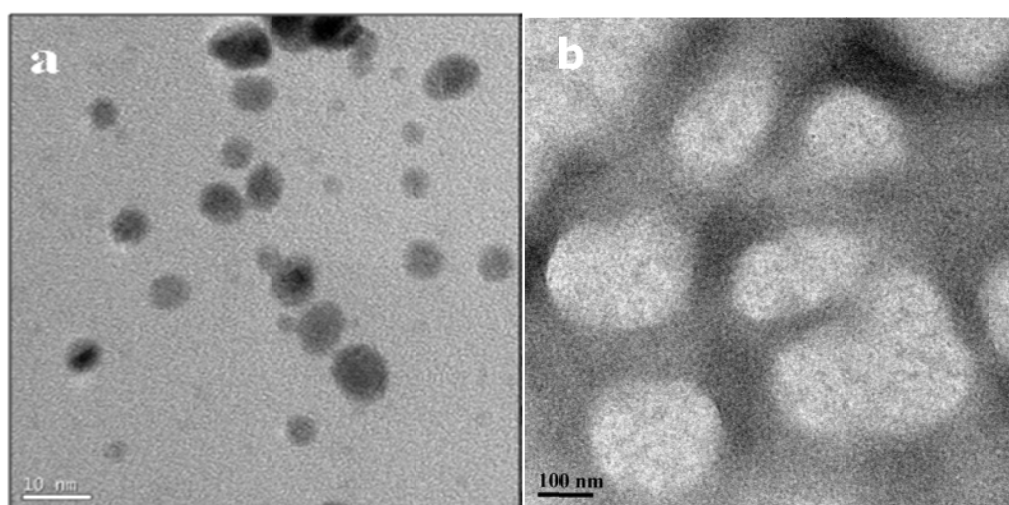


**Figure 4.26** TEM images of a) Poly(DSDMA) stabilized 6 nm AuNPs b) Nanocapsules formed on etching

#### 4.4 Conclusions

In conclusion, we have demonstrated that the use of a poly dentate ligand viz poly(DSDMA) containing pendant unsaturation can be used as a substrate for the synthesis of AuNPs upto  $2.2 \pm 0.2$  nm diameter. The stability of the nanoparticles so

formed in solvents and towards competitive ligand DTT, was considerably enhanced over that exhibited by nanoparticles stabilized on the monomer DSDMA. The thermal stability of the nanoparticles stabilized on poly(DSDMA) was further enhanced as a result of cross linking of the pendant vinyl unsaturation during the thermal treatment as was clearly demonstrated by no change in the size of the nanoparticles before and after thermal treatment. Moreover, the nanoparticles containing gold core can be readily etched by methyl iodine to yield soluble nanoparticles containing nanocavities as demonstrated by TEM and AFM analysis. Extension of this concept to hydrophilic monomers would lead to nanoparticles which will find applications in drug delivery and imaging.

**References**

1. Boyer C, Whittaker M. R., Nouvel C., Davis T. P., *Macromolecules*, 43, **2010**, 1792–1799.
2. Daniel M-C., Astruc D., *Chem. Rev.*, 104, **2004**, 293-346.
3. Ghosh S. K., Pal T., *Chem. Rev.*, 107, **2007**, 4797-4862.
4. Koenig S., Chechik V., *Langmuir*, 22, **2006**, 5168-5173.
5. Koenig S., Chechik V., *Chem. Commun.*, **2005**, 4110–4112.
6. Li C., Jiang L., Liu H., Li Y., Song Y., *ChemPhysChem*, 10, **2009**, 2058-2065.
7. Li Z., Jin R., Mirkin C.A., Letsinger R.L., *Nucleic Acid Res.*, 30, **2002**, 1558-1562.
8. Lim J., Yang H., Paek K., Cho C., Kim S., J. Bang, B. J. kim, *J. Poly. Sci. Part A: Poly. Chem.*, 49, **2011**, 3464–3474.
9. Liu X., Li C., Xu J., Lv J., Zhu M., Guo Y., Cui S., Liu H., Wang S., and Li Y., *J. Phys. Chem. C*, 112, **2008**, 10778-10783.
10. Love C. S., Ashworth I., Brennan C., Chechik V., Smith D. K., *Langmuir*, 23, **2007**, 5787-5794.
11. Love C.S., Chechik V., Smith D.K., and Brennan C., *J. Mat. Chem.*, 14, **2004**, 919.
12. Merican Z., Schiller T. L., Hawker C. J., Fredericks P. M., Blakey I., *Langmuir*, 23, **2007**, 10539-10545.
13. Pellegrino T., Kudera S., Liedl T., Javier A. M., Manna L., Parak W. J., *Small*, 1, **2005**, 48-63.
14. Rastogi S. K., Denn B. D., Branen A. L., *J. Nano. Res.* 14, **2012**, 673.
15. Roux S., Garcia B., Bridot J-L, Salome M., Marquette C., Lemelle L., Gillet P., Blum L., Perriat P., Tillement O., *Langmuir*, 21, **2005**, 2526-2536.

16. Sakata T., Maruyama S., Ueda A., Otsuka H., Miyahara Y., *Langmuir*, 23, **2007**, 2269-2272.
17. Satav S.S., Karmalkar R.N., Kulkarni M.G., Mulpuri N., Sastry G.N., *J. Am. Chem. Soc.*, 128, **2006**, 7752-7753.
18. Shan J., Nuopponen M., Jiang H., Kappinen E., Tenhu H., *Macromolecules*, 36, **2003**, 4526 – 4533.
19. Shimmin R.G., Schoch A.B., Braun P.V., *Langmuir*, 20, **2004**, 5613-5620.
20. Sun L., Crooksa R.M., Chechik V., *Chem. Commun.*, **2001**, 359–360.
21. Wang Z., Tan B., Hussain I., Schaeffer N., Wyatt M. F., Brust M., Cooper A. I., *Langmuir*, 23, **2007**, 885-895.
22. Wu M., O'Neill S. A., Brousseau L.C., McConnell W. P., Shultz D. A., Linderman R. J., Feldheim D. L., *Chem. Commun.*, **2000**, 775–776.
23. Wuelfing W. P., Gross S. M., Miles D. T., Murray R. W. *Journal of American Chemical Society*, 120, **1998**, 12696 – 12697.
24. Yoo M., Kim S., Lim J., Kramer E.J., Hawker C. J., Kim B. J., Bang J., *Macromolecules*, 43, **2010**, 3570–3575.
25. Yonezawa T., Yasui K. and Kimizuka N., *Langmuir*, 17, **2001**, 271-273.
26. Zhang S., Leem G., Srisombat L., Lee T. R., *J. Am. Chem. Soc.*, 1, **2001**, 113-120.



---

---

**Chapter 5**  
**Characterization of gold nanoparticles**

---

---

## 5.1 Introduction

Gold nanoparticles (AuNPs) are of particular interest because of their unique electronic, optical, thermal and magnetic properties (Daniel and Astruc 2004, Ghosh and Pal 2007, Liu et al 2008, Rastogi et al 2012), which are useful in drug delivery and catalysis (Torchilin 2006). Physicists predicted that AuNPs in the size range 1-5 nm, would exhibit distinct electronic and magnetic properties, (Daniel and Astruc 2004) depending on the particle size, interparticle distance, nature of the protecting ligand, and shape of the AuNPs (Brust et al 2002).

In chapter 4 we demonstrated that stability of poly(DSDMA) stabilized AuNPs against solvent, thiol exchange and temperature could be enhanced as result of polydentate character. In this chapter we report characterization of poly(DSDMA) stabilized AuNPs using XRD for particle size, XPS for oxidation state, DPV and STM for size dependent electronic properties and ESR for magnetic properties.

## 5.2 Experimental section

### 5.2.1. Materials

Purified AuNPs of size 2.2 nm to 8 nm. Dichloromethane (DCM) (GR grade), were purchased from SD fine chemicals, India.

### 5.2.2 Instrumentation

#### 5.2.2.1 Wide angle X-ray diffraction (XRD)

Powder X-ray diffraction (XRD) patterns of poly(DSDMA) AuNPs were recorded on a Rigaku Dmax 2500 diffractometer with Cu K $\alpha$  (1.541Å) radiation (40 kV, 100 mA). Powder samples were mounted on a sample holder and scanned in the range  $2\theta = 30$  to  $80^\circ$ .

### 5.2.2.2 Electron paramagnetic resonance (EPR)

The EPR spectra were recorded on a Bruker EMXEPR spectrometer at liquid nitrogen temperature.

## 5.3 Results and discussion

Tailoring electronic properties of AuNPs is critical for developing electrical devices superior to semiconductor based integrated circuits and information storage devices. There is therefore growing interest in nanoparticles which exhibit Coulomb blockade that manifests single electron tunnelling at room temperature. (Drexler 1986, Zaitoun et al 2001, Grohn et al 2003)

### 5.3.1 XRD Analysis

Figure 5.1 shows the XRD analysis of AuNPs using poly(DSDMA) concentration 1 to 25 mM and auric chloride 1 to 10 mM. The particle size calculated from Scherrer's equation decreased from 8.3 nm, to 2.2 nm with increase in disulfide to gold ratio from 25:1 to 1:10. The results are consistent with the findings from UV-Visible spectrum as well as TEM analysis. The diffraction peaks in figures 5.1d, e and f of AuNPs size 8.3 nm, 6.4 nm and 3.3 nm are typical of fcc structure. For particle size less than 3.3 nm, only broad prominent 111 peak was observed (Figure 5.1b and c). These results are similar to those Chen and Kimura (1999) who demonstrated a decrease in the particle size from 3.4 nm to 1 nm with increasing thiol to gold ratio from 0.5 to 2.5 and that at particle size 3.4 nm all fcc planes were seen and at 1.2 nm particle size only 111 plane was seen.

### 5.3.2 X-ray photoelectron spectroscopy (XPS)

XPS analysis of poly(DSDMA) stabilized AuNPs of size 2.2 to 3.2 nm was undertaken. The binding energies (Au 4f<sub>7/2</sub> 83.9 eV and Au 4f<sub>5/2</sub> 87.8 eV) of AuNPs size 2.2 nm were comparable to those of bulk (Au 4f<sub>7/2</sub> 84.0 eV and Au 4f<sub>5/2</sub> 87.6 eV).

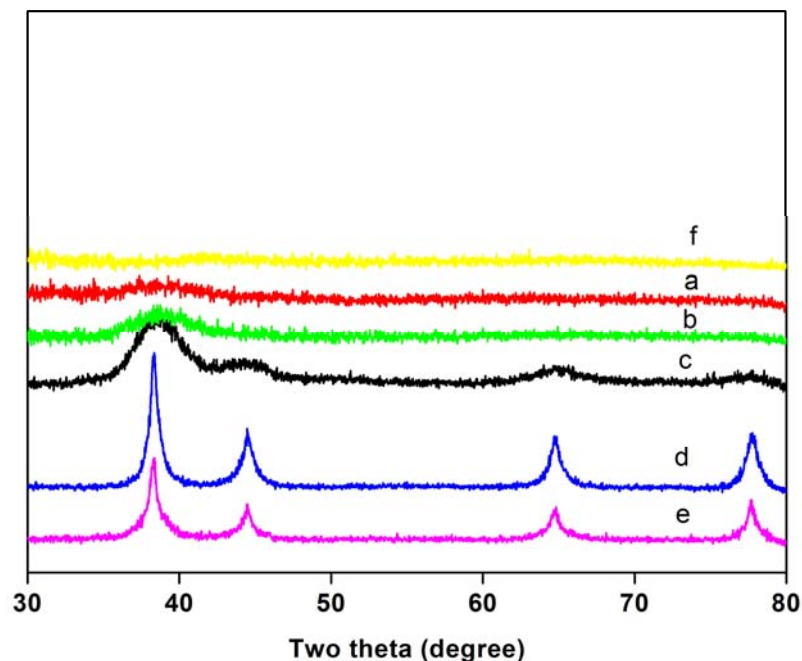


**Figure 5.1** XRD of AuNPs prepared at disulfide to gold a) 25:1 b) 10 :1 c) 1:1 d) 1:5 e) 1: 10 f) polymer

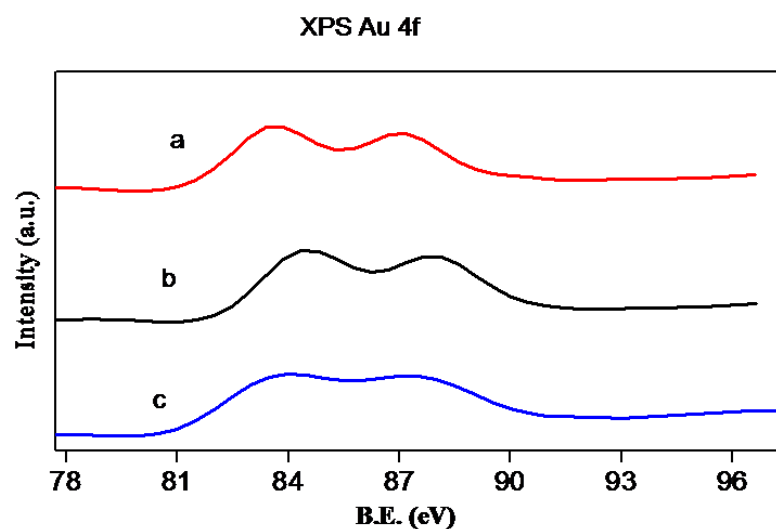


**Figure 5.2** Binding energies of poly(DSDMA) stabilized AuNPs of particle size a) 2.2 nm b) 2.8 nm c) 3.2 nm.

The difference could be attributed to the particle size (Wang et al 2008). Increase in particle size from 2.8 nm to 3.2 nm resulted in increase in binding energy (Au4f<sub>7/2</sub> 84.5 eV and Au 4f<sub>5/2</sub> 88.32 eV) (Au 4f<sub>7/2</sub> 85.1 eV and Au 4f<sub>5/2</sub> 89.02 eV). The observation is in agreement with that of Radnik et al (2003) and Balamurgan et al

(2005). These binding energies confirm that AuNPs are in zero oxidation state (Figure 5.2).

### 5.3.3 Differential pulse voltametry (DPV)

One of the distinctive features of ultra small nanoparticles is the room temperature single electron tunneling also known as “Coulomb blockade effect”, which is the energy necessary to place an extra electron on a nanoparticle, arising due to the Coulombic repulsion among electrons (Dorogi et al 1995, Andres et al 1996, Feldheim, et al 1998, Thomas et al 2000). This electrostatic energy can be viewed as the difference between the electron affinity and the ionization potential of the nanoparticle, termed as the charging energy ( $E_C = e^2/2C \gg k_B T$  where  $C$  is the capacitance of the particle). To observe single electron tunneling,  $E_C$  should be greater than  $k_B T$ , in order to restrict the thermal motion of electrons. Accordingly, for each extra electron to be tunneled an “ $e/C$ ” amount of voltage is required for an increase of “ $e/R_T C$ ” amount of tunneling current ( $R_T$  is the tunnel resistance). The Coulomb blockade effect was initially observed for metal islands at low temperature, and subsequently for passivated nanoparticles attached on electrode surface. Evaluation of monolayer stabilized metallic nanoparticles, especially thiol stabilized AuNPs (1.1-3 nm) investigated in the past, revealed quantized double layer charging (QDL) resulting from sub autofarad capacitance, which led to coulomb blockade at room temperature. For example, Chaki et al (2004) reported that  $3.72 \pm 0.4$  nm AuNPs stabilized by dodecane thiol were accessible to single electron charging. More interestingly, differential pulse voltametry (DPV) revealed multiple QDL charging events. In this context, it was interesting to investigate the DPV characteristics of the AuNPs stabilized on DSDMA as well as poly(DSDMA). The superimposed DPV responses for 2.2, 2.8 and 3.2 nm AuNPs stabilized on poly(DSDMA) using 0.5 mM

TBAHFP as supporting electrolyte in dichloromethane using Pt ultra microelectrode (20  $\mu\text{m}$ ) at scan rate 25 mV/s are shown in Figure 5.3. Since AuNPs were formed by reduction in the presence of  $\text{NaBH}_4$ , they were considered to have a charge  $Z = -1$ . Accordingly, the first oxidation and reduction processes were  $-1/0$  and  $-2/-1$ . The  $-1/0$  as well as  $0/1$  charge steps are marked with respect to platinum quasi reference electrode. It is interesting to note that full width at half maximum (FWHM) value of 94 mV for 2.2 nm AuNPs is very close to that for an ideal single electron transfer process, 90.6 mV (Chen et al 1998) for conventional redox species and yields a capacitance of 1.7 aF obtained from the Z plot. Increase in particle size to 2.8 and 3.2 nm, results in decrease in FWHM values to 64 and 61 mV, which are greater than the range 50-55 mV reported for dodecane thiol stabilized AuNPs and demonstrate the QDL process for these AuNPs. The corresponding capacitance values are 2.5 and 2.62 aF respectively (Chaki et al 2004). More particularly, the results signify that the AuNPs stabilized on the polydentate ligand poly(DSDMA) are accessible to single electron charging. In contrast, the 2.8 nm AuNPs stabilized on DSDMA did not exhibit these characteristics probably because of broader size distribution which would result in still higher capacitance (Chen et al 1998) as well as differences in ligand binding.

The DPV plots (Figure 5.4) revealed a highly populated evenly spaced (ca.80-90 mV) current peaks for AuNPs stabilized on poly(DSDMA) (2.2 nm size) before crosslinking. After crosslinking these are lost despite the fact that the particle size is constant. This could be attributed to crosslinking of polymer shell, which forms an impermeable coating around AuNPs.

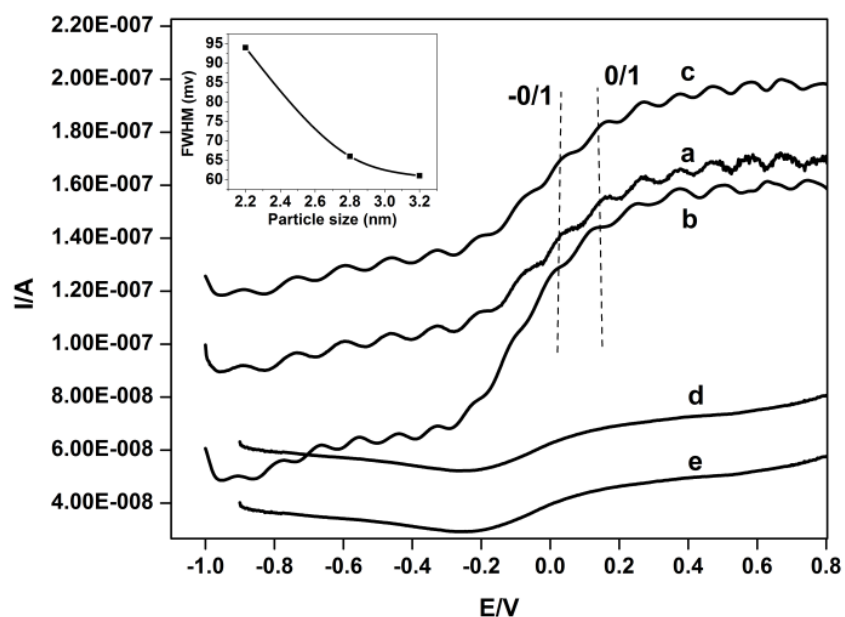


**Figure 5.3** Superimposed DPV responses of AuNPs for particle size a) 2.2 nm b) 2.8 nm c) 3.2 nm stabilized on Poly DSDMA d) 2.8 nm stabilized on DSDMA e) Blank.

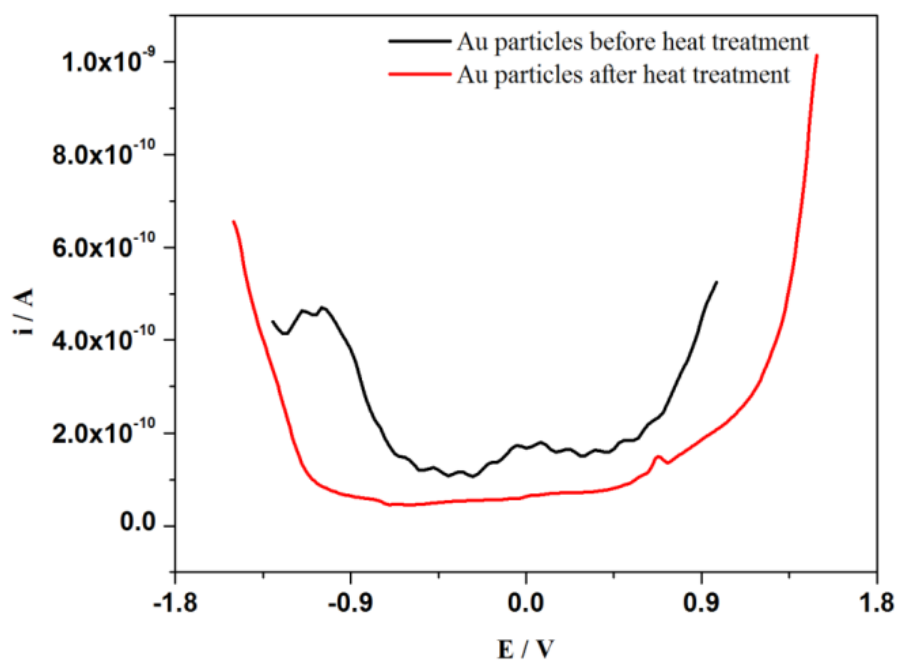


**Figure 5.4** DPV responses of AuNPs size 3 nm before and after heating.

### 5.3.4 Scanning tunnelling microscope (STM)

Like high-resolution electron microscopy, STM techniques also have facilities for direct imaging of structures. As discussed in previous section DPV clearly shows coulomb blockade effect. Similarly STM is a technique which can we monitor the

single electron charging of AuNPs. The poly(DSDMA) stabilized 3.2 nm particles are investigated for single electron charging, results are shown in Figure 5.5.

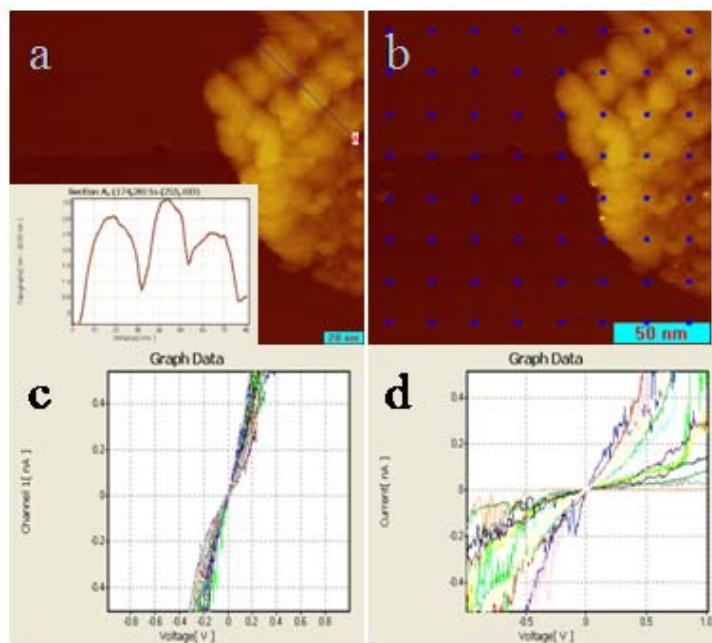


**Figure 5.5** STM image of a) AuNPs with height profile b) AuNPs c) I-V profile on HOPG surface d) I-V curve on AuNPs.

The sample for STM analysis was prepared depositing a drop of dilute nanoparticle solution on highly oriented pyrolytic graphite (HOPG) substrate followed by drying for 5 min. STM studies were carried out immediately after deposition. The particle size measured from STM is 3.5 nm which is in good agreement with particle size obtained from TEM (3.2 nm). STM studies indicate that these particles are accessible for single electron charging. I-V behaviour obtained from the STM measurements on a single particle shows a clear Coulomb blockade effect (Figure 5.5d).

### 5.3.5 Electron paramagnetic resonance (EPR) characterization

Interaction between thiol and Au atoms on the surface of nanoparticles which alters the electronic structure of the latter, is known to induce localized magnetic moment and influence the magnetic behavior. While bulk gold is diamagnetic, AuNPs stabilized with alkanethiols exhibit ferromagnetic behavior at room temperature,



below a critical threshold size. The presence of iron impurities if any, does not contribute to this behavior (Zhu et al 2009, Marquez et al 2010). However, the interpretation of the results is often rendered difficult by the differences in particle size and size distribution (Zhu et al 2009). Since the AuNPs stabilized on poly(DSDMA) are in the range  $2.2\text{-}3.2 \pm 0.1$  nm, it was interesting to evaluate their magnetic behavior. From Figure 5.6 A (plots a, b and c) the paramagnetic behavior at 77 K. The g values were 2.017, 2.015 and 2.013 for 2.2, 2.8 and 3.2 nm particles with significant peak broadening at room temperature. As the particle size increased to 6 and 8 nm, diamagnetic behavior was observed even at 77 K was evident (Figure 5.6 B plots d and e).

Guerrero et al (2008) synthesized thiol stabilized 2-2.5 nm AuNPs using dodecanethiol and tiopronin. The AuNPs synthesized using tetraoctyl ammonium bromide exhibited bimodal distribution with diameters 1.5 and 5 nm. Dodecanethiol capped AuNPs exhibited behavior characteristic of ferromagnetic materials, tiopronin stabilized AuNPs exhibited paramagnetic behavior while tetraoctyl ammonium bromide stabilized AuNPs were diamagnetic. The differences in the magnetic behavior were shown to result from differences in the surface electronic structure caused by binding between Au atoms and thiol ligands. In the case of linear dodecanethiols, intermolecular interactions between Au and dodecanethiol are enhanced as the latter can self assemble. Interactions are not as strong in the case of tiopronin as it does not favor self assembly. Thus paramagnetic behavior results from fluctuations in orientation of spins, induced through binding of sulfur and Au atoms. Clearly the presence of disulfide in the pendent chain of poly(DSDMA) precludes formation of self assembled monolayers and binding enhancement of the type possible in the case of dodecanethiol. Yet binding between polydentate

poly(DSDMA) and gold atoms on the surface of AuNPs is more extensive as compared to that in the case of DSDMA. This is probably why AuNPs stabilized on poly(DSDMA) are paramagnetic. In contrast the AuNPs stabilized on DSDMA are diamagnetic at 77 K even for the particle size of 2.8 nm (Figure 5.6 B plot f) which could be attributed to weaker binding in the case of DSDMA.

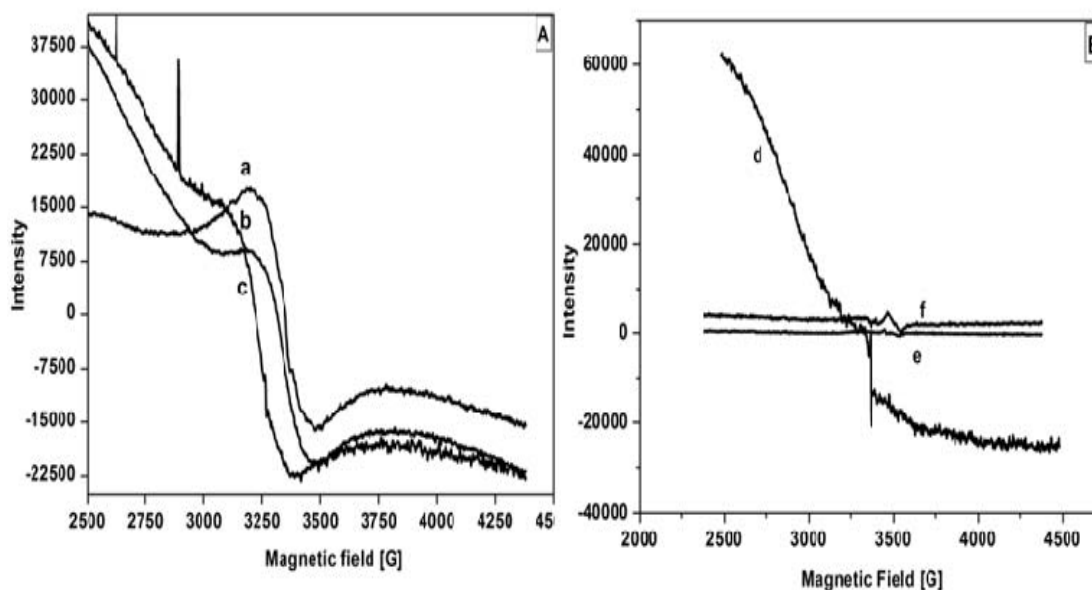


**Figure 5.6** Electron Paramagnetic Resonance spectra (EPR) of AuNPs stabilized on Poly (DSDMA) of size a) 2.2 nm b) 2.8 nm c) 3.2 nm d) 6 nm e) 8 nm f) DSDMA stabilized 2.8 nm AuNPs.

Venta et al (2007) recently showed that the magnetic properties are unaffected when the thiol stabilized AuNPs are incorporated in polyethylene matrices and that such composite could be useful for the development of devices. Poly(DSDMA) stabilized AuNPs can be easily cast in to films from solution and crosslinked which should be especially beneficial in such applications.

#### 5.4 Conclusions

Gold nanoparticle sizes calculated using Scherer equation were comparable with those obtained from TEM results and XPS confirmed that AuNPs were in zero oxidation state. Poly(DSDMA) stabilized AuNPs of size 2.2 nm to 3.2 nm were small

enough to exhibit coulomb blockade in DPV and STM at room temperature and exhibited paramagnetic behavior at 77K. These characteristics would be useful for electronic storage devices.

**References**

1. Andres R. P., Bein T., Dorogi M., Feng S., Henderson J. I., Kubiak C. P., Mahoney W., Osifchin R. G., Reifengerger R., *Science*, 272, **1996**, 1323–1325.
2. Balamurugan B., Maruyama T., *Appl. Phys. Lett.*, 87, **2005**, 143105.
3. Brust, M., Kiely, C. J., *Colloids Surf. A: Physicochem. Eng. Asp*, 202, **2002**, 175-186.
4. Chaki N., Singh P., Dharmadhikari C. V., Pillai V. K., *Langmuir*, 20, **2004**, 10208–10217.
5. Chen S., Ingram R. S., Hostetler M. J., Pietron J. J., Murray R. W., Schaaff T. G., *Science*, 280, **1998**, 2098–2101.
6. Chen S., Kimura K., *Langmuir*, 15, **1999**, 1075-1082.
7. Chen S., Murray R. W., Feldberg S. W., *J. Phys. Chem. B*, 102, **1998**, 9898–9907.
8. Daniel M.-C., Astruc D., *Chem. Rev.*, 104, **2004**, 293–346.
9. Dorogi M., Gomez J., Osifchin R., Andres R. P., Reifengerger R., *Phys. Rev. B: Condens. Matter Mater. Phys.*, 52, **1995**, 9071–9077;
10. Drexler, K. E., *Engines of Creation: The Coming Era of Nanotechnology*; Anchor Press/ Doubleday: New York, **1986**.
11. Drexler, K. E. *Nanosystems: molecular machinery, manufacturing and computation*; John Wiley & Sons: New York, **1992**.
12. Feldheim D. L., Keating C. D., *Chem. Soc. Rev.*, 27, **1998**, 1–12.
13. Ghosh S. K., Pal T., *Chem. Rev.*, 107, **2007**, 4797–4862.
14. Guerrero E., Munoz -Marquez M. A., Garcia M. A., Crespo P., Fernandez-Pinel E., Hernando A., Fernandez A., *Nanotechnology*, 19, **2008**, 175701.

15. Grohn, F., Bauer B. J., Amis E., *J. Phys. Chem. A*, 107, **2003**, 3424
16. Liu X., Li C, Xu J., Lv J., Zhu M., Guo Y., Cui S., Liu H., Wang S., Li Y., *J. Phys. Chem. C*, 112, **2008**, 10778–10783.
17. Lucena R., Conesa J. C., *J. Nano Res.*, 12, **2010**, 1307–1318.
18. Munoz-Marquez M. A., Guerrero E., Fernandez A., Crespo P., Hernando A., Thomas P. J., Kulkarni G. U., Rao C. N. R., *Chem. Phys. Lett.*, 321, **2000**, 163–168.
19. Munoz - Marquez M. A., Guerrero E, Fernandez A., Crespo P., Hernando A., Lucena R., Conesa J. C., *J. Nano Res.*, 12, **2010**, 1307–1318.
20. Radnik J., Mohr C., Claus P., *Phys. Chem. Chem. Phys.*, 5, **2003**, 172–177.
21. Rastogi S. K., Denn B. D., Branen A. L., *J. Nano Res.*, 14, **2012**, 673.
22. Torchilin V. P., *Adv. Drug Delivery Rev.*, 58, **2006**, 1532.
23. Venta J. D., Pucci A., Pinel E. F., Garcia M. A., Fernandez C. J., Crespo P., Mazzoldi P., Ruggeri G., Hernando A., *Adv. Mater.*, 19, **2007**, 875–877
24. Wang Z., Zhang Q., Kuehner D., Ivaskab A., Niu L., *Green Chem.*, 10, **2008**, 907–909.
25. Zaitoun, M. A., Mason W. R., Lin C. T., *J. Phys. Chem. B*, 105, **2001**, 6780.
26. Zhu M., Aikens C. M., Hendrich M. P., Gupta R., Qian H., Schatz G. C. Jin R., *J. Am. Chem. Soc.*, 131, **2009**, 2490–2492.
27. Munoz M. A., Guerrero E, Fernandez A., Crespo P., Hernando A., Lucena R., Conesa J. C., *J. Nano Res.*, 12, **2010**, 1307–1318.

---

---

**Chapter 6**  
**One pot room temperature synthesis of robust gold nanochains**

---

---

## **6.1 Introduction**

Research efforts on tailoring metal nanoparticles have focused on a) manipulation of shape, size and distribution nanoparticles and b) controlled aggregation of the nanoparticles into arrays, which exhibit unusual properties and lead to applications not hitherto realized (Wang et al 2002, Wu et al 2008, Lee et al 2011). While significant progress has been made in the design of 3D and 2 D assemblies, (Kotov et al 1994, Pileni 2001, Lin et al 2001, Shi et al 2007) the design of 1D assemblies still poses challenges in view of the need for directional aligning of zero dimensional nanoparticles which do not exhibit anisotropic properties. The unique optical, magnetic and electrical properties of nanochains lead to applications in optoelectronics, as single electron transistors, as interconnects in electronic and sensing devices, wave guides, as well as miniaturized photonic devices and biomedical devices (Pissuwan et al 2006, Yurekli et al 2003, Bae et al 2005, Dimitrakopoulos et al 2002 Rezaee et al 2010, Yang and Kim 2002, Gunawidjaja et al 2009, Biswas et al 2010). This has motivated researchers to explore new approaches for the synthesis of robust nanochains.

Strategies for the synthesis of nanochains were summarized by Zhang and Zeng (2006). Murugadoss and Chattopadhyay (2008) reported that citrate stabilized AuNPs form nanochains at pH 3.5, on increasing concentration of acetanilide as a result of interaction between negatively charged AuNPs and protonated acetanilide. Tsai et al (2010) showed that an increase in ion concentration of solution containing nanoparticles results in gold nanochains as attractive van der Waals forces overcome repulsive Coulomb forces.

Apart from these physical interactions, formation of nanochains as a result of chemical linkages between AuNPs has been reported. Wang et al (2002) reported the

formation of gold nanochains from alkane thiol and pyrrole functionalized alkane thiol AuNPs via chemical oxidation of pyrrole unit in solution. Lai et al (2011) synthesized gold nanochains in aqueous medium by the UV light triggered photolysis of light responsive o - nitro benzyl derivative thioctic acid 3-3 (3-hydroxymethyl-4-nitro phenoxy) - propyl ester functionalized AuNPs, which leads to condensation with (thioctic acid 4-amino methyl benzyl amide) functionalized AuNPs resulting in indazolone linkages. More recently, Lee et al (2011) demonstrated synthesis of gold nanochains by the interaction of carboxylates on the citrate stabilized AuNPs with the imine in N-ethyl-N'-(dimethyl amino propyl) carbodiimide (EDC).

In view of limited stability of gold nanochains, efforts have been made to enhance the same by encapsulation in suitable matrices. Fernandes et al (2010) exploited the electric dipole dipole interaction resulting from ligand exchange between [(bis(p-sulfonato-phenyl) phenylphosphine (BSPP) or citrate] and AuNPs capped partially with [(46-mercapto-22,43-dioxo - 3,6,9,12,15,18 - hexaoxa - 21,44 - diazahexatetraconta-31,33-diyne-1-oic acid] (DA-PEG). These were destabilized by centrifugation to yield nanochains, which were then encapsulated in the polymer formed by UV induced photocrosslinking of DA-PEG. Similarly the citrate capped AuNPs were exchanged with 2 mercapto ethanol and destabilized by incubation to yield nanochains which were then encapsulated in a silica layer formed by the polycondensation of mercapto propyl triethoxysilane and tetra ethyl orthosilicate. However, during the process  $\lambda_{max}$  blue shifted by 34 nm to 668 nm. Cho et al (2010) formed linear assemblies from AuNPs by adding alkane thiol carboxylic acids in the mixture of water and ethanol. The chain length was governed by the ligand concentration and the inter particle separation by the number of alkane groups in the ligand. The stability of chains was enhanced by encapsulation in silica or gelatin.



Poly(amidoamine) dendrimers and hyperbranched poly(amidoamines) have been shown to reduce and stabilize the AuNPs at room temperature (Shi et al 2009, Zhang et al 2008 and Harada et al 2009). In contrast, the AuNPs formed on linear poly(amidoamines) were unstable, which was attributed to the chain entanglements (Zhang et al 2008).

The stability of the AuNPs could be enhanced by enhancing the binding between the ligand and the AuNPs. In a recent communication, we showed how the stability of AuNPs could be enhanced by using a polydentate thiol (Biradar et al 2012). We now explore new strategies to obtain stable nanochains from AuNPs. Amine functionalized polymers stabilize AuNPs by physisorption and are therefore not so robust. Chen et al (2011) reacted amines in the pendent chain of poly (allyl amine hydrochloride) with carbon disulfide to yield a dithiocarbamate, which chemisorbed AuNPs. The multi point binding of dithiocarbamate on the polymer chain with AuNPs enhanced the stability of AuNPs, although no chains were reported.

In this communication we show that the low molecular weight PAmAm acts as both reducing and stabilizing substrate during the synthesis of AuNPs at room temperature. With decreasing ratio of poly(amidoamine) to auric chloride, there is a transition from isolated nanoparticles to linear chain, which suggests that the linear morphology probably results from non uniform distribution of the stabilizer as suggested by Wu et al (2008). However, a more systematic analysis reveals that the pH of the medium plays a more crucial role. The nanochains are formed as a result of dipolar coupling between AuNPs and tertiary amine group under acidic pH conditions (Murugadoss and Chattopadhyay 2008) and the isolated nanoparticles are formed at basic pH as a result of coordination of t-amino group with the AuNPs (Miyamoto et al 2008). Under both conditions the binding between the nanoparticles and amine group in the

main chain of the polymer is so strong that the morphologies are stable towards change in pH, temperature and salt concentration.

## **6.2. Experimental section**

### **6.2.1. Materials**

Bisacrylamide (MBA), Piperazine (PY), Deuterated water (D<sub>2</sub>O) (99.9 % D), Auric chloride (HAuCl<sub>4</sub>.3H<sub>2</sub>O) (99.9%) were purchased from Aldrich chemicals USA. Acetone (GR grade), was purchased from SD fine chemicals India. Sodium hydroxide and Hydrochloric acid (35%) were purchased from Merck, India.

### **6.2.2. Measurements**

#### **6.2.2.1. UV-Vis spectrophotometry**

UV-Vis absorption spectra were recorded on Shimadzu UV-Visible spectrophotometer UV-1601PC model, in the wavelength range 200 - 1000 nm.

#### **6.2.2.2. Fourier transform infrared (FT-IR) spectroscopy**

The FTIR studies were carried out using Perkin Elmer Spectrophotometer, UK in diffused reflectance mode. The samples were milled with KBr. The spectra were recorded over the frequency range 3500 -500 cm<sup>-1</sup> at resolution 4 cm<sup>-1</sup>.

#### **6.2.2.3 Gel permeation chromatography (GPC)**

Molecular weight of PAmAm was determined at 25 °C using aqueous size exclusion chromatography equipped with TSK-GEL columns using 0.2 M NaNO<sub>3</sub> at a flow rate 1 mL min<sup>-1</sup>. The columns were calibrated using Polyethylene Glycol standards.

#### **6.2.2.4 Nuclear magnetic resonance (NMR) spectroscopy**

<sup>1</sup>H NMR measurements were carried out on DRX -200 spectrometer, operating at a proton frequency 200 MHz.

**6.2.2.5. Dynamic light scattering (DLS)**

The particle size was measured on Malvern Brookhaven Instrument Corporation 90 plus particle size analyser at 25 °C in water with the laser operating at 659 nm. The scattered light intensity was measured at 90°.

**6.2.2.6 Transmission electron microscopy (TEM)**

FEI Technai, Transmission electron microscope was operated at accelerating voltage 200 kV. The samples were prepared by drop casting on carbon coated grid and dried at room temperature overnight.

**6.2.3 Polymer synthesis**

The procedure reported by Day and Ray (2003) was slightly modified. 2 g MBA (0.014 moles) was dissolved in 10 ml DI water and cooled to 5 °C since the condensation with amine is exothermic. 1.2 g (0.015 moles) piperazine dissolved in 5 ml water, was added dropwise. After the addition was complete, the solution was stirred under nitrogen atmosphere for 24 h at room temperature, which turned viscous with time. It was poured into acetone to precipitate PAmAm as a white powder which was filtered, washed with acetone and dried under vacuum. (Yield 80 %).

**6.2.4 AuNP synthesis**

50 ml 1mM auric chloride solution was added to 50 ml aqueous PAmAm solution. The polymer concentration was varied in the range 30 mM to 1.5 mM (Figure 6.1). The nanoparticles were recovered by centrifugation at 10,000 rpm and were washed repeatedly with water.

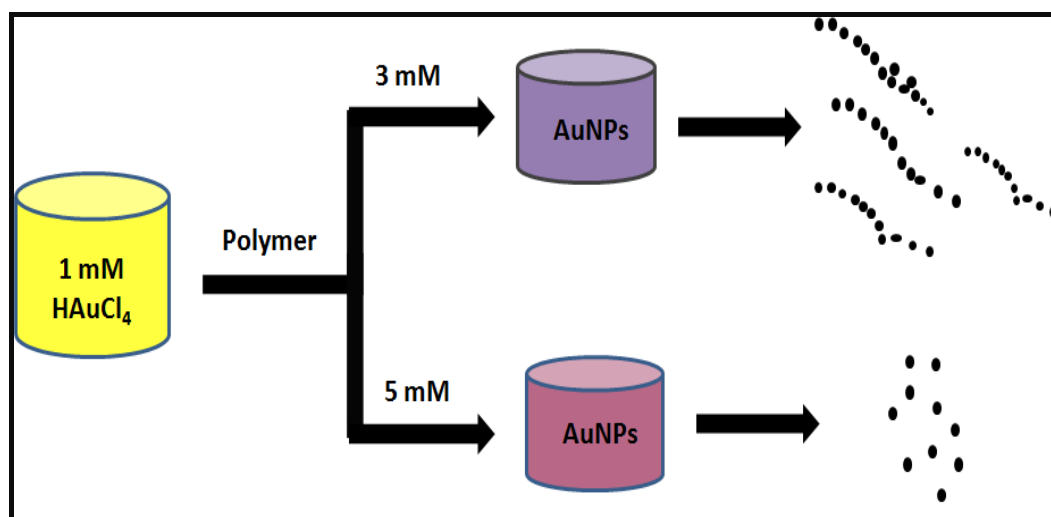


**Figure 6.1** Schematic for synthesis of gold nanoparticles and nanochains

### 6.3 Results and discussion

The importance of gold nanochains, the strategies for their synthesis using both template based and template free methods and the merits of the latter have been well documented (Tsai 2010). While Wu et al (2008) reported a single step synthesis of gold nanochains using low mol wt Chitosan, the synthesis had to be carried out at 125<sup>0</sup> C. In view of the reduction of Au<sup>+3</sup> to Au<sup>0</sup> at room temperature by tertiary amines, (Kuo2005, Zhou 2002) particularly Piperazine (Zhang 2008), we selected a linear polyamidoamine based on Bisacrylamide and Piperazine. It was believed that the AuNPs would be further stabilized by the polyvalency effect, resulting from the presence of t-amines along the main chain repeat unit (Miyamoto 2008). Since earlier reports attributed failure of linear polyamidoamines to stabilize AuNPs to chain entanglements, a low mol wt polymer of mol wt 632 g mol<sup>-1</sup> was used. In the following sections we describe one pot synthesis of gold nanochains at room temperature using low mol wt polyamidoamine, the parameters influencing the morphology of AuNPs formed and stability of morphologies under various conditions.

### 6.3.1. PAmAm characterization

#### 6.3.1.1. Confirmation of polymerization by FT-IR

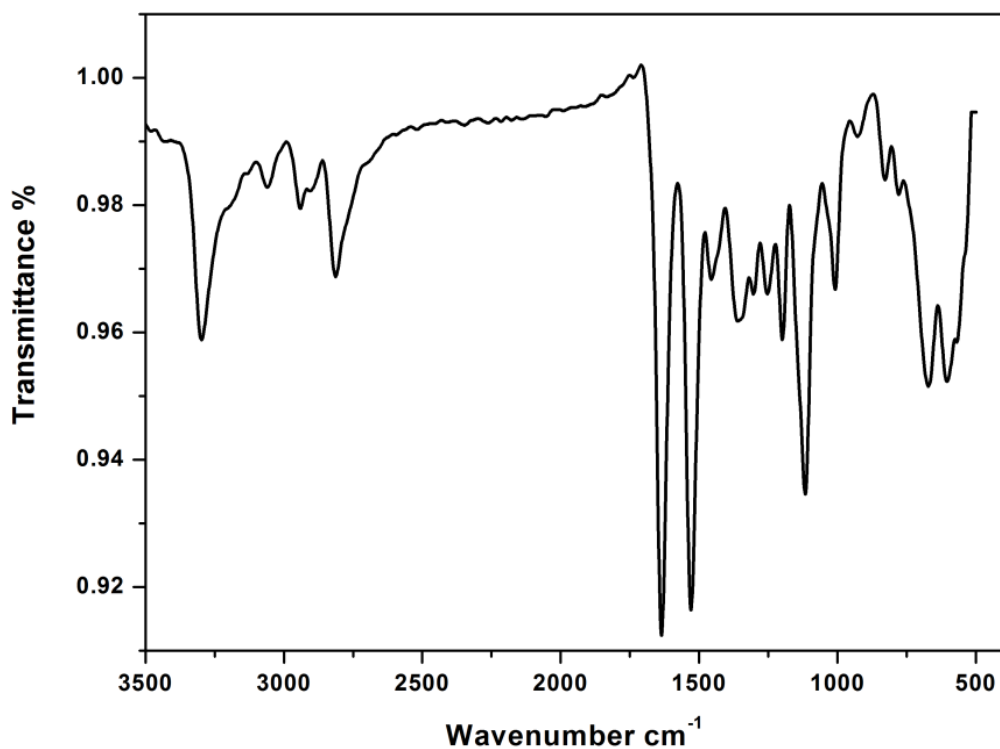


Figure 6.2 FT-IR spectrum of PAmAm

#### 6.3.1.2. Confirmation of polymerization by $^1\text{H}$ NMR

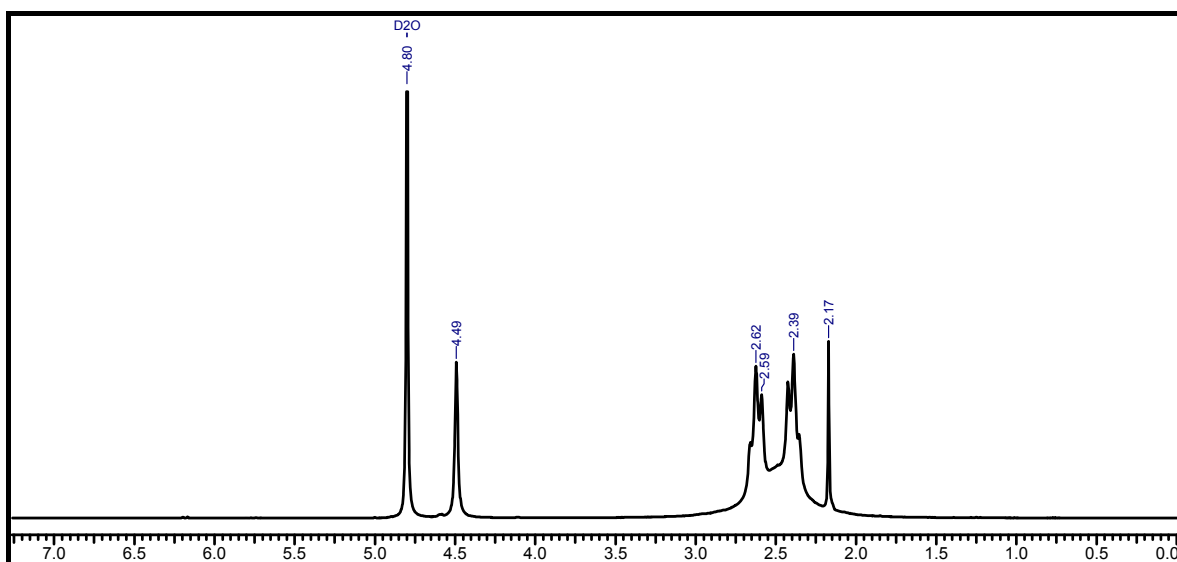


Figure 6.3  $^1\text{H}$  NMR of PAmAm with terminal amine

The FT-IR spectrum of PAmAm shows disappearance of peak at  $1640\text{ cm}^{-1}$  corresponding to double bond in Bisacrylamide and amide peak shift confirms formation of linear polymer. Peaks at  $1654$ ,  $1542$  and  $1384\text{ cm}^{-1}$  are seen for amide I, II and III respectively. Peak at  $3315\text{ cm}^{-1}$  confirms presence of secondary amine (Figure 6.2).

$^1\text{H}$  NMR analysis shows peak at  $2.39\text{ ppm}$  which corresponds to  $\text{CH}_2$  protons of piperazine and peak at  $4.49\text{ ppm}$  which corresponds to  $\text{CH}_2$  protons of MBA. The absence of vinyl peak of MBA in the range  $5.5$  to  $6.5\text{ ppm}$  confirms polymerization of MBA (Figure 6.3).

### **6.3.2 Effect of PAmAm concentration on morphology of AuNPs**

$50\text{ ml}$   $1\text{ mM}$  auric chloride solution was added to  $50\text{ ml}$  aqueous PAmAm solution. The polymer concentration was varied in the range  $30\text{ mM}$  to  $1.5\text{ mM}$ . At  $30\text{ mM}$  PAmAm concentration, the color changed from light yellow to colourless then red and finally dark red. The nanoparticle formation was monitored by UV-Vis spectrophotometry. The SPR peak first appeared at  $547\text{ nm}$  after  $20\text{ mins}$  and shifted to  $540\text{ nm}$  after  $1\text{ h}$ . The peak intensity reached maximum and the peak position blue shifted to  $536\text{ nm}$  at the end of  $12\text{ h}$  (Figure 6.4a). TEM analysis of the AuNPs formed at the end of  $12\text{ h}$  revealed  $10\text{ nm}$  particles (Figure 6.5a). Sun et al (2006) reported that addition of N-[3-(trimethoxysilyl) propyl] polyethylenimine to auric chloride solution resulted in initial SPR peak at  $580\text{ nm}$ , which was attributed to the surface plasmon resonance of the closely associated gold clusters initially formed chain. The disappearance of the peak at  $580\text{ nm}$  with time was attributed to the disintegration of cluster and formation of isolated AuNPs resulted in SPR peak at  $528\text{ nm}$ .

As the concentration of PAmAm decreased from 30 mM to 5 mM, the time required for the emergence of the SPR peak decreased from 20 mins to 3 mins. Similar trends were reported by Harada et al (2009) who attributed this to decrease in the pH of the medium which resulted in increase in the conc of the  $\text{AuCl}_4^-$  and/or  $[\text{AuCl}_3(\text{OH})]^-$  species which was more reactive. Further,  $\lambda_{\text{max}}$  showed a blue shift from 536 nm to 525 nm (Figure 6.4b), indicating a decrease in particle size from 10 nm to 5 nm as was confirmed by TEM (Figure 6.5d).

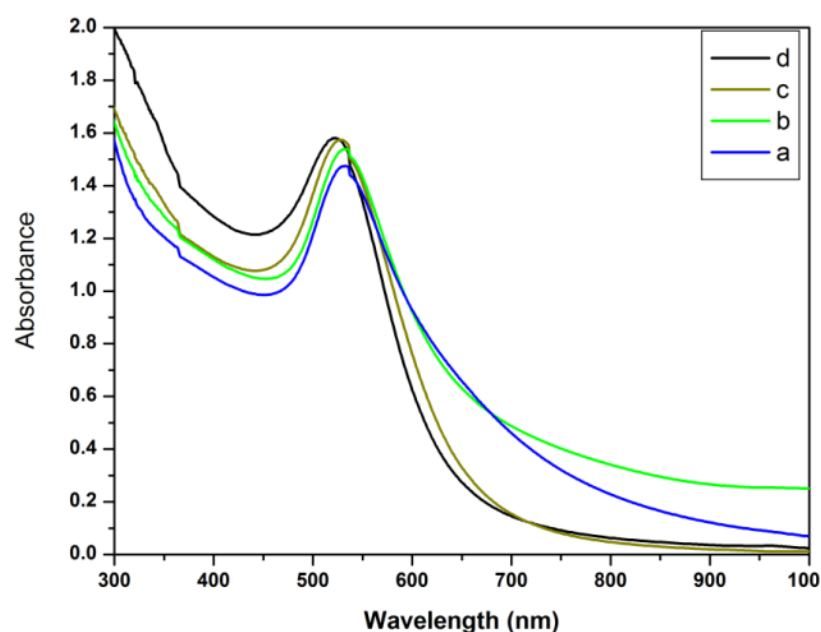


**Figure 6.4** UV spectra of AuNPs prepared at PAmAm concentration a) 30 mM b) 20 mM c) 10 mM d) 5 mM

When PAmAm concentration was further lowered to 3 mM, the color changed from yellow to colourless to red and finally turned blue indicating agglomeration. UV-Vis spectral analysis showed emergence of peak at 524 nm in 2 mins followed by a peak at 710 nm, after 200 mins, which could be attributed to LSPR (Figure 6.6a). TEM analyses showed that LSPR peak at 710 nm was a result of 1D assembly (Figure 6.7a). The appearance of SPR peak due to AuNPs at 535 nm followed by the emergence of second peak at 700 nm was concomitant with colour change in solution

from red to pale pink to blue (Wu et al 2008 and Murugadoss and Chattopadhyay 2008).

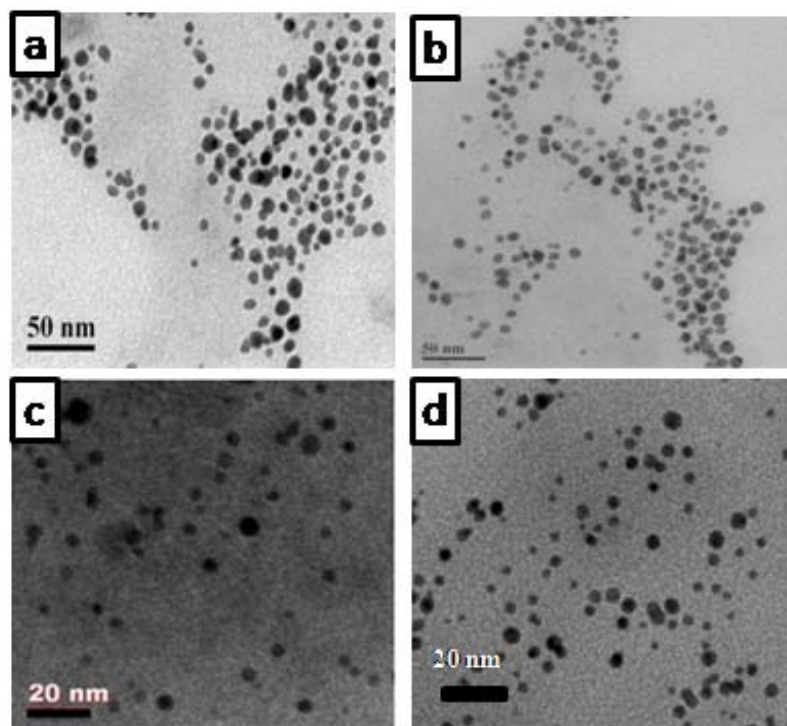


**Figure 6.5** TEM images of AuNPs formed at PAMAm concentration a) 30 mM b) 20 mM c) 10 mM d) 5 mM.

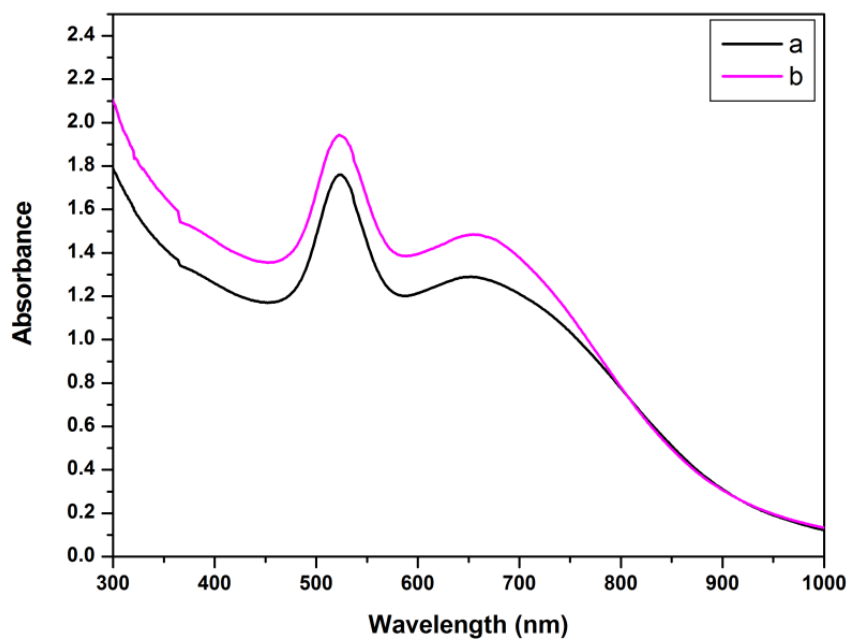


**Figure 6.6** UV –Vis spectra of AuNPs at PAMAm concentration a) 3 mM b) 1.5 mM.



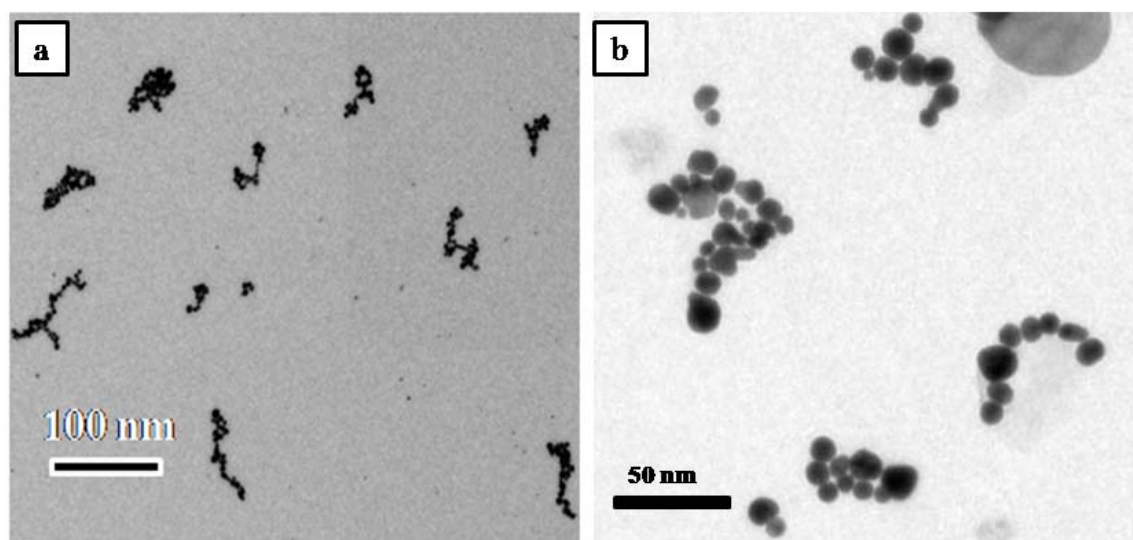


**Figure 6.7** TEM images of AuNPs prepared at concentration a) 3 mM b) 5 mM

With further decrease in PAmAm concentration to 1.5 mM, the LSPR peak exhibited blue shift to 650 nm (Figure 6.6b). This is consistent with the results of TEM analysis which showed that Au nanochains formed, were shorter in length (Figure 6.8b). Further decrease in PAmAm concentration to 0.75 mM revealed two peaks at 524 nm and 610 nm respectively. However, the nanoparticles precipitated out within 12 hrs. To our knowledge this is the first report of single step synthesis of Au nanochains formed at room temperature. Linear PAmAm used as substrate acts both as a reducing as well as stabilizing agent. Stabilization of AuNPs on PAmAm dendrimers reported in the past resulted in nanoparticles but not chains (Shi et al 2009 and Divsar et al 2009). While stabilization on lower PAmAm concentration resulted in precipitation.

### 6.3.2.1 In situ investigation of nanochain formation

Addition of 50 ml 1 mM auric chloride to 50 ml 3 mM PAmAm solution resulted initially in peak at 524 nm because of surface plasmon resonance (SPR) which confirmed reduction of auric chloride and formation of isolated gold nanoparticles. After 5 mins, another peak emerged at 640 nm as a result of longitudinal surface plasmon resonance (LSPR). The peak shifted to 680 nm, which increased in intensity

and shifted to 710 nm at the end of 200 mins. Thereafter the peak position remained constant indicating no further growth (Figure 6. 8).

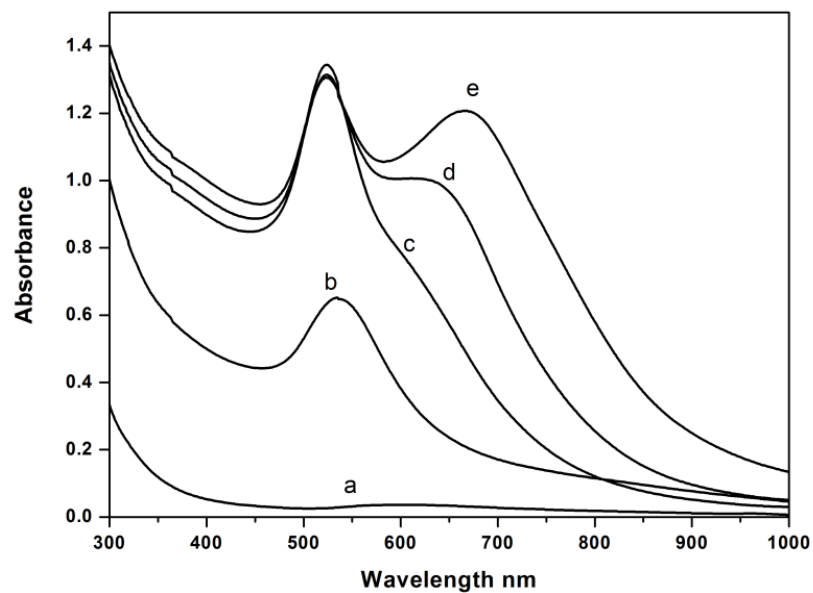


**Figure 6.8** UV – Vis spectra of Au nanochain formed at 3 mM PAMAm concentration a) 0 min b) 5 min c) 20 min d) 60 min e) 200 min

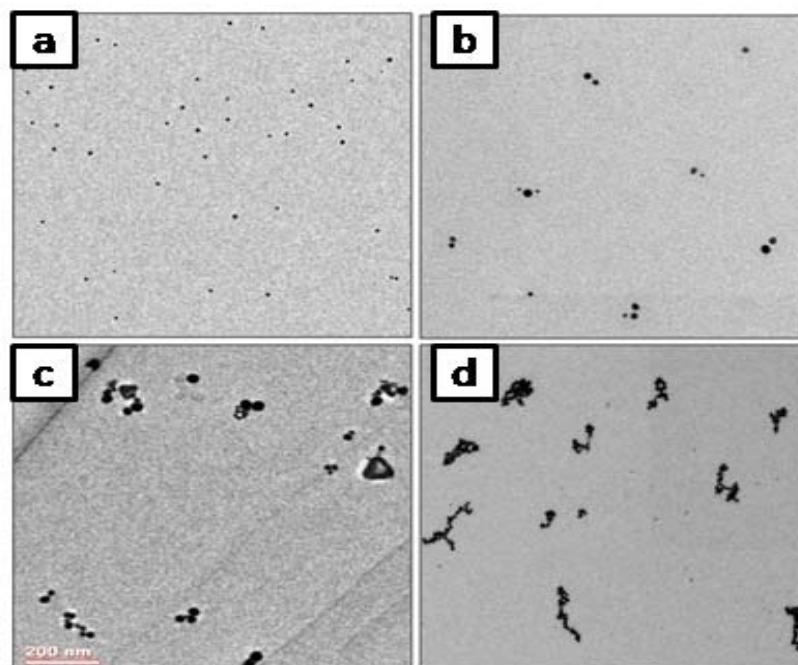


**Figure 6.9** TEM images of AuNPs formed at 3 mM PAMAm concentration at a) 5 min b) 20 min c) 60 min d) 200 min

TEM analyses of AuNPs formed at time intervals of 5, 20, 60 and 200 mins shown in Figure 6.9 reveal that auric chloride is reduced by PAmAm to form isolated nanoparticles first, followed by aggregation to dimers and trimers which subsequently resulted in 1D assembly. Wu et al (2008) reported a one pot method for the synthesis of linear assembly of AuNPs at 125 °C using Chitosan as reducing and stabilizing agent and monitored the morphology as a function of time by TEM wherein isolated particles were initially formed and 1D assembly resulted over 200 mins. Thus, the kinetics of nanochain formation is analogous in both cases, except that in the present case, the synthesis has been possible at room temperature because of tertiary amines which are known to effect reduction at room temperature (Shi et al 2009).

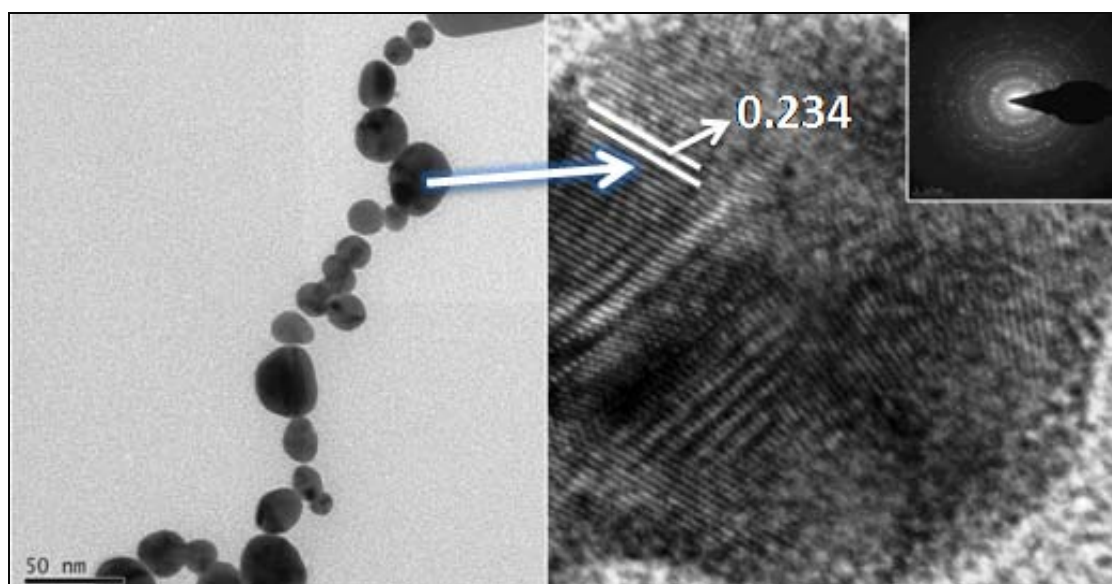


**Figure 6.10** HR-TEM image of Au nanochains

Figure 6.10a shows HR- TEM image of gold nanochains at higher magnification  
Figure 6.10b shows the image for selected single particles with clear lattice fringes showing an inter planar distance of 0.234 nm which is consistent with the value for bulk Au (0.235 nm).

In summary, we have shown that linear PAmAm forms AuNPs at room temperature and that the polymer acts both as a reducing agent as well as a stabilizer. These results are significant in the context of the report by Zhang et al (2008) who showed that reduction of auric chloride in the presence of linear polyamidoamine of Molecular weight  $1.4 \times 10^5 \text{ gmol}^{-1}$  resulted in insoluble precipitates, which was attributed to chain entanglement. The PAmAm used in this work has molecular weight of only  $632 \text{ gmol}^{-1}$ . It therefore appears that the choice of lower molecular weight, which avoids chain entanglement, leads to stabilization of AuNPs. The formation of nanochains observed with decreasing concentration of PAmAm could probably be attributed to the unsymmetrical distribution of ligands on AuNPs as reported by Wu et al (2008) for Chitosan stabilized AuNPs. At this stage, it may be noted that Chitosan was dissolved in 1% acetic acid. The pH of Chitosan solution in 1% acetic acid was 4.2 and decreased to 3.8 when it was mixed with auric chloride solution. PAmAm used by us is dissolved in water. In the present case the pH of the solution decreased from 6.3 to 3.3 when 1 mM auric chloride solution was mixed with 30 mM and 3 mM PAmAm solution respectively. The effect of pH rather than that of concentration in governing the morphology of the AuNPs is discussed in subsequent sections.

#### **6.3.2.2 Effect of polymer concentration on AuNP morphology at pH 3.3**

Si and Mandal (2007) investigated assembly of AuNPs on the peptide ( $\text{NH}_2\text{-Leu-Aib-Tyr-OMe}$ ) in the pH range 2.5 to 10. 3D AuNP assemblies were formed at pH 2.5. At pH 4, controlled assembly resulting in the formation of 1D chain from intermolecular H-bonding between two carboxylic acid groups of peptides bound to the two adjacent AuNPs was observed. The 1D assembly was converted to particulate morphology as the pH of the medium was switched to 10 and the transition was reversible. It was therefore interesting to investigate if the 1 D AuNP assembly reported by us in the

previous section was reversible and whether it was a result of lower concentration or variation of the pH. A systematic investigation of the effect of pH at varying concentrations of PAmAm was therefore undertaken (Figure 6.11).

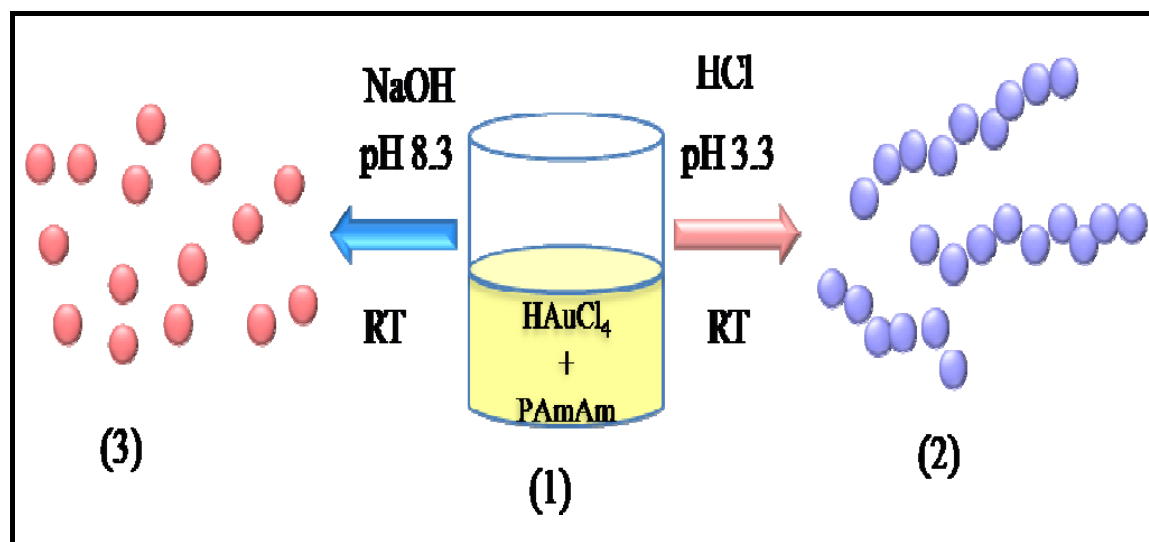


**Figure 6.11** Schematic for pH dependent morphology of gold nanoparticles

Polymer concentration was varied in the range 5 mM to 20 mM. In each case pH was adjusted to 3.3 by adding 1 M HCl. At 5 mM concentration UV-Visible spectrum showed two peaks at 524 nm and at 725 nm (Figure 6.12b), indicating possible formation of 1 D assembly. Longitudinal surface plasmon resonance (LSPR) peak can be attributed to very low interparticle spacing which results in very strong coupling of localized surface plasmon. TEM analyses confirmed that 1D assembly was indeed formed and that the chain length increased as compared to that observed at 3 mM concentration (Figure 6.13a). At 10 mM concentration, the LSPR peak was observed at 750 nm (Figure 6.12c), indicating that the chain length increased further. TEM analyses indicated that this was accompanied by branching (Figure 6.13b). Thus our results evaluating effect of polymer concentration at constant pH 3.3 on the morphology of AuNPs exhibit similar trends as reported by Murugadoss and Chattopadhyay (2008). At 20 and 30 mM PAmAm concentration, the nanoparticles

precipitated out due to destabilizing effect by a large concentration of PAMAm Wu et al (2008).

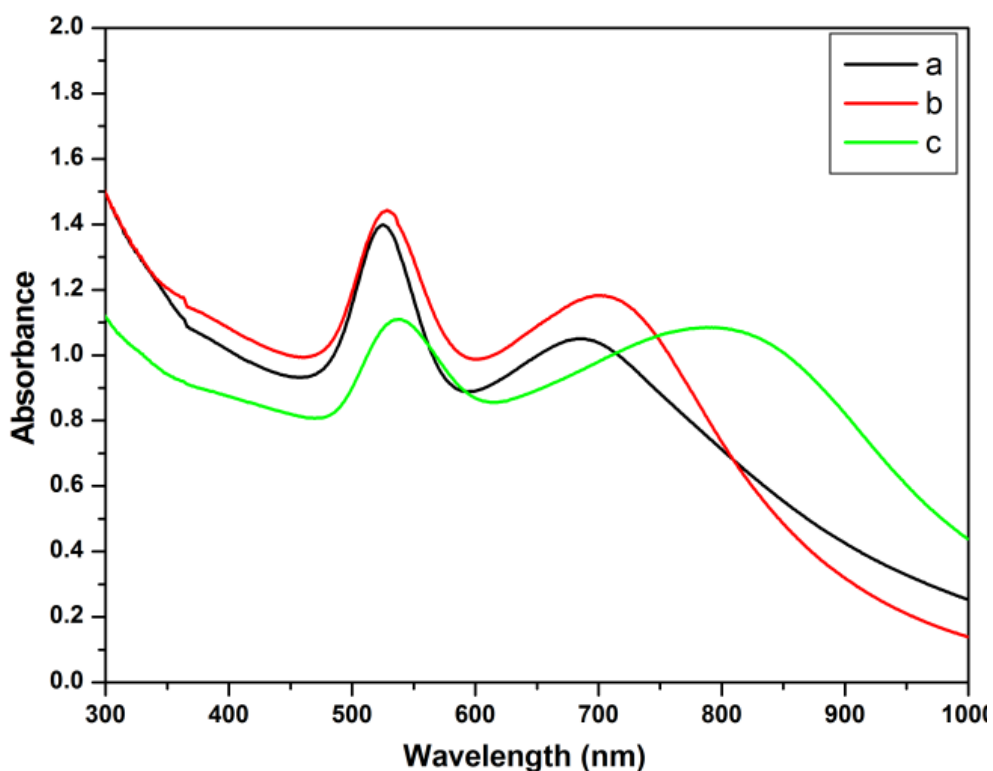


**Figure 6.12** UV- Vis spectra of AuNPs formed at pH 3.3 and concentration a) 3 mM b) 5 mM c) 10 mM

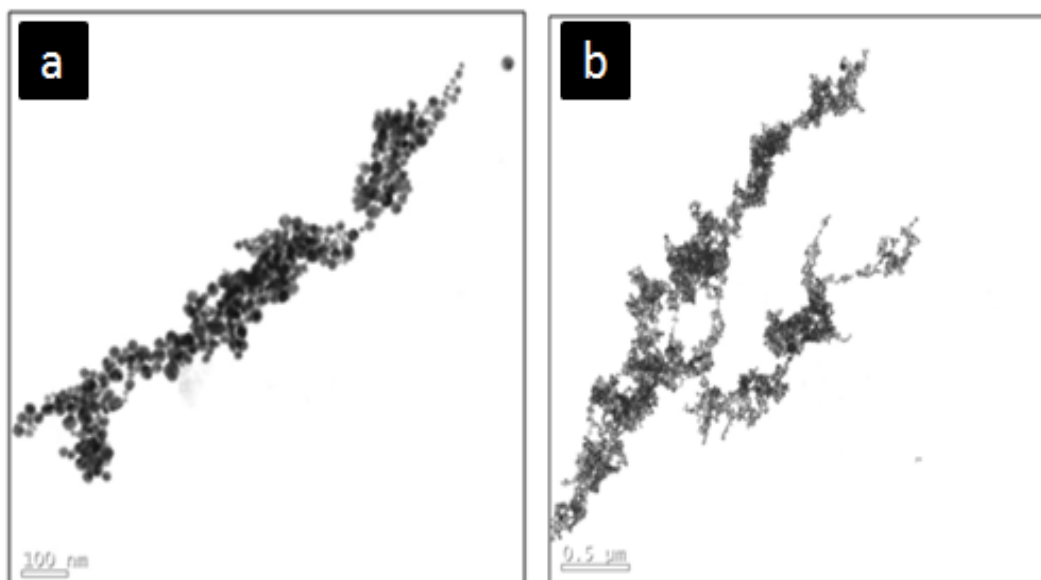


**Figure 6.13** TEM images of AuNPs at a) 5 mM b) 10 mM and pH 3.3

### 6.3.2.3 Effect of polymer concentration on AuNPs morphology at pH 8.3

In order to further ascertain if the morphology of AuNPs observed was governed by polymer concentration or pH of the medium, we examined the effect of polymer concentration on morphology of AuNPs at pH 8.3. It was noted that SPR peak at 525 nm appeared much later than at acidic pH since the predominant species  $[\text{AuCl}_2(\text{OH})_2]^-$  and/or  $[\text{AuCl}(\text{OH})_3]^-$  have low reactivity (Harada et al 2010). Polymer concentration was varied in the range 5 mM to 30 mM and the pH was adjusted to 8.3 using 1 M NaOH. UV-Vis spectra and TEM analyses of these AuNPs indicated that in all cases isolated AuNPs were formed (Figures 6.14 and 6.15). These results suggest that pH of the solution plays a more dominant role in governing the morphology than the polymer concentration. The AuNPs formed were stable upto three months.

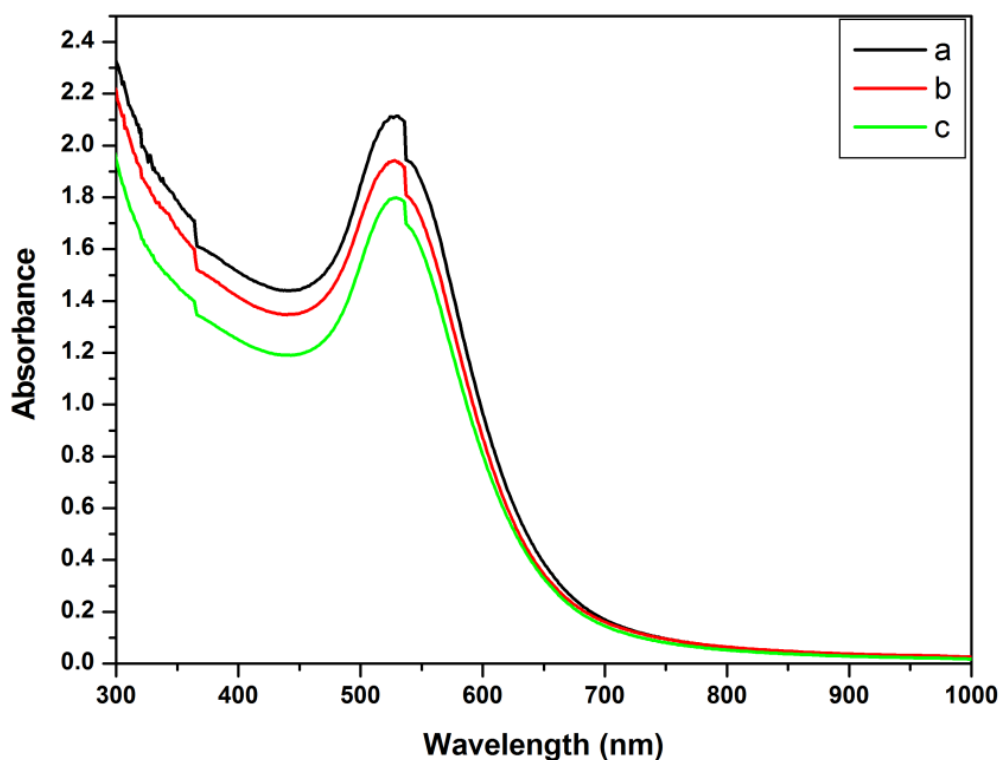


**Figure 6.14** UV-Vis spectra of AuNPs prepared at pH 8.3 using polymer concentration a) 5 mM b) 10 mM c) 20 mM

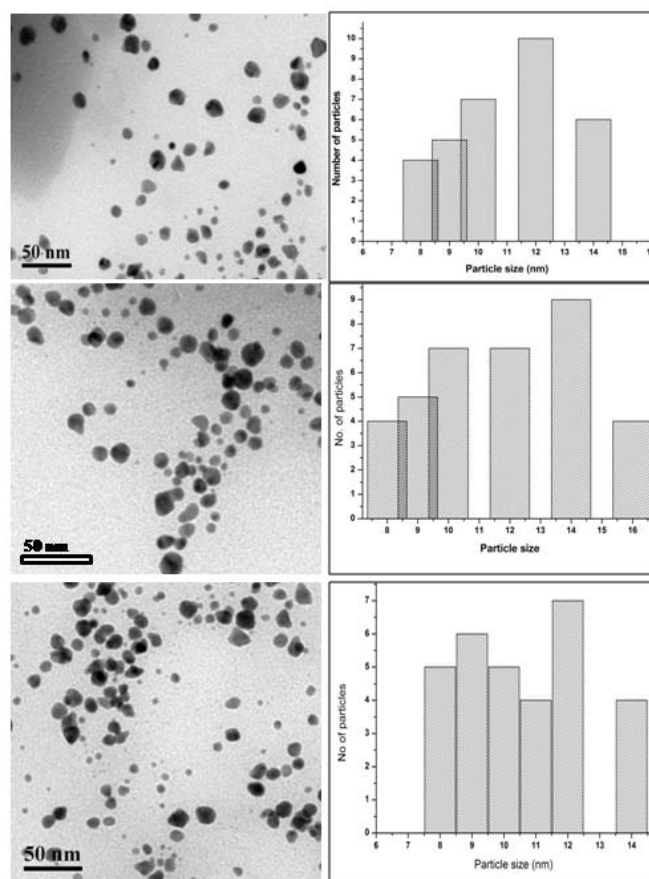


**Figure 6.15** TEM images of AuNPs formed at PAmAm concentration a) 5 mM b) 10 mM d) 20 mM at pH 8.3.

#### 6.3.2.4 Effect of pH on morphology of AuNPs prepared at constant polymer concentration

The pH of 3 mM PAmAm solution was adjusted in the range 3.3 to 8.3 by adding few drops of 1M NaOH solution. The effect of pH on SPR and LSPR peak position is summarized in table 1.

The AuNPs prepared at pH 3.3 and 4.3 showed two peaks. The peak at 524 nm corresponds to isolated nanoparticles. The peak in the range 700-725 nm could result from aggregation or 1D assembly. With further increase in pH from 5.3 to 8.3, the peak at 524 nm shifted to 540 nm (Figure 6.16d-f) indicating increase in particle size (5 nm to 10 nm). However the second peak at longer wavelength was no more observed, indicating that only isolated AuNPs were formed. The TEM analyses of



AuNPs formed at pH 3.3 clearly showed 1D assembly. On the contrary, AuNPs formed at pH 4.3 exhibited aggregation (Figure 6.17a). As pH was further increased from 5.3 to 7.3 (Figure 6.17b-c), aggregation of AuNPs decreased and finally at pH 8.3 isolated AuNPs were formed as shown in Figure 6.17d. These experiments

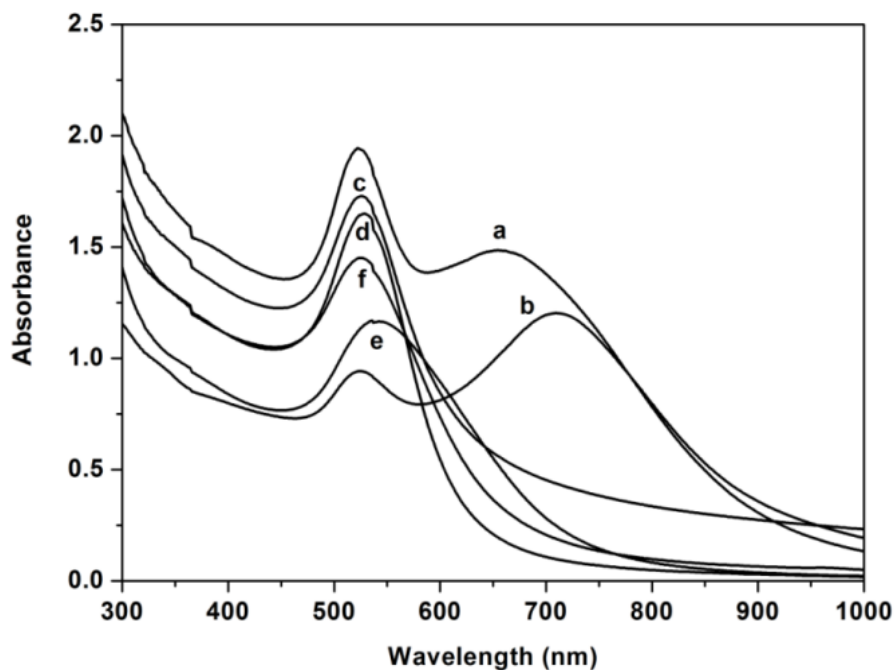


**Figure 6.16** UV - Visible spectra at pH a) 3.3 b) 4.3 c) 5.3 d) 6.3 e) 7.3 f) 8.3

**Table 1** Effect of pH on SPR and LSPR peak

| pH  | SPR peak (nm) | LSPR peak (nm) |
|-----|---------------|----------------|
| 3.3 | 524           | 710            |
| 4.3 | 524           | 725            |
| 5.3 | 525           | Not seen       |
| 6.3 | 531           | Not seen       |
| 7.3 | 535           | Not seen       |
| 8.3 | 540           | Not seen       |

indicate that in the present case the acidic pH 3.3 leads to the formation of nanochains rather than PAmAm concentration. At this pH the polyamidoamine is partially

protonated. It is therefore logical to conclude that the unprotonated t-amines effect the reduction of  $\text{Au}^{+3}$  to AuNPs which interact with protonated amidoamine to form structures facilitating dipolar coupling leading to nanochains.

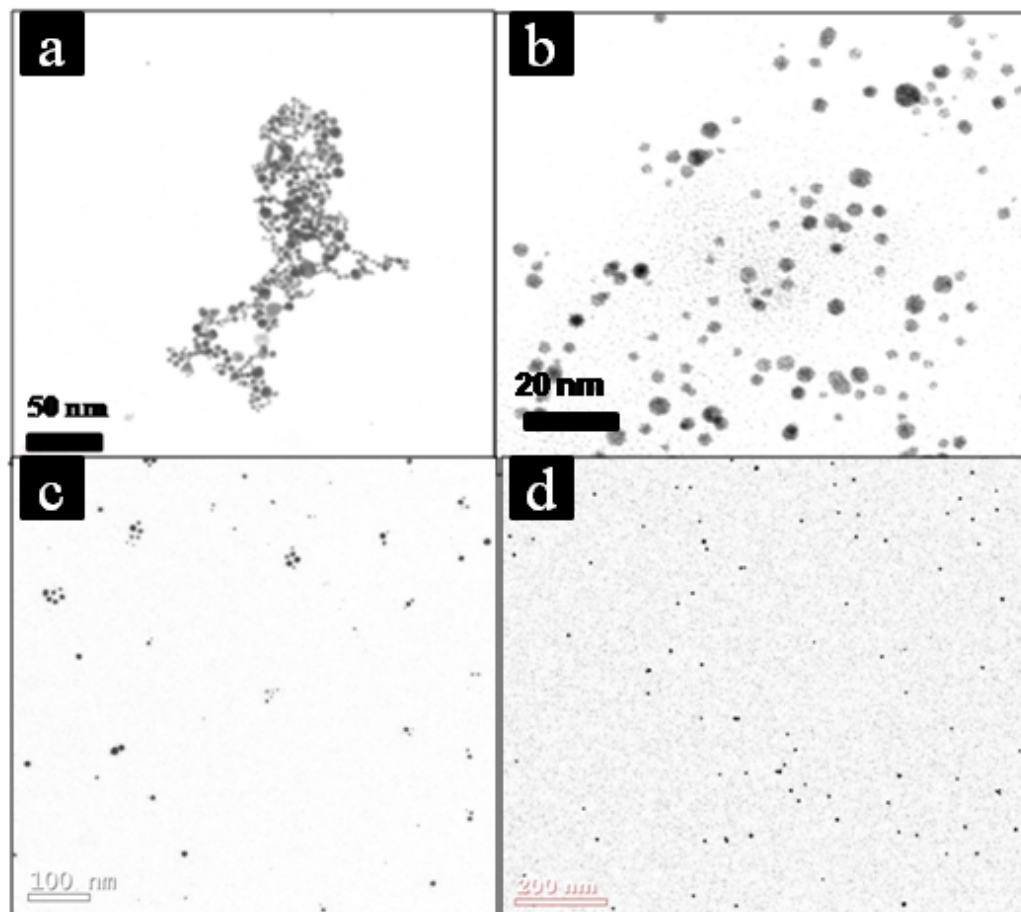


**Figure 6.17** TEM analyses of AuNPs formed at pH a) 4.3 b) 5.3 c) 7.3 d) 8.3

### 6.3.2.5 Effect of solvent on chain length

According to Zhang et al (2008) the anisotropic assembly of AuNPs resulting from dipolar coupling could be manipulated by varying the dielectric constant (DEC) of the medium. Thus the nanochains synthesized in the water / DMF mixtures were shorter than those in the water / acetone mixtures since the dielectric constant of DMF (38.3) is greater than that of Acetone (20.7) leading to stronger electrostatic repulsion of AuNPs in water / DMF mixtures than in water / acetone mixtures. In order to further validate the mechanism of chain formation in present case the AuNPs were formed in

aqueous PAmAm solution containing 50 % Methanol (DEC 33) and Acetonitrile (DEC 37.5). The UV-Vis spectra and TEM analyses of these particles shown in Figure 6.18 and 6.19 reveal that when Acetonitrile was added during the preparation of AuNPs, the  $\lambda_{\max}$  shifted to 710 nm and that the length of the nanochain as measured by TEM increased to 550 nm as compared to 500 nm in water alone. The effect was more pronounced as methanol was added as cosolvent where upon  $\lambda_{\max}$  shifted to 735 nm and the length of the nanochain increased to 800 nm. Methanol having lower DEC lowered the surface charge of nanoparticle and enhanced the aggregation of the nanoparticles.

The increase in chain length on the incorporation of cosolvent could be attributed to lower dielectric constant of the solvent which lowers the surface charge of nanoparticles and hence leads to increase in the chain length. The effect of the DEC of co solvent observed by us is consistent with that reported by Zang et al (2008) and corroborates the rate of dipolar coupling in chain formation.

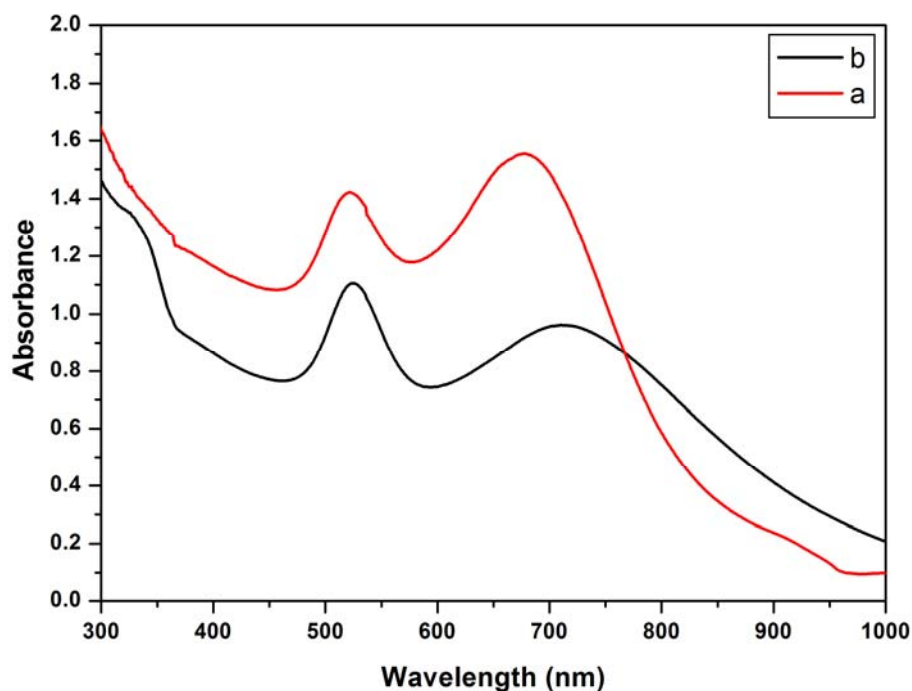


**Figure 6.18** UV-Vis spectra of AuNPs prepared in the presence of cosolvent a) Acetonitrile b) Methanol (50% vol /vol).

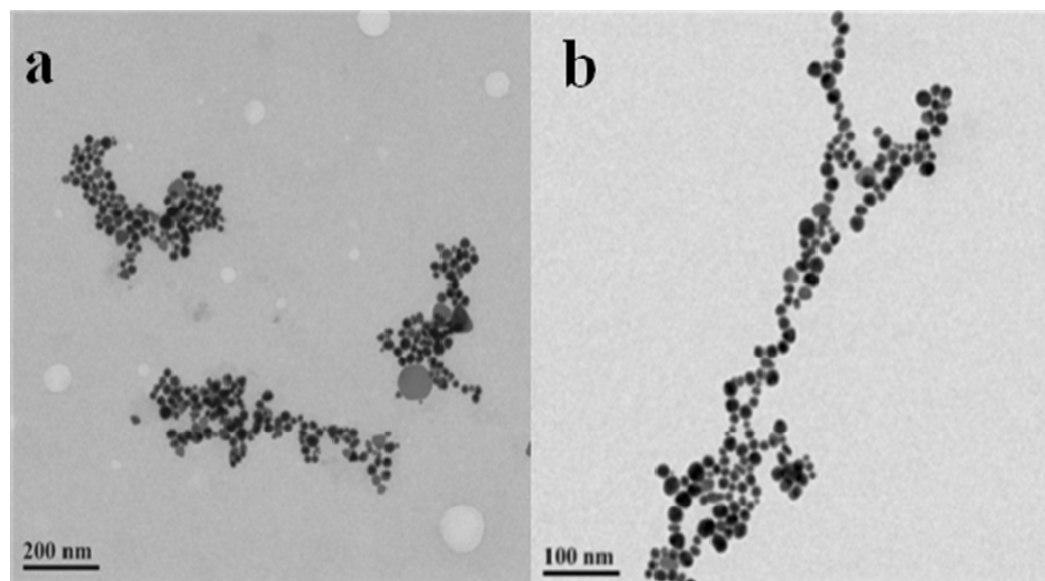


**Figure 6.19** TEM of AuNPs prepared in the presence of a) Acetonitrile b) methanol (50% vol / vol) .

### 6.3.3 Stability

The importance of stability of nanochain in various environments was highlighted by Fernandes et al (2010).

#### 6.3.3.1 Effect of pH on stability.

Si and Mandal (2007) reported that during stabilization of AuNPs at pH 3.3 hydrogen bonding of carboxylated peptide groups led to linear assembly of AuNP, whereas at pH 10 deprotonation of carboxylated peptide groups resulted in isolated nanoparticles. The linear assembly obtained at pH 3.3 underwent a reversible transformation to isolated nanoparticles when pH was shifted to 10. Guo et al (2007) reported aggregation of AuNPs in the presence of Polylysine at pH 11.5. At pH 6.5, protonation of amine groups occurred and isolated AuNPs were formed. The reversible morphological transformation on shifting pH from 11.5 to 6.5 as result of change in conformation of Polylysine from  $\alpha$  -helix-rich structure to  $\beta$  -helix-rich structure could be exploited as a probe to detect the conformational transition. Dynamic light scattering analysis of PAmAm in aqueous medium showed a change in

size from 110 nm at pH 3.3 to 35 nm at pH 8.3. It was therefore interesting to investigate the effect of pH on the stability of gold nanochains.

pH of nanochains formed at pH 3.3 was switched to pH 8.3 using 1 M NaOH. The UV-Visible spectrum showed no change in peak position (Figure 6.20) indicating that nanochains formed were stable under basic condition. This was further confirmed by TEM analysis (Figure 6.21). Similarly when the pH of isolated AuNPs formed at pH 8.3 was switched to 3.3 using 1M HCl, UV-Visible spectrum and TEM analysis confirmed that there was no change in peak position and morphology, which indicates that the morphology was not altered by pH switching (Figures 6.22 and 6.23).

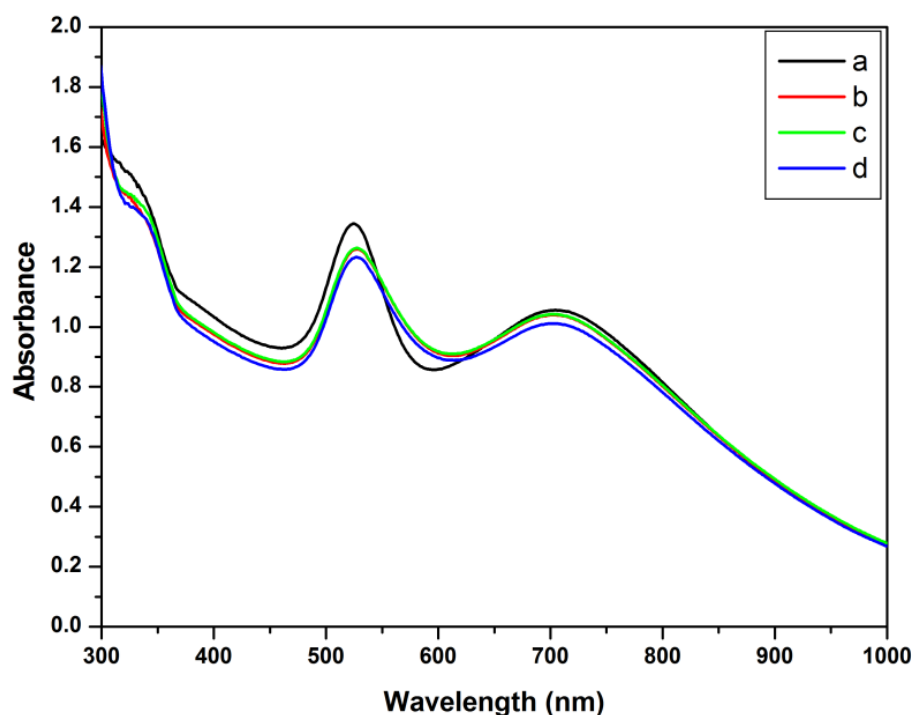


**Figure 6.20** UV-Vis spectra of nanochains a) before and b) after addition of NaOH at pH 8.3

The DLS measurements showed that the size of the PAmAm chain at pH 3.3 was 110 nm. Stabilization of the AuNPs on the chain at this pH resulted in decrease in size to 40 nm. Increase in pH to 8.3 resulted in only a small decrease in chain dimension to 35 nm. Similarly PAmAm chain dimension decreased from 35 nm to 23 nm when AuNPs were stabilized at pH 8.3. Further decrease in pH to 3.3 resulted in only small

increase to 25 nm. The results indicate that the change in the effective size due to protonation / deprotonation as a result of pH switching was arrested when the AuNPs were stabilized on the polymer.

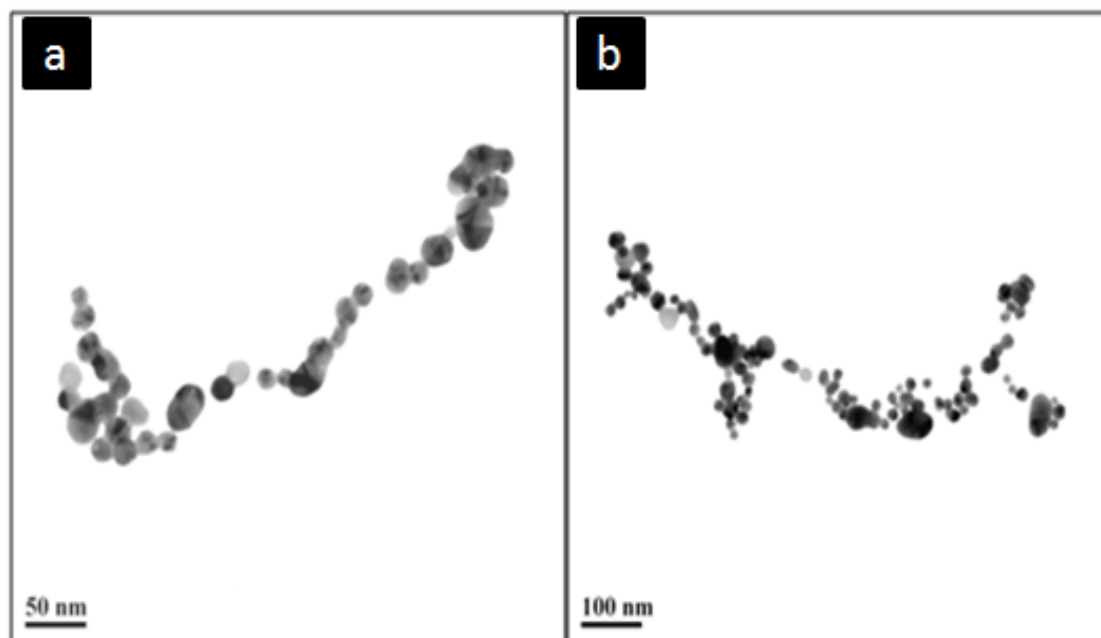


**Figure 6.21** TEM of AuNPs formed at 3 mM a) at pH 3.3 b) on switching to 8.3.

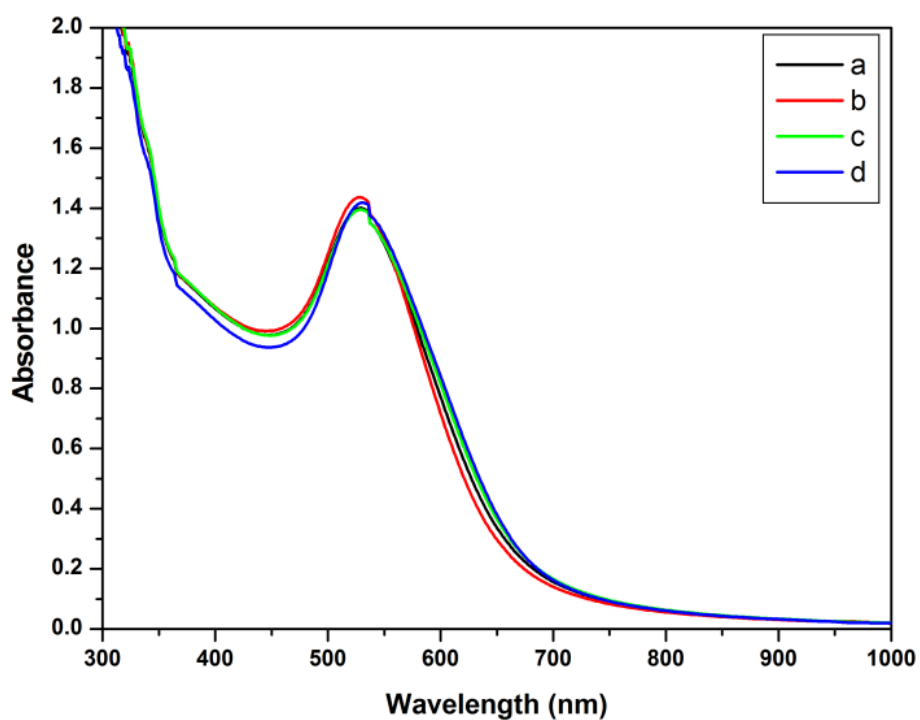


**Figure 6.22** UV-Vis spectra of isolated AuNPs a) at pH 8.3 b) on switching to 3.3

Zeta potential of the nanochains at pH 3.3 was + 40.03 and was lowered to – 31.53 as pH was switched to 8.3. Similarly Zeta potential of nanoparticles prepared at pH 8.3 was -17.04 and changed to +15.86 as pH was switched to 3.3. However these changes didnot influence the chain dimensions significantly as described above.

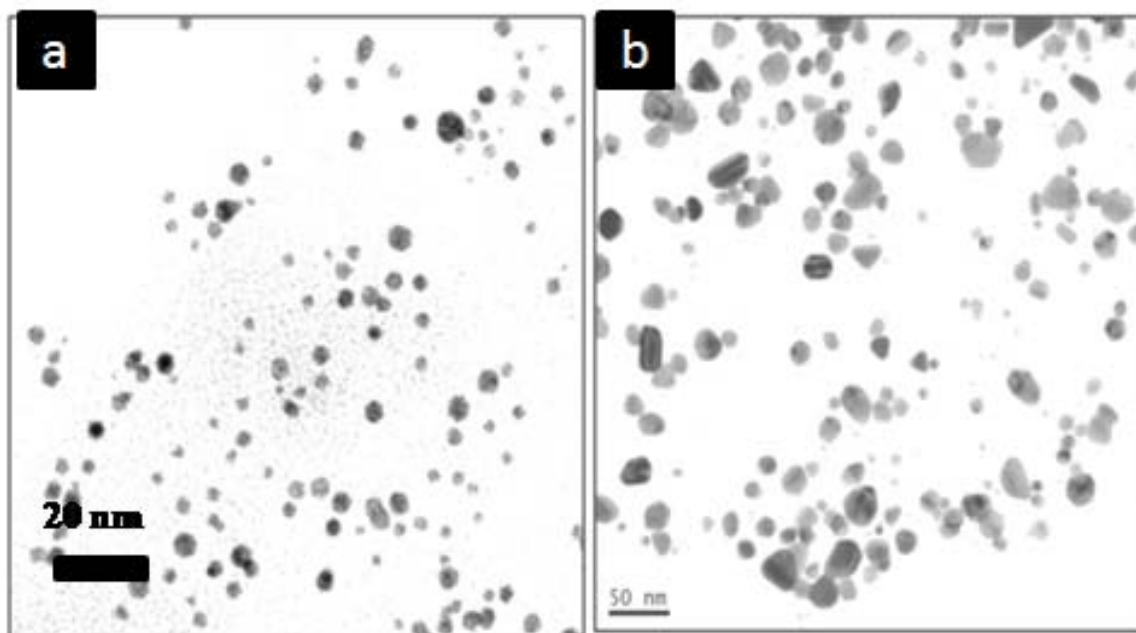


**Figure 6.23** TEM of AuNPs at 3 mM concentration a) at pH 8.3 b) on switching to pH 3.3

### 6.3.3.2 Stability against temperature

Fernandes et al (2010) synthesized gold nanochains using DA-PEG ligands and crosslinked the same using photo irradiation. These nanochains were stable at 70 °C upto 1 h. The nanochains encapsulated in MPTES / TEOS matrix were stable at 70 °C for 10 h. In the present case Au nanochains formed at pH 3.3 were monitored for stability at 70 °C using UV- Visible spectra. The Au nanochains were stable up to 24 h (Figure 6.24). This is particularly significant since the nanochains were not crosslinked / encapsulated. With further increase in temperature to 100 °C, LSPR peak at 710 nm shifted to 750 nm (Figure 6.24d) due to desorption of polymer and eventually the nanochains precipitated out.

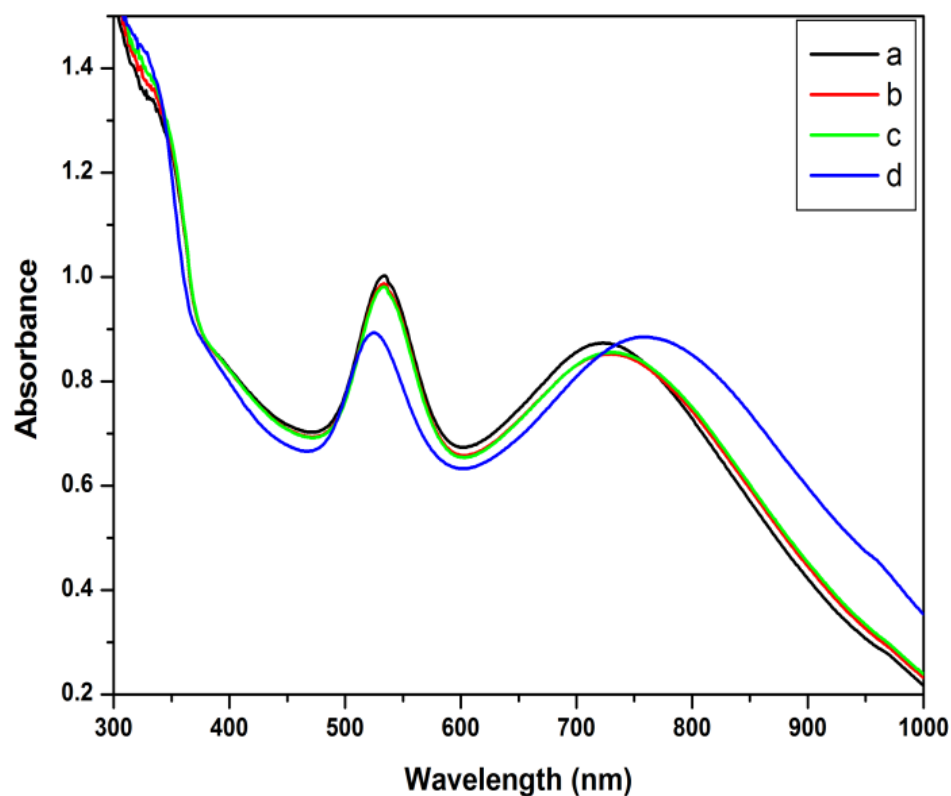


**Figure 6.24** UV spectra of AuNPs at 70 °C, after a) 1 h b) 12 h c) 24 h e) at 100 °C

### 6.3.3.3 Stability against thiol exchange

Sardar et al (2008) reported that amine in poly(allylamine) could be used for stabilization of AuNPs and could be exchanged with mercapto-propionic acid. For biological applications stability against thiol is critical (Subramaniam 2005). Therefore the effect of thiol on stability of nanochains was investigated.

The Au nanochains prepared at pH 3.3 and 3 mM concentration were stable against exchange with 10 mM cysteine hydrochloride. The initial LSPR peak at 710 nm showed blue shift to 660 nm (Figure 6. 25). However, TEM showed that nanochains were stable (Figure 6.26). The stability of nanochains in the present case could be attributed to increased ligand binding between AuNPs and the t- amino group which is on the main chain of the polymer and the multiple binding of the AuNPs constituting the nanochain. The shift in LSPR could therefore be probably due to change in dielectric constant of the medium on addition of thiol.



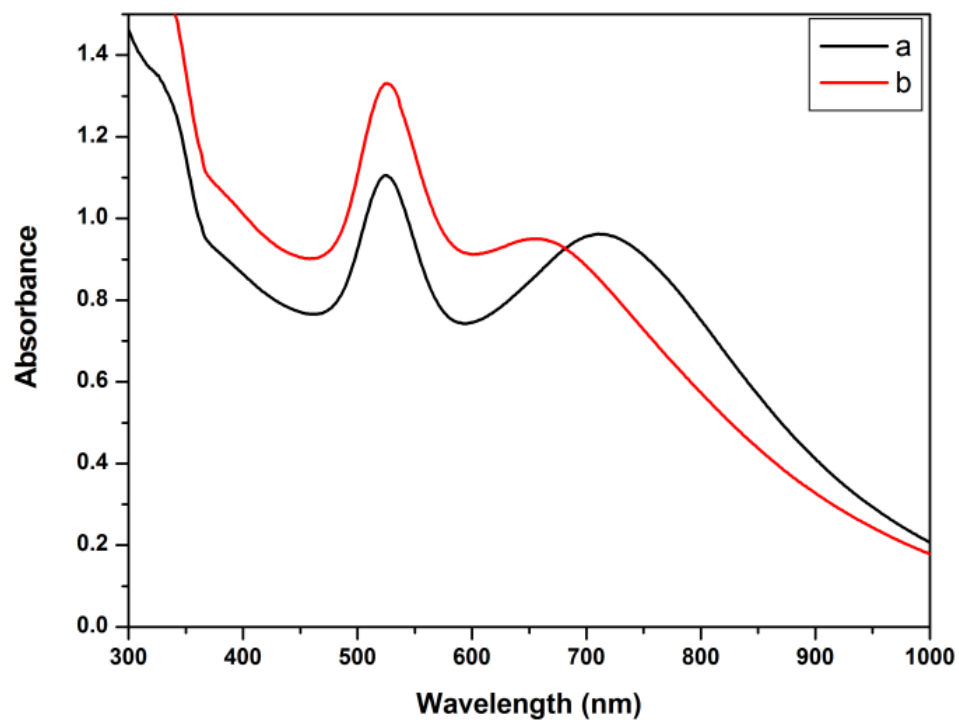


**Figure 6.25** UV-Vis spectra of Au nanochains exchanged with thiol a) before addition b) 24 h after addition of 10 mM thiol.

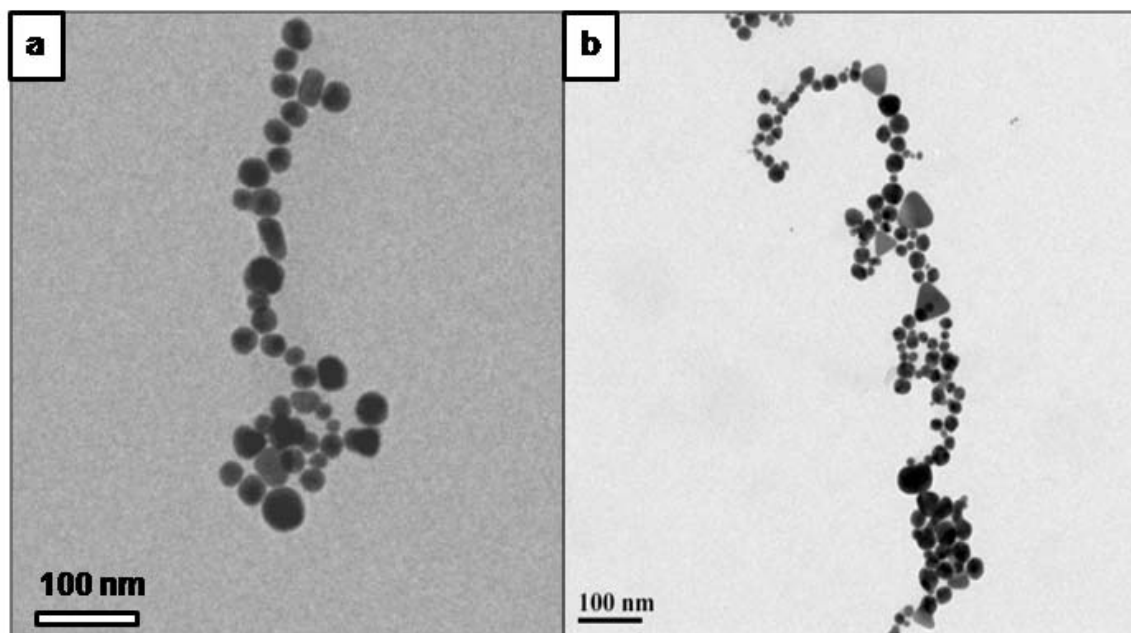


**Figure 6.26** TEM of AuNPs against thiol exchange before and after.

#### 6.3.3.4 Stability against salt

Stability of AuNPs in the presence of salt is critical in biological application. (Zhou et al 2006 and Wang et al 2007). We monitored the stability of Au nanochains in the

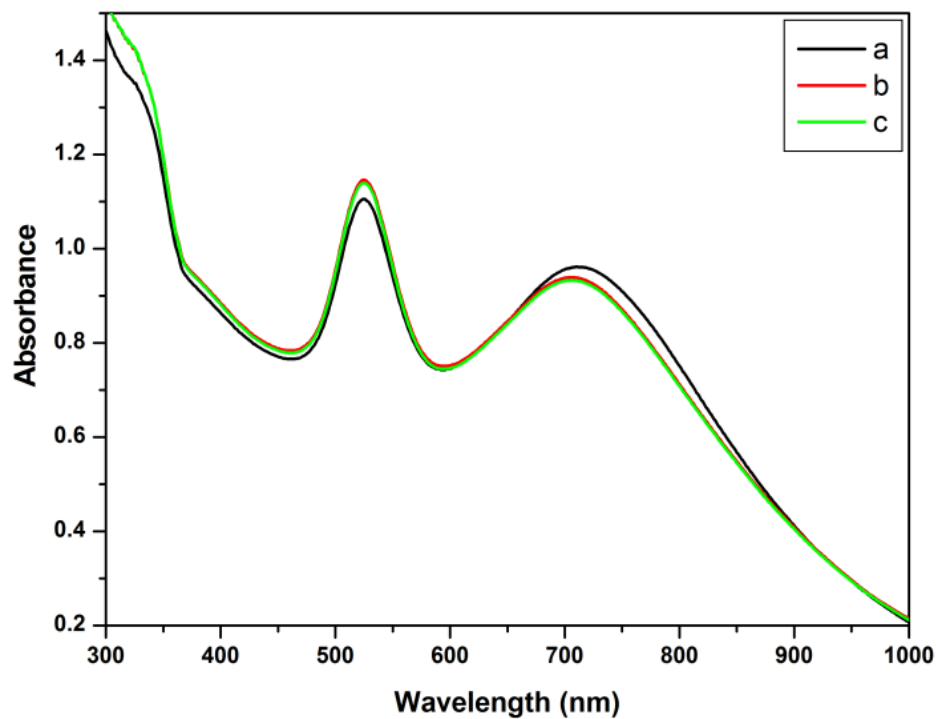


**Figure 6.27** UV-Vis spectra of a) AuNPs b) 1h c) 24 h after addition of 1mM NaCl

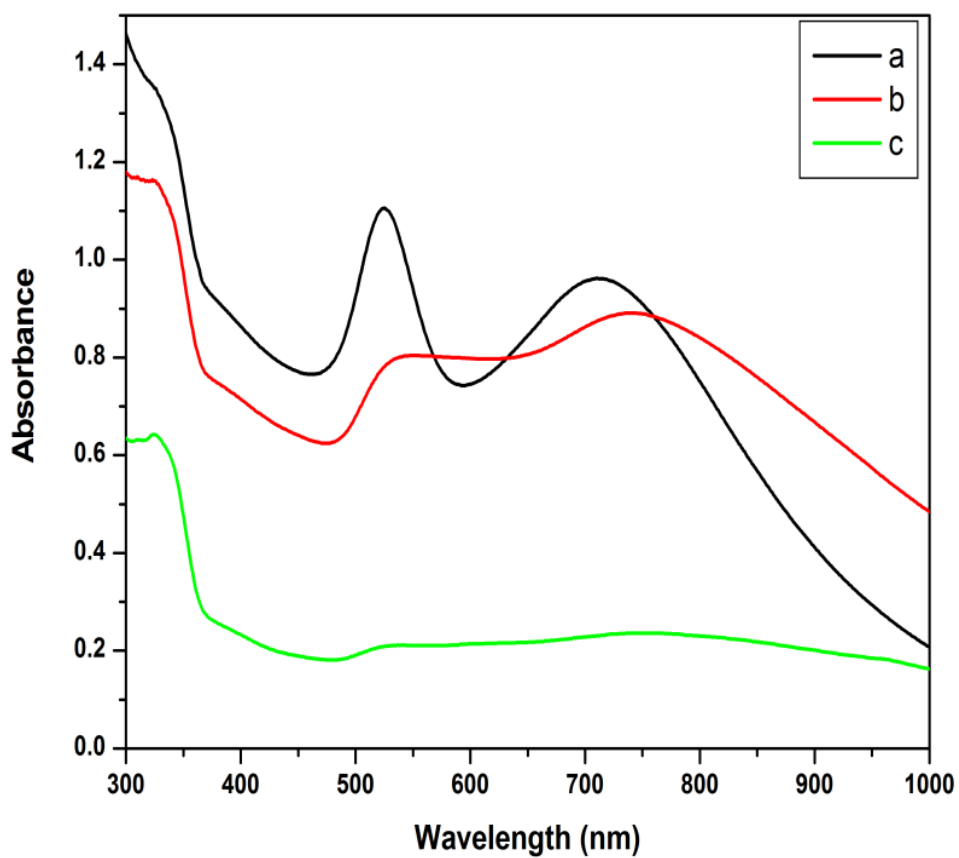


**Figure 6.28** UV-Vis spectra of a) AuNPs b) 1h c) 24 h after addition of 10 mM NaCl

presence of 1 mM sodium chloride. The gold nanochains prepared at 3 mM PAmAm concentration were stable as confirmed by UV-Vis spectra (Figure 6.27). The peaks remained unaltered up to 24 h which confirm that these nanochains were stable against 1 mM salt. Nanochains were unstable at 5 mM salt concentration (Figure 6.28). Unfortunately there are no reports on stability of Au nanochains in the presence of salt against which our result could be compared.

#### **6.4 Conclusions**

Low molecular weight linear PAmAm effects synthesis of AuNPs at room temperature by serving as reducing as well as stabilizing substrate. The nanochain formation at lower PAmAm concentration suggests that this is a result of non uniform distribution of the polymer. Syntheses at constant pH 3.3 and 8.3 at varying concentrations and at 3.3 mM PAmAm concentration at varying pH, suggest that pH plays a more critical role than PAmAm concentration. The results are particularly significant as the nanochains are stable towards change in pH, temperature, salt concentration and do not need encapsulation in polymer matrices as in the past. These would be useful in biomedical applications.

**References**

1. Bae A. H., Numata M., Hasegawa T., Li C., Kaneko K., Sakurai K., Shinkai S., *Angew. Chem., Int. Ed.*, 44, **2005**, 2030.
2. Biradar S. C., Shinde D. B., Pillai V. K., Kulkarni M. G., *J. Mater. Chem.*, 22, **2012**, 10000-10008.
3. Biswas A., Wang T., Biris A. S., *Nanoscale*, 2, **2010**, 1516.
4. Chen K., Robinson H. D., *J. Nanopart. Res.*, 13, **2011**, 751–761.
5. Cho E. C., Choi S.W., Camargo Pedro H. C., Xia Y., *Langmuir*, 26, **2010**, 10005-10012.
6. Dimitrakopoulos C. D., Malenfant P. R. L., *Adv. Mater.*, 14, **2002**, 99.
7. Divsar F., Nomani A., Chaloosi M., Haririan I., *Microchim. Acta.*, 165, **2009**, 421–426.
8. Deya R. K., Raya A. R., *Biomaterials*, 24, **2003**, 2985-2993.
9. Fernandes R., Mei L., Dujardin E., Mann S., Kanaras A. G., *Chem. Commun.*, 46, **2010**, 7602–7604.
10. Gunawidjaja R., Kharlampieva E., Choi I., Tsukruk V. V., *Small*, 5, **2009**, 2460.
11. Guo Y., Ma Y., Xu L. Jun L., Yang W., *J. Phys. Chem. C*, 111, **2007**, 9172-9176.
12. Harada A., Yuzawa A., Kato T., Kojima C., Kono K., *J. Poly. Sci: Part A: Poly. Chem.*, 48, **2010**, 1391–1398.
13. Kotov N. A., Meldrum F. C., Wu, C., Fendler J. H., *J. Phys. Chem.*, 98, **1994**, 2735-2738.
14. Kuo P.L., Chen C.C, Jao M.W., *J. Phys. Chem. B.*, 109, **2005**, 9445.

15. Lai J., Xu Y., Mu X., Wu X., Li C., Zheng J., Wu C., Chen J., Zhao Y., *Chem. Commun.*, **47**, **2011**, 3822–3824.
16. Lee J., Zhou H., Lee J., *J. Mater. Chem.*, **21**, **2011**, 16935.
17. Lin, X. M., Jaeger H. M., Sorensen, C. M., Klabunde K. J., *J. Phys. Chem. B.*, **105**, **2001**, 3353-3357.
18. Miyamoto D., Oishi M., Kojima K., Yoshimoto K., Nagasaki Y., *Langmuir*, **24**, **2008**, 5010-5017.
19. Murugadoss A., Chattopadhyay A., *J. Phys. Chem. C*, **112**, **2008**, 11265–11271.
20. Pissuwan, D., Valenzuela, S. M., Cortie, M. B., *Trends in Biotechnol.*, **24**, **2006**, 62-67.
21. Pileni, M. P., *J. Phys. Chem. B*, **105**, **2001**, 3358-3371.
22. Rezaee A., Aliganga A. K. A., Pavelka L. C., Mittler S., *Phys. Chem. Chem. Phys.*, **12**, **2010**, 4104.
23. Sardar R., Bjorge N.S., Shumaker-Parry J. S., *Macromolecules*, **41**, **2008**, 4347-4352.
24. Shi, C., Tian, L., Wu, L., Zhu J., *J. Phys. Chem. C*, **111**, **2007**, 1243-1247.
25. Si S., Mandal T. K., *Langmuir*, **23**, **2007**, 190-195.
26. Sun X., Dong S., Wang E., *Materials Chem. and Phy.*, **96**, **2006**, 29-33.
27. Shi X., Sun Kai, Baker J. R., *J. Phys. Chem. C Nanomater Interfaces.*, **112**, **2009**, 8251–8258.
28. Subramaniam C., Tom R. T., Pradeep T., *J. Nano. Res.*, **7**, **2005**, 209-217.
29. Tsai L-C., Cheng I-C., Tu M-C., Chen C-D., Lin H-Y., *J. Nanopart Res*, **12**, **2010**, 2859-2864.
30. Wang T., Zhang D., Xu W., Li S., Zhu D., *Langmuir*, **18**, **2002**, 8655-8659.

31. Wang Z., Tan B., Hussain I., Schaeffer N., Wyatt M. F., Brust M., Cooper A. I., *Langmuir*, 23, **2007**, 885–895.
32. Wu L, Shi C., Tian L., Zhu J., *J. Phys. Chem. C Letters*, 112, **2008**, 319-323.
33. Yang P. D., Kim F., *ChemPhysChem*, 3, **2002**, 503.
34. Zhang H., Fung K-H, Hartmann J., Chan C. T, Wang D., *J. Phys. Chem. C*, 112, **2008**, 16830–16839.
35. Zhang H., Wang D., *Angew. Chem. Int. Ed.*, 47, **2008**, 3984 –3987.
36. Zhang Y. Peng H., Huang W., Zhou Y. Yana D., *Journal of Colloid and Interface Science*, 325, **2008**, 371–376.
37. Zhou Y., Itoh H., Uemura T., Naka K., Chujo Y., *Langmuir*, 18, **2002**, 277.
38. Zhou J., Beattie D. A., Ralston J., Sedev R., *Langmuir*, 23, **2007**, 12096-12103.

---

---

**Chapter 7**  
**Conclusions and recommendations for**  
**further work**

---

---

## 7.1 Introduction

Present investigation was undertaken to explore the utility of polydentate ligands as substrates for enhancing stability of AuNPs. Poly(DSDMA) stabilized AuNPs exhibited enhanced stability in solvents, against temperature, competing ligands as well as during etching to yield nanocapsules. The methodology could be used for synthesis of nanocapsules for applications in drug delivery. Poly(DSDMA) stabilized AuNPs exhibited lower particle size, narrower size distribution and unique properties such as coulomb blockade and paramagnetic characteristics.

The research work further demonstrates utility of low molecular weight poly amidoamines for stabilization of AuNPs. The morphology of AuNPs was governed by pH of the medium. At pH 3.3 nanochains were formed and at pH 8.3 isolated nanoparticles were formed. The nanochains were stable against pH shift from 3.3 to 8.3 and elevated temperature, salt concentration and thiol exchange.

This chapter summarizes significant findings of the present investigation followed by the recommendations for further work.

## 7.2 Significant findings

1. Bis (2-methacryloylhydroxyethyl) disulfide (DSDMA) stabilized AuNPs, The particle size decreased with increasing disulfide to Au ratio. The lowest particle size was 2.8 nm. (*Chapter 3 section 3.3.1.1*)
2. DSDMA stabilized 3.2 nm AuNPs could be photo polymerized. UV-Vis spectra and TEM analysis confirmed no change in particle size. (*Chapter 3 section 3.3.1.3*)
3. Photo polymerization enhanced the thermal stability of AuNPs at 140 °C upto 1h. (*Chapter 3 section 3.3.2.3*)



4. DSDMA formed 1:1 inclusion complex with  $\beta$ -cyclodextrin. (*Chapter 4 section 4.3.1*) (*Chapter 4 section 4.2.3.2*)
5. Inclusion complex mediated homopolymerization of DSDMA led to the formation of latent cross-linkable polymers containing disulfide in every repeat unit, since the vinyl group included in  $\beta$ -Cyclodextrin did not participate in radical polymerization. (*Chapter 4 section 4.3.1*)
6. Selective polymerization of DSDMA was confirmed by  $^1\text{H-NMR}$ . (*Chapter 4 section 4.3.1*)
7. At identical disulfide: Au ratio, poly(DSDMA) stabilized AuNPs characterized by UV-Vis spectra and TEM were 3.2 nm to 2.2 nm and were monodisperse compared to DSDMA stabilized AuNPs. (*Chapter 4 section 4.3.3.1*)
8. Poly(DSDMA) stabilized AuNPs were stable in DMF upto one year and against thiol exchange in 10 mM DTT upto 72 h. (*Chapter 4 section 4.3.3.1 and 4.3.3.2*)
9. Poly(DSDMA) stabilized AuNPs exhibited enhanced thermal stability upto 4h due to crosslinking of pendent unsaturation. UV-Vis spectra and TEM of AuNPs confirmed the stability of nanoparticles. FT-IR confirmed the crosslinking of poly(DSDMA). (*Chapter 4 section 4.3.3.3*)
10. Enhanced thermal stability of poly(DSDMA) stabilized AuNPs could be attributed to higher graft density of poly(DSDMA) stabilized AuNPs (37 DSDMA units  $\text{nm}^{-2}$ ) vis a vis that of DSDMA stabilized AuNPs (9 DSDMA units  $\text{nm}^{-2}$ ). (*Chapter 4 section 4.3.3.3*)
11. Etching of AuNPs from poly(DSDMA) resulted in 5 nm cavities as confirmed by TEM and 7 nm capsules as confirmed by AFM. (*Chapter 4 section 4.3.3.4.1*)
12. The particle sizes determined by XRD using Scherer equation are comparable with those obtained by TEM results. (*Chapter 5 Section 5.3.1*)

13. XPS analysis confirmed that AuNPs were in zero oxidation state. (*Chapter 5 Section 5.3.2*)
14. Poly(DSDMA) stabilized AuNPs (2.2 nm to 3.2 nm) exhibited size dependent coulomb blockade at room temperature and paramagnetic character at liquid nitrogen temperature. (*Chapter 5 Section 5.3.3 and (Chapter 5 Section 5.3.5)*)
15. Polyamidoamines served as both stabilizer and reducing agent to yield both gold nanoparticles and nanochains. (*Chapter 6 Section 6.3.2*)
16. The kinetics of chain formation suggested nanochains were from isolated nanoparticles leading to dimer / trimer and subsequent linear aggregation. (*Chapter 5 Section 6.3.2.1*)
17. Morphology of AuNPs was primarily governed by pH rather than concentration. (*Chapter 6 Section 3.2.2 and Chapter 6 Section 6.3.2.3*)
18. Nanochains formed robust against pH switching, thiol exchange and salt concentration (*Chapter 6 Section 6.3.3*)

### **7.3 Recommendation for further work**

No investigation of this kind can address all the issues, especially those generated during the course of the investigation, and could form the basis for subsequent investigations. In this context following recommendations can be made for future work in this area.

1. Explore if polydentate ligand approach can be extended to synthesis of water soluble polydentate ligands for enhancing stability of AuNPs especially against DTT for biological application. Nanocapsules so formed could be evaluated for drug delivery.
2. Explore if increase in size of AuNPs leads to larger nanocavities and stable nanocapsules.

3. Explore if poly(DSDMA) could be used for stabilization of silver and palladium nanoparticles. Silver nanoparticles are well known to exhibit antimicrobial activity which depends on the particles size and stability of nanoparticles. Stability of Palladium nanoparticles is critical in various organic reactions.
4. Explore other nondegradable polymers containing amines (e.g. Polyallylamine and Polyethylene imines) for robust nanochains formation which can be utilized for electronic application.
5. Evaluation of robust gold nanochains for SERS substrate and electronic applications could be explored

# List of publications

## Communications

1. **Satish C. Biradar**, Dhanraj B. Shinde, Vijayamohanan K. Pillai and Mohan G. Kulkarni. 'Polydentate disulfides for enhanced stability of AuNPs and facile nanocavity formation' **Journal of Material Chemistry**, 2012, 22, 10000-10008.
2. **Satish C. Biradar** and Mohan G. Kulkarni 'One pot room temperature synthesis of robust gold nanochains' *communicated to Chemistry of Materials*.

## Patent

1. **Satish C. Biradar**, Mohan G. Kulkarni "Robust gold nanochains and process for preparation thereof" (US patent application filed)

## Satish Chaturrao Biradar

### Institution address

Polymer Science and Engineering Division,  
National Chemical Laboratory,  
Pune, India-411 008.

E-mail. [biradarsc@gmail.com](mailto:biradarsc@gmail.com) [biradarsc@yahoo.co.in](mailto:biradarsc@yahoo.co.in)

Phone No. (Off) +91-20-2590 2307, Mobile. +91 9922052568

---

### Residential address

SA-17, NCL colony  
Pahan, Pune - India  
Pin: 411008

### Educational Qualifications:

- **Ph.D. (Polymer science)**

**Thesis Title: Role of polymer functionality and architecture on morphology of gold nanoparticles.**

**Research Guide:** Dr. M. G. Kulkarni,  
Head, Polymer Science and Engineering division,  
National Chemical Laboratory (CSIR) Pune, India.

- **M.Sc. (Chemistry)** First Class, SRTMU Nanded, India. June 2004.
- **B.Sc. (Chemistry)** First Class, SRTMU Nanded, India. June 2001.

### Awards/ Scholarships

1. **NET-JRF** (National Eligibility Test), **2005**, conducted by Council of Scientific and Industrial Research (CSIR), New Delhi, India, Government of India.
2. **GATE** (Graduate Aptitude Test in Engineering, Subject: Chemistry) **2005**, conducted by Ministry of Human Resource Development, Govt. of India.

### Research Interest

- Synthesis of novel polymer architectures
- Synthesis of nanomaterials
- Drug delivery
- Micro- encapsulation

## Strengths

- A broad, interdisciplinary scientific background in organic, polymer and materials chemistry
- Experience in synthesis of novel monomers, polymers, nanomaterials and their characterization by instrumental techniques such as UV, NMR, FTIR, DSC, TEM, AFM and DLS.
- Excellent interpersonal skills and ability to work individual as well as in team.

## Technical Skills

### Area of Expertise

- Design and synthesis of monomers and polymers for stabilization of gold nanoparticles

### Experimental Techniques

- Acquainted with basic organic and polymer synthesis techniques. Hands on experience in handling equipments and analysis using FTIR, UV-Visible spectroscopy, DSC, TGA and DLS.

### Computer Skills:

- Knowledge ACS Chemical Abstract (CA on CD), Web of Science, Scopus, Scifinder (for searching scientific information)
- Knowledge of scientific softwares like Chem office, Origin and photoshop

## Publications

1. **Satish C. Biradar**, Dhanraj B. Shinde, Vijayamohanan K. Pillai and Mohan G. Kulkarni. 'Polydentate disulfides for enhanced stability of AuNPs and facile nanocavity formation' *Journal of Material Chemistry*, 2012, 22, 10000-10008

2. **Satish C. Biradar** and Mohan G. Kulkarni 'One pot room temperature synthesis of robust gold nanochains' *communicated to Chemistry of Materials*.

## **Patent :**

### **US patent application filed**

1. **Satish C. Biradar**, Mohan G. Kulkarni “Robust gold nanochains and process for preparation thereof”

### **Posters Presented:**

1. **Satish C. Biradar**, Dhanraj B. Shinde, Vijayamohanan K. Pillai and Mohan G. Kulkarni ‘Polydentate disulfides for enhanced stability of AuNPs and facile nanocavity formation’ on the occasion of celebration of *Science day* held at NCL, Pune. **Feb 2012.**
2. **Satish C. Biradar** and Mohan G. Kulkarni ‘One pot facile synthesis of robust gold nanochains’ *Material science and technology event held at NCL, PUNE*, in **April, 2012.**